RAONI PAIS SIQUEIRA

SERINE/ARGININE PROTEIN KINASE (SRPK) INHIBITION AS A POTENTIAL THERAPEUTIC STRATEGY AGAINST LEUKEMIA CELLS

Tese apresentada à Universidade Federal de Viçosa, como parte das exigências do Programa de Pós-Graduação em Bioquímica Aplicada, para obtenção do título de *Doctor Scientiae.*

VIÇOSA
MINAS GERAIS – BRASIL
2018

Ficha catalográfica preparada pela Biblioteca Central da Universidade Federal de Viçosa - Câmpus Viçosa

T
S618s
2018

Siqueira, Raoni Pais, 1988-
Serine/arginine *protein kinase* (SRPK) inhibition as a potential therapeutic strategy against leukemia cells / Raoni Pais Siqueira. – Viçosa, MG, 2018.
ix, 90f. : il. (algumas color.) ; 29 cm.

Orientador: Gustavo Costa Bressan.
Tese (doutorado) - Universidade Federal de Viçosa.
Referências bibliográficas: f.77-86.

1. Inibidor de quinase. 2. Leucemia. 3. Serine/arginine protein kinase. I. Universidade Federal de Viçosa. Departamento de Bioquímica e Biologia Molecular. Programa de Pós-Graduação em Bioquímica Aplicada. II. Título.

CDD 22 ed. 582

RAONI PAIS SIQUEIRA

SERINE/ARGININE PROTEIN KINASE (SRPK) INHIBITION AS A POTENTIAL THERAPEUTIC STRATEGY AGAINST LEUKEMIA CELLS

Tese apresentada à Universidade Federal de Viçosa, como parte das exigências do Programa de Pós-Graduação em Bioquímica Aplicada, para obtenção do título de *Doctor Scientiae.*

APROVADA: 28 de fevereiro de 2018.

Patrick Eyers

Luciana Maria Silva

Raphael de Souza Vasconcellos

Robson Ricardo Teixeira
(Coorientador)

Gustavo Costa Bressan
(Orientador)

To my family

TABLE OF CONTENTS

LIST OF FIGURES

LIST OF TABLES

ABSTRACT

SIQUEIRA, Raoni Pais, D.Sc., Universidade Federal de Viçosa, February, 2018. **Serine/Arginine Protein Kinase (SRPK) Inhibition as a Potential Therapeutic Strategy Against Leukemia Cells.** Adviser: Gustavo Costa Bressan. Co-advisers: Juliana Lopes Rangel Fietto, Márcia Rogéria de Almeida Lamêgo, Abelardo Silva Júnior and Róbson Ricardo Teixeira.

Serine/Arginine protein kinase (SRPK) are key components of the splicing machinery trough the phospho-regulation of SR Proteins, which are crucial for exon selection in the alternative splicing. However, SRPK have frequently been found overexpressed or/and with altered activity in a number of cancers, including leukemias. Thus, the discovery of small molecule inhibitors against these kinases is of potential interest to identify novel therapeutic opportunities. Here, it is described the pharmacological inhibition of SRPK by *N*-(2-(piperidin-1-yl)-5-(trifluoromethyl)phenyl)isonicotinamide (SRPIN340) on the viability of lymphoid and myeloid leukemia cell lines. Along with significant cytotoxic activity, the effect of treatments in regulating the phosphorylation of the SR protein family and in altering the expression of MAP2K1, MAP2K2, VEGF and FAS genes were also assessed. Furthermore, it was found that pharmacological inhibition of SRPKs can trigger early and late events of apoptosis. Finally, intrinsic tryptophan fluorescence emission, molecular docking and molecular dynamics were analyzed to gain structural information on the SRPK/SRPIN340 complex. In a second study, it is described the synthesis of a series of twenty-two trifluoromethyl arylamides based on the SRPIN340 scaffold and the evaluation of their antileukemia effects. Some derivatives presented superior cytotoxic effects against myeloid and lymphoid leukemia cell lines compared to SRPIN340. In particular, compounds *N*-(2-(4-bromophenylamino)-5-(trifluoromethyl)phenyl)-2-chloronicotinamide (**24**), *N*-(2-(4-bromophenylamino)-5-(trifluoromethyl)phenyl)nicotinamide (**30**), and *N*-(2-(4-bromophenylamino)-5-(trifluoromethyl)phenyl)benzamide (**36**) presented IC_{50} values within the 6.0 – 35.7 μM (μmol L^{-1}) range. In addition, these three compounds were able to trigger apoptosis and autophagy, and they exhibited synergistic effects in combination with the chemotherapeutic agent vincristine. Moreover, compound **30** was more efficient than SRPIN340 in impairing the intracellular phosphorylation status of SR proteins as well as the expression of MAP2K1, MAP2K2, VEGF, and RON oncogenic isoforms in leukemia cells. Taken together, these results suggest that SRPK pharmacological inhibitors may be considered for the development of novel therapeutic strategies against leukemias and other types of cancers.

RESUMO

SIQUEIRA, Raoni Pais, D.Sc. Universidade Federal de Viçosa, fevereiro de 2018. **Inibição de Serine/Arginine Protein Kinase (SRPK) como Estratégia Terapêutica contra Linhagens Leucêmicas.** Orientador: Gustavo Costa Bressan. Coorientadores: Juliana Lopes Rangel Fietto, Márcia Rogéria de Almeida Lamêgo, Abelardo Silva Júnior e Róbson Ricardo Teixeira.

Serine/Arginine protein kinases (SRPKs) são componentes chave da maquinaria de splicing através da regulação por fosforilação das proteínas SR, as quais são cruciais para a seleção dos sítios de splicing alternativo. Entretanto, as SRPKs são frequentemente encontradas superexpressas ou com atividade alterada em diversos tipos de cânceres, inclusive em leucemias. Dessa forma, a busca por pequenas moléculas inibidores destas quinases são de potencial interesse para o delineamento de novas estratégias terapêuticas. Nesta tese, descreve-se a avaliação da inibição farmacológica de SRPKs pelo inibidor seletivo *N*-(2-(piperidin-1-il)-5-(trifluorometil)fenil)isonicotinamida (SRPIN340) sobre a viabilidade de linhagens leucêmicas linfoides e mieloides. Além de mostrar atividade citotóxica significativa, o efeito dos tratamentos na regulação da fosforilação das proteínas SR e na alteração da expressão dos genes MAP2K1, MAP2K2, VEGF e FAS foram também identificados. Além disso, a inibição farmacológica de SRPKs foi capaz de desencadear eventos precoces e tardios de apoptose. Por último, estudos de fluorescência intrínseca de triptofano, docking molecular e dinâmica molecular foram analisados a fim de se obter informações estruturais acerca do complexo SRPK/SRPIN340. No segundo estudo, é descrita a síntese de uma série de vinte e duas trifluorometil arilamidas baseadas na estrutura molecular do SRPIN340, além da avaliação dos seus efeitos antileucêmicos. Alguns dos derivados apresentaram efeitos citotóxicos superiores contra linhagens de leucemia mieloide e linfoide em comparação com o SRPIN340. Em particular, os compostos *N*-(2-(4-bromofenilamino)-5-(trifluorometil)fenil)-2-cloronicotinamida (**24**), *N*-(2-(4-bromofenilamino)-5-(trifluorometil)fenil)nicotinamida (**30**), e *N*-(2-(4-bromofenilamino)-5-(trifluorometil)fenil)benzamida (**36**) apresentaram valores de IC_{50} na faixa de 6,0 – 35,7 μM (μmol L^{-1}). Estes três compostos também foram capazes de desencadear eventos de apoptose e autofagia, além de exibir efeito sinergístico em combinação com o agente quimioterápico vincristina. Além disso, o composto **30** se mostrou mais eficiente que o SRPIN340 na diminuição da fosforilação das proteínas SR bem como na diminuição da expressão de isoformas oncogênicas dos genes MAP2K1, MAP2K2, VEGF, e RON. Tomados conjuntamente, estes resultados sugerem que inibidores de SRPKs são capazes de suprimir o crescimento celular através da regulação dos eventos de splicing e podem ser considerados como ponto de partida importante para desenvolvimento de novas estratégias terapêuticas contra leucemias e outros tipos de cânceres.

Chapter 1: General Introduction

1. General Introduction

1.1 Alternative splicing and its role in cancer

One of the most intriguing findings in the central dogma of molecular biology was the discovery that eukaryotic genes are discontinuous, with coding DNA segments (exons) disrupted by long noncoding sequences (introns) (Matera and Wang, 2014). Through advances in the field of genome sequencing, it has been increasingly evident that precursor messenger RNA (pre-mRNA) splicing can occur as a way of generating an additional complexity in the process of gene expression that scales with organism complexity (Lee and Rio, 2015). More than 95% of human genes have been found to undergo splicing in a developmental, tissue-specific or signal transduction-dependent manner, and more than 90% of human genes undergo alternative splicing (Wang et al., 2008, 2015). Therefore, alternative splicing is a molecular mechanism from which the inclusion or exclusion of different exons or parts of exons in mRNA, responsible for generating new isoforms from a single gene can occur (Kozlovski et al., 2017).

The splicing consists in two transesterification reactions catalyzed by the spliceosome, a multisubunit complex of ribonucleoproteins that assembles around splice sites at each intron-exon boundaries (Salton and Misteli, 2016). Each splice site consists of a consensus sequence that is flexibly recognized by spliceosomal components (Kornblihtt et al., 2013). Thus, the spliceosome complex and its associated regulatory factors are composed of more than 200 proteins and five small nuclear RNAs (snRNAs), and catalyzes both constitutive and regulated alternative splicing. The U1, U2, U4, U5, and U6 snRNAs participate in several key RNA–RNA and RNA–protein interactions during spliceosome assembly and splicing catalysis (Anczuków and Krainer, 2016). In a simplified way, spliceosome assembly is initiated when U1 snRNP U1 is recruited to the 5’ splicing site and U2 snRNP stably associates with the branch site (E complex). In a subsequent step, the U4/U6.U5 tri-snRNP is then recruited, generating the catalytic complex that removes the intron (C complex) (**Figure 1**).

Since pre-mRNA splicing is an essential process in mammalian cells, it is not surprising that the deregulation of these events is the cause of many human diseases, including cancer. In fact, several studies have demonstrated that tumors exhibit abnormal splicing patterns and these changes in splicing occur in favoring the process of cellular transformation (Singh and Eyras, 2017). Some examples of splicing isoforms found in cancers include the increased expression of anti-apoptotic isoforms of genes such as BCL2L1, CASP2, or FAS; pro-invasive isoforms of CD44, FGFR2, or RAC1; and pro-angiogenic VEGF spliced isoform (Anczuków and Krainer, 2016).

However, it is important to mention that global alterations in splicing behavior in cancer can be caused by changes in expression or activity of particular components of the splicing machinery (Salton and Misteli, 2016). Tumors exhibit somatic mutations in splicing regulators

encoding genes, or changes in splicing-factor levels in response to cell signaling or transcriptional regulation, which in turn promote the differential splicing patterns in tumors compared to normal tissues. Alterations in the activity of splicing factors can lead to the production of pro-tumorigenic isoforms that have been linked tumorigenesis processes, such as proliferation, apoptosis, invasion, metabolism, angiogenesis, DNA damage, or even drug resistance and immune response (**Figure 2**) (Anczuków and Krainer, 2016).

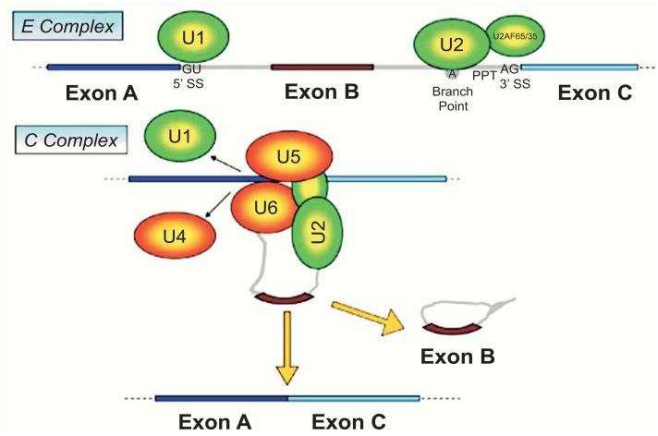

Figure 1: Simplified scheme of spliceosome assembly. To form E complex, U1 is recruited to the 5'-splice site, whereas U2 is recruited to the branch-point. Then, the U4/U6.U5 tri-snRNP associates with the forming spliceosome, removing U1 and U4 (C complex). In this scheme, the 'exon B' is removed along with two introns, exemplifying an alternative splicing event (This figure was extracted from La Cognata et al., 2014).

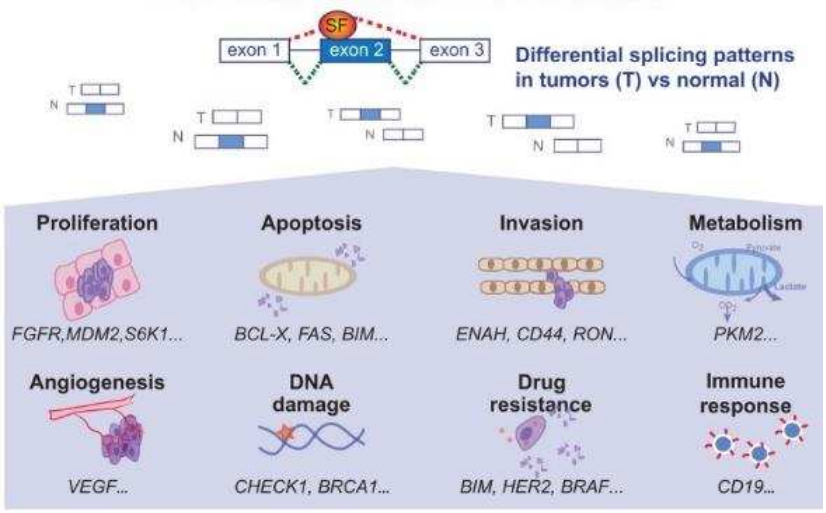

Figure 2: Differential splicing pattern in tumor and normal tissues. Alterations in the splicing patterns in favoring the tumorigenic process. SF: splicing factor (This figure was extracted from Anczuków and Krainer, 2016).

1.2 SR Proteins and their roles in pre-mRNA splicing

One well-studied family of splicing factors that regulate the assembly of the spliceosome complex is the SR proteins. These proteins are highly conserved in metazoa and plants and, typically, contain one or two RNA-binding motifs (RRM domain) and a carboxy terminal domain rich in serine and arginine residues (RS domain) (Syed et al., 2012) (**Figure 3**). Binding of SR proteins to cis-elements in pre-mRNA exons, called exonic splicing enhancers (ESE), acts to prevent exon skipping and ensures the correct 5' to 3' linear order of exons in spliced mRNA (Aubol et al., 2013; Long and Caceres, 2009) (**Figure 4**). Consequently, the portion of the exon delimited by binding of these proteins tends to be maintained in the mature mRNA transcript, but they can inhibit splicing when associated with introns (Cho et al., 2011; Wang et al., 2013). In addition, the coordinated performance of SR family members with other splicing factors results in a differential recognition of introns and exons by the spliceosome complex which, through alternative splicing, can be included or excluded in the mature mRNA (Wang et al., 2013).

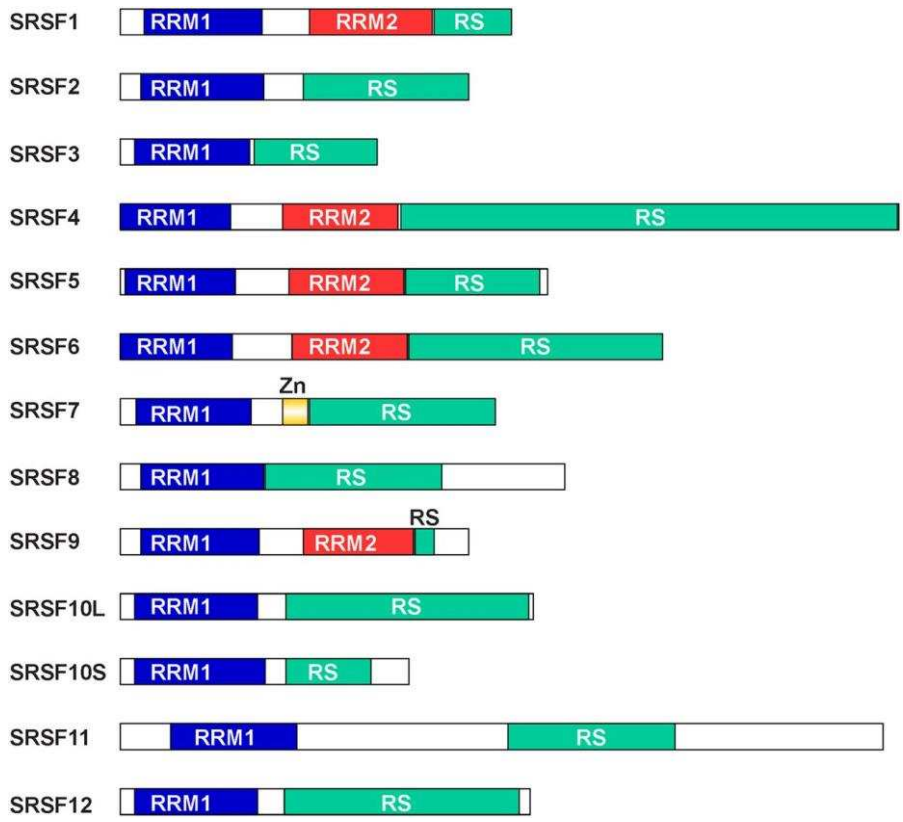

Figure 3: SR splicing factors family present in humans. The RNA-binding motifs (RRM domains; blue/red) and the carboxy terminal domain rich in serine and arginine residues (RS domain; green) are highlighted (This figure was extracted from Mahiet and Swanson, 2016).

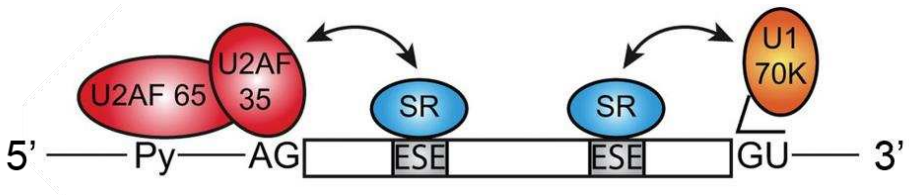

Figure 4: Role of SR proteins in splicing site selection. SR protein binds to an ESE through its RRMs domains and contacts the splicing factor U2 and/or the snRNP protein U1 at the adjacent splice sites through its RS domain (This figure was extracted from Long and Caceres, 2009).

Phosphorylation of the RS domain of SR proteins has a great impact on their regulation, as it may affect their binding to target mRNAs, their interaction with other proteins and their intracellular localization (Naro and Sette, 2013). Two families of protein kinases are the main responsible for extensively phosphorylating these essential splicing factors. The serine/arginine protein kinases (SRPK1-3) strictly phosphorylate Arg-Ser dipeptides, whereas the CDC2-like kinases (CLK1-4) can phosphorylate both Arg-Ser and Ser-Pro dipeptides, common in all SR proteins (Aubol et al., 2016).

When dephosphorylated, SR proteins are predominantly located in the cytoplasm. In its turn, SRPKs that are located also in the cytoplasm phosphorylate SR proteins, a key modification that facilitates the shuttling of these splicing factors into the nucleus where they aggregate in nuclear speckles, which are nuclear domains enriched in pre-mRNA splicing factors (Aubol et al., 2013; Zhong et al., 2009). Further phosphorylation by SRPKs or CLKs release the SR proteins from these nuclear corpuscles, allowing recognition and interaction with pre-mRNA (Zhong et al., 2009). Therefore, the phosphorylation levels of RS domains in SR proteins can actively regulate the splicing by controlling protein-protein or protein-RNA interactions in the spliceosome, influencing the production of a spliced isoform in detriment of another (Aubol et al., 2013).

1.3 SRPKs and their oncogenic activity

As previously stated, one of the most important group of kinase related to the phospho-regulation of SR proteins are the serine/arginine protein kinases (SRPKs). These kinases have conserved residues of the catalytic domains of serine/threonine kinases and they have a central role in the regulatory network for splicing - controlling the intranuclear distribution of splicing factors, reorganization of nuclear speckles, protein-protein and RNA-protein interaction, and ultimately the action of SR factors on the pre-mRNA (Giannakouros et al., 2011; Zhou and Fu, 2013). SRPK1 was the first SR kinase to be described (Gui et al., 1994). Through homology studies, two other SR kinases, SRPK2 (Kuroyanagi et al., 1998) and SRPK3 (Nakagawa et al., 2005), have been identified. Lastly, a product of the SRPK1 gene produced by alternative splicing

(named SRPK1a) has been also reported (Sanidas et al., 2010). While SRPK1 is ubiquitously expressed, SRPK2 is expressed mainly in the nervous system and the expression of SRPK3 seems to be restricted to muscle cells (Zhou and Fu, 2013).

SRPKs are characterized by an N-terminal extension and a bipartite catalytic domain bifurcated by a large spacer insert domain (SID) (**Figures 5** and **6**) (Aubol and Adams, 2014). The SID is an intrinsically unstructured region with critical modulatory role on SRPK subcellular localization, as deletion of this sequence changes the distribution pattern of the kinase from mainly cytoplasmic to exclusively nuclear (Koutroumani et al., 2017). Thus, SRPKs are mainly localized in the cytoplasm of mammalian cells due to the presence of a cytoplasmic retention signal localized in the SID, which is involved in the interaction with the HSP70 and HSP90 molecular chaperones (Naro and Sette, 2013). However, these kinases can translocate into the nucleus of cells under several conditions, mainly as a consequence of activation of the signal transduction pathway EGF-PI3K-AKT-SRPK (Naro and Sette, 2013; Zhou and Fu, 2013). In this context, Zhou and colleagues (2012) showed the AKT-mediated SRPK1 autophosphorylation switched this splicing kinase from Hsp70- to Hsp90-containing complexes, enhancing SRPK nuclear translocation and SR protein phosphorylation (Zhou et al., 2012). In turn, recent studies have shown a different mechanism that regulates the cellular activity of SRPK2, which must be doubly phosphorylated by S6K and CK1 via mTORC1-activation before its nuclear import (Lee et al., 2017). Therefore, these studies highlight the SRPKs as key point in regulating the cellular splicing activity through SR proteins phosphorylation in response to external and internal stimuli.

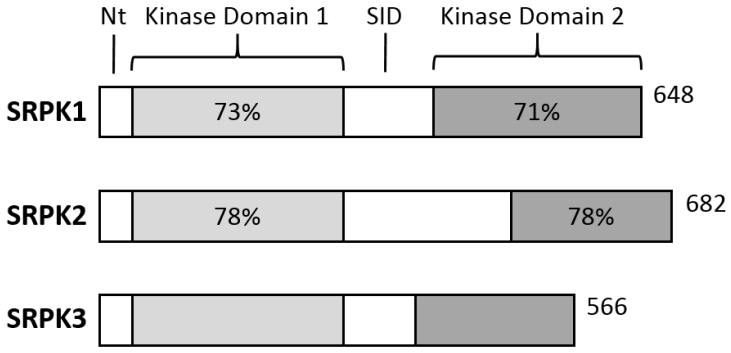

Figure 5: Schematic representation of the domain architecture of mouse SRPK family. In each structure, the percentages represent the homology of the kinase domains of SRPK1 and SRPK2 compared to SRPK3. The N-terminus (Nt) and the spacer insert domain (SID) are also highlighted. (This figure was extracted from Nakagawa et al., 2005).

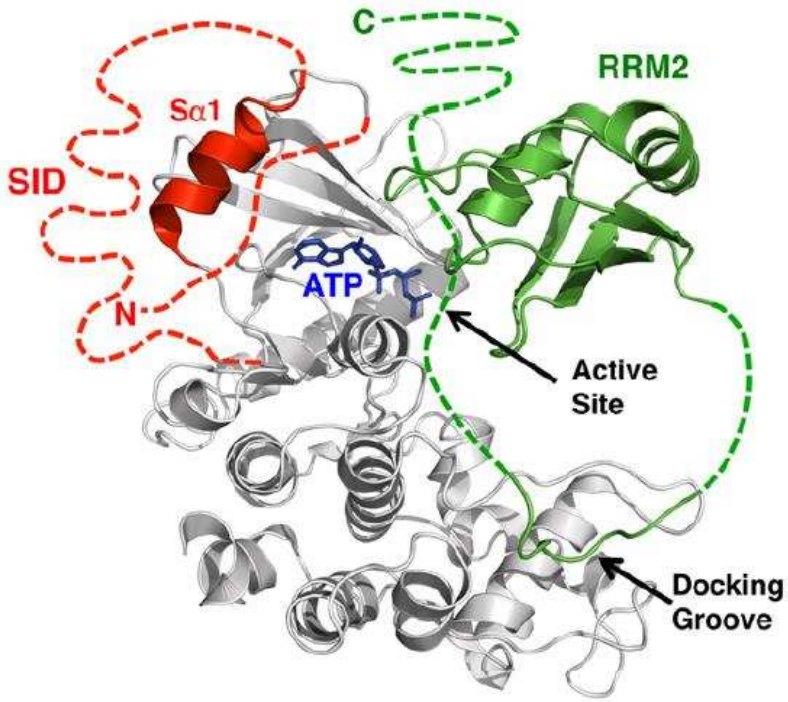

Figure 6: Structure of SRPK1 in complex with SR protein SRSF1. The catalytic domain composed of C- and N-lobe is shown in gray and the spacer insert domain (SID) is in red. There is also the C-lobe region called docking groove that binds SRSF1 (green). The dashed lines represent the intrinsically unstructured regions absent in the crystal structures obtained. The ATP are highlighted in blue (This figure was extracted from Aubol and Adams, 2014).

Despite the importance in splicing regulation, SRPK1 and SRPK2 have been found overexpressed and/or with oncogenic activity in different types of cancer including breast, colon, gastric cancer, leukemia, melanoma, non small cell lung carcinoma, squamous cell lung carcinoma, glioma, ovary, prostate, among others (Bullock et al., 2016; Gammons et al., 2014; Goncalves et al., 2014; Gout et al., 2012; Jang et al., 2008; Odunsi et al., 2012; Van Roosmalen et al., 2015; Wu et al., 2014; Xu et al., 2017). Mechanistically, the role of SRPKs in tumorigenesis, has been credited, for example, to their benefits to the expression of pro-oncogenic MAP2K1 and MAP2K2 and pro-angiogenic VEGF (Gammons et al., 2014; Hayes et al., 2007). Moreover, recent studies showed that high SRPK1 expression correlates with poor outcome of patients and metastasis of breast and prostate cancers (Bullock et al., 2016; Van Roosmalen et al., 2015).

Regarding leukemia, the oncogenic activity of SRPKs has already been demonstrated as crucial for the leukomogenesis process. Leukemia is the cancer of blood cells that results from cell differentiation and uncontrolled proliferation during hematopoiesis in the bone marrow (**Figure 7**) (Morlando et al., 2015). Thus, leukemia refers to a heterogeneous group of hematologic malignancies classified into chronic and acute leukemia and further classified based

on cell lineage into myeloid and lymphoid. There are four major types of leukemia: chronic myeloid leukemia (CML), chronic lymphocytic leukemia (CLL), acute myeloid leukemia (AML), and acute lymphocytic leukemia (ALL) (Al Omair, 2015; Arber et al., 2016). Leukemia is the most common cancer in children and teens, accounting for almost 1 out of 3 cancers. Most childhood leukemias are acute lymphocytic leukemia (ALL). Most of the remaining cases are acute myeloid leukemia (AML). Estimates from the Instituto Nacional de Câncer José Alencar Gomes da Silva (INCA-Brazil) indicate that in 2013 occurred more than 6000 deaths in Brazil due to leukemia and by the year 2018 are expected 10800 new cases of the disease. SRPK1 has been found to be overexpressed in patients with acute lymphocytic leukemia and chronic myeloid leukemia (Hishizawa et al., 2005; Salesse et al., 2004). In this context, a recently study based on CRISPR dropout screen identified SRPK1 as a key epigenetic regulator of BRD4, a gene often required for the expression of Myc and other tumor driving oncogenes in hematologic cancers (Tzelepis et al., 2016). High levels of SRPK2 has been also found overexpressed in acute myeloid leukemia cell lines and in acute lymphocytic leukemia specimens from clinically diagnosed patients. In this case, the overexpression of SRPK2 have been correlated to cell proliferation through the SR protein hyperphosphorylation and cyclin A1 expression (Jang et al., 2008).

Although the role of SRPKs in the alternative splicing in leukemias still needs to be better elucidated, Cunningham and colleagues (2013) showed that the tumor suppressor WT1 regulates murine hematopoiesis via alternative splicing of VEGF (Cunningham et al., 2013). It is clear that WT1 mediates transcriptional repression of SRPK1, which alters mRNA splicing of VEGF reducing the expression of the pro-angiogenic isoform $VEGF_{165}b$ (Amin et al., 2011).

In addition, the key role played by SRPKs in mRNA processing is particularly apparent in studies on other pathological conditions, such as viral infection by herpes simplex, hepatitis B, papilloma virus and HIV (Giannakouros et al., 2011); vascular disorders such as neovascularization choroidal (Gammons et al., 2013); and neurodegenerative diseases, in which SRPK2 participates in the neuronal survival, cell cycle progression, and memory determination in Alzheimer's disease (Chan and Ye, 2013).

Therefore, these data collectively suggest that SRPK are potential targets for the development of new chemotherapeutic agents for treating cancer and other disorders.

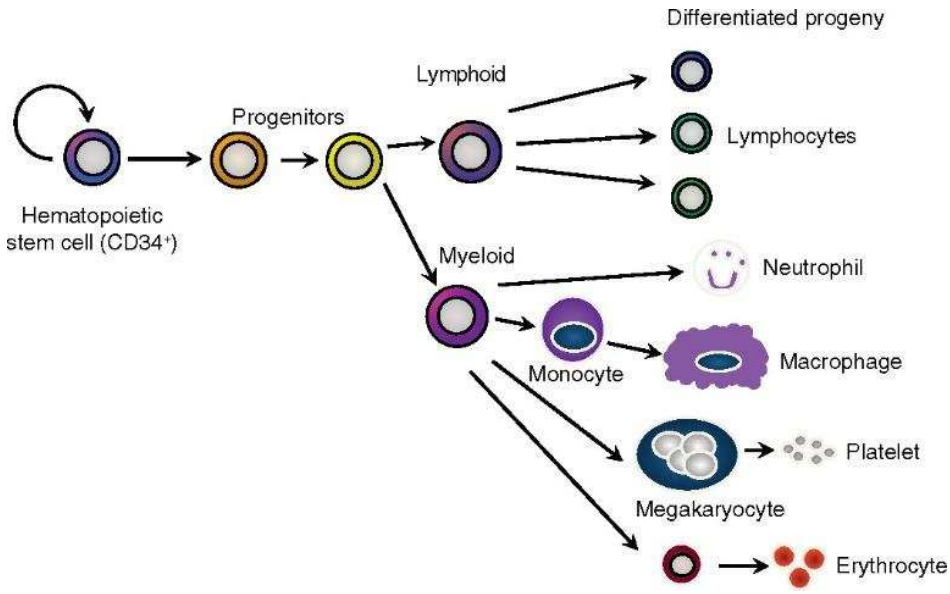

Figure 7: Differentiation of the hematopoietic system. Hematopoietic stem cells can give rise to all the cell types of the peripheral blood through the development of lymphoid and myeloid progenitors (This figure was extected from King and Goodell, 2011).

1.4 SRPK as drug target

Not so long ago, the approval of imatinibib (Gleevec, Novartis) targeting the Bcr-Abl oncoprotein for the treatment of patients with chronic myeloid leukemia (CML) was not only an important discovery in targeted cancer therapy, but also highlighted the protein kinases as potential drug targets (Wu et al., 2016). Since then, The US Food and drug Administration (FDA) has approved other 36 small-molecule kinase inhibitors (KIs) for use in cancer and/or other human disorders (Klaeger et al., 2017). However, the present success of these drugs is mainly achieved by targeting tyrosine protein kinases in the human kinome, which still account for more than 75% of all approved small-molecule kinase inhibitor (Wu et al., 2016). These data indicate that a small part of the human kinoma have been explored so far and, therefore, that there is still a potential in human "drugable" kinoma to be understood and explored more fully.

Due to their important role in the development and progression of different diseases, the serine/threonine protein kinases SRPK1 and SRPK2 have been suggested as potential therapeutic targets and some small-inhibitors with important biological effects have already been described (Da Silva et al., 2015; Lee and Abdel-Wahab, 2016). In this section, the main SRPKs inhibitors described in the literature will be summarized.

The first inhibitor of SRPK1/2 described was the *N*-(2-(piperidin-1-yl)- 5-(trifluoromethyl)phenyl)isonicotinamide, also named SRPIN340 (**Figure 8**). This molecule has been described as an ATP-competitive inhibitor highly selective for both kinases (Fukuhara et

al., 2006). Considering its biological effects, SRPIN340 has been characterized as an antiviral agent against the replication of several viruses, such as HIV, Sindbis virus, HCV and hepatitis C (Anwar et al., 2011; Fukuhara et al., 2006; Karakama et al., 2010). In addition, it presented anti-angiogenic activity in an ocular murine angiogenesis model (Amin et al., 2011; Dong et al., 2013; Gammons et al., 2013) and antitumor activity in a murine xenograft model of melanoma (Gammons et al., 2014).

These promising results stimulated the search for new and more potent inhibitors of SRPKs (**Figure 8**). This is the case of a disubstituted furan inhibitor named SPHINX, which is a SRPIN340 derivative able to reduce the expression of pro-angiogenic VEGF isoforms and consequently choroidal neovascularization *in vivo* (Gammons et al., 2013). Pharmacophore docking models followed by a high-throughput screening of a large chemical library identified the inhibitor SRPIN803, able to promote the dual inhibition of SRPK1 and CK2. This inhibitor prevented pro-angiogenic VEGF production more effectively than SRPIN340 and significantly inhibited choroidal neovascularization in a mouse model of age-related macular degeneration (Morooka et al., 2015). More recently, a more potent and selective inhibitor of SRPK1 has been described, SPHINX31. Treatments with this compound inhibited phosphorylation of the splicing factor SRSF1, resulting in alternative splicing of VEGF from pro-angiogenic to antiangiogenic isoforms. This property resulted in a potent inhibition of blood vessel growth in choroidal angiogenesis *in vivo* (Batson et al., 2017).

Therefore, these data indicates that the SRPKs inhibitors described so far may be considered as starting point for the development of novel potential antineoplastic drugs.

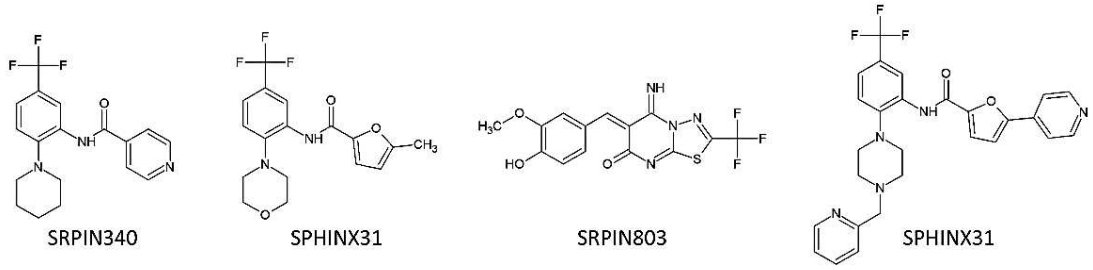

Figure 8: SRPK inhibitors with relevant biological activity. With exception of SRPIN803, all these inhibitors have in common the trifluoromethyl arylamide moiety.

1.5 Aims of the thesis

Based on the hypothesis that SRPK1 and SRPK2 dysregulation can lead to the biogenesis and progression of several cancers, including leukemia, the specific objectives of this thesis were:

- To investigate the *in vitro* antileukemia potential of SRPK pharmacological inhibition by SRPIN340 (Chapter 2).
- To assess the antileukemia potential of novel trifluoromethyl arylamides derived from SRPIN340 (Chapter 3).

Chapter 2: Research Article I

2. Research Article I

Potential Antileukemia Effect and Structural Analyses of SRPK Inhibition by *N*-(2-(Piperidin-1-yl)-5-(Trifluoromethyl)Phenyl)Isonicotinamide (SRPIN340)

Raoni Pais Siqueira[1], Éverton de Almeida Alves Barbosa[1], Marcelo Depólo Polêto[1], Germanna Lima Riguetto[2], Thiago Vargas Seraphim[3], Rafael Locatelli Salgado[1], Joana Gasperazzo Ferreira[1], Marcus Vinícius de Andrade Barros[4], Leandro Licursi de Oliveira[5], Angelo Brunelli Albertoni Laranjeira[6], Márcia Rogéria Almeida[1], Abelardo Silva júnior[7], Juliana Lopes Rangel Fietto[1], Jörg Kobarg[8], Eduardo Basílio de Oliveira[9], Róbson Ricardo Teixeira[4], Júlio César Borges[3], Jose Andrés Yunes[6] and Gustavo Costa Bressan[1]

[1]Departamento de Bioquímica e Biologia Molecular, Universidade Federal de Viçosa, Viçosa, Minas Gerais, Brasil.

[2]Instituto de Biologia, Universidade Estadual de Campinas, Campinas, São Paulo, Brasil.

[3]Instituto de Química, Universidade de São Paulo, São Carlos, São Paulo, Brasil.

[4]Departamento de Química, Universidade Federal de Viçosa, Viçosa, Minas Gerais, Brasil.

[5]Departamento de Biologia Geral, Universidade Federal de Viçosa, Viçosa, Minas Gerais, Brasil.

[6]Centro Infantil Boldrini, Campinas, São Paulo, Brasil.

[7]Departamento de Veterinária, Universidade Federal de Viçosa, Viçosa, Minas Gerais, Brasil.

[8]Laboratório Nacional de Biociências, Centro Nacional de Pesquisa em Energia e Materiais, Campinas, São Paulo, Brasil.

[9]Departamento de Engenharia de Alimentos, Universidade Federal de Viçosa, Viçosa, Minas Gerais, Brasil.

PLoS One, v. 10, p. 1 – 21, e0134882, 2015

2.1 Abstract

Dysregulation of pre-mRNA splicing machinery activity has been related to the biogenesis of several diseases. The serine/arginine-rich protein kinase family (SRPKs) plays a critical role in regulating pre-mRNA splicing events through the extensive phosphorylation of splicing factors from the family of serine/arginine-rich proteins (SR proteins). Previous investigations have described the overexpression of SRPK1 and SRPK2 in leukemia and other cancer types, suggesting that they would be useful targets for developing novel antitumor strategies. Herein, we evaluated the effect of selective pharmacological SRPK inhibition by *N*-(2-(piperidin-1-yl)-5-(trifluoromethyl)phenyl)isonicotinamide (SRPIN340) on the viability of lymphoid and myeloid leukemia cell lines. Along with significant cytotoxic activity, the effect of treatments in regulating the phosphorylation of the SR protein family and in altering the expression of MAP2K1, MAP2K2, VEGF and FAS genes were also assessed. Furthermore, we found that pharmacological inhibition of SRPKs can trigger early and late events of apoptosis. Finally, intrinsic tryptophan fluorescence emission, molecular docking and molecular dynamics were analyzed to gain structural information on the SRPK/SRPIN340 complex. These data suggest that SRPK pharmacological inhibition should be considered as an alternative therapeutic strategy for fighting leukemias. Moreover, the obtained SRPK-ligand interaction data provide useful structural information to guide further medicinal chemistry efforts towards the development of novel drug candidates.

Keywords

Serine/arginine-rich protein kinases, SR proteins, cancer, leukemia, SRPIN340, pre-mRNA splicing, docking, molecular dynamics, intrinsic fluorescence analyses, MAP2K1, MAP2K2, VEGF, FAS, mAb1H4

2.2 Introduction

More than 90% of all human transcribed genes may undergo alternative splicing, a mechanism that allows a considerable increase of the encoding potential of eukaryotic genomes (Wang et al., 2008). This process leads to the expression of different protein isoforms that may possess even antagonistic functions, as occurs with VEGF pro- and anti-angiogenic isoforms (Fedorov et al., 2011; Harper and Bates, 2008). Pre-mRNA splicing flexibility plays a key role in tissue development and cell response to external stimuli, unsurprisingly explaining why dysregulation of these events has been related to the biogenesis of many human diseases, including cancer (Bourgeois et al., 2004; Fedorov et al., 2011; Ward and Cooper, 2010).

Regulation of pre-mRNA splicing involves hundreds of auxiliary factors that control splicing site selection, spliceosome assembly and splice reaction (Bourgeois et al., 2004; Wahl et al., 2009). The serine/arginine protein family (SR proteins) constitutes an important group of splicing factors responsible for delimitating intron and exon boundaries in pre-mRNAs (Bourgeois et al., 2004; Long and Caceres, 2009). These proteins act in response to environmental changes and are structurally characterized by an amino-terminal portion possessing one or two RNA-binding domains (RRM) and a carboxy-terminal portion comprising a domain rich in serine and arginine residues (RS) (Cho et al., 2011; House and Lynch, 2008). These serine residues are extensively phosphorylated by different kinases, notably by serine/arginine-rich protein kinases (SRPKs) (Giannakouros et al., 2011). This kinase family possesses a bi-lobular kinase domain separated by a divergent spacer region that is targeted by molecular chaperones in the context of the EGFR/PI3K/Akt/SRPK signaling pathway (Giannakouros et al., 2011). The signaling module EGFR/PI3K/AKT is commonly related to multiple cancers and constitutes the major activation mechanism known for SRPKs to date (Courtney et al., 2010; Wong et al., 2010; Zhong et al., 2009; Zhou and Fu, 2013). Activated SRPKs, in turn, regulate SR proteins' cellular sublocalization, splicing site selection and interaction with additional protein factors (Aubol et al., 2013; Jang et al., 2008). Moreover, SRPKs can also activate AKT in the cytosol through a mechanism involving the phosphatase pleckstrin homology (PH) domain leucine-rich repeat protein phosphatase PHLPP (Wang et al., 2014).

Overexpression and dysregulation of SRPKs have been characterized as important factors in promoting cell proliferation in many human cancers including leukemia, pancreatic, breast, colon, lung, ovarian and melanoma (Gammons et al., 2014; Gout et al., 2012; Hayes et al., 2007, 2006; Jang et al., 2008; Wu et al., 2014). Considering leukemias, SRPK1 has been found to be overexpressed in patients with acute lymphoblastic leukemia and chronic myeloid leukemia (Hishizawa et al., 2005; Salesse et al., 2004). High levels of SRPK2 in some acute myeloid

leukemia cell lines and in acute lymphoblastic leukemia specimens have been correlated to cell proliferation through the acinus SR protein hyperphosphorylation and cyclin A1 expression (Jang et al., 2008). In general, it is believed that overexpression of SRPKs may alter the proper activity of SR factors on their primary transcript target, favoring the expression of splicing isoforms that contribute to tumorigenic processes (Zhou and Fu, 2013). Hence, the available data suggest that SRPK inhibition could control tumor cell proliferation (Hayes et al., 2006; Jang et al., 2008).

Previous high throughput screening campaigns have identified the *N*-(2-(piperidin-1-yl)-5-(trifluoromethyl)phenyl)isonicotinamide, also named SRPIN340, as an ATP-competitive inhibitor that is highly selective for SRPK1 and SRPK2 (Fukuhara et al., 2006). This inhibitor has been characterized as an antiviral agent against the replication of several viruses, such as HIV, Sindbis virus, HCV and hepatitis C (Anwar et al., 2011; Fukuhara et al., 2006; Karakama et al., 2010). In addition, it presented anti-angiogenic activity in an ocular murine angiogenesis model (Amin et al., 2011; Dong et al., 2013; Nowak et al., 2010; Oltean et al., 2012) and antitumor activity when locally injected into human melanoma tumors developed in mice transplanted with human melanoma cells (Gammons et al., 2014).

Considering that SRPK dysregulation can lead to AKT hyperactivation and can additionally generate multiple abnormal protein isoforms involved in the biogenesis and progression of several cancers, this work describes an *in vitro* evaluation of the antileukemia potential of SRPK pharmacological inhibition. In addition, structural data that might explain SRPIN340's inhibitory activity on SRPK2 are also described.

2.3 Experimental Procedures

2.3.1 Cell lines

The leukemia cell lines used were K562 (chronic myelogenous leukemia - CML); KG1 and HL60 (acute myelogenous leukemia - AML); Jurkat, TALL, and Molt4 (T-cell acute lymphoblastic leukemia – ALL-T); and RS4, 697, and Nalm6 (B-cell acute lymphoblastic leukemia – ALL-B). K562, HL60, RS4, and 697 were kindly provided by Dr. Sheila A. Shurtleff (St. Jude Children's Research Hospital, Memphis, TN). The Nalm6 cell line was provided by Dr. Angelo Cardoso (Dana-Farber Cancer Institute, Boston, MA). TALL was kindly provided by Dr. Joao T. Barata (Instituto de Medicina Molecular, Lisboa, Portugal). The KG1, Molt4, and Jurkat cell lines were provided by Dr. Alexandre E. Nowill (Centro Integrado de Pesquisas Oncohematológicas da Infância, UNICAMP, Campinas, Brazil). Cells were cultivated in RPMI 1640 (Sigma) medium supplemented with 10% (v/v) fetal bovine serum (FBS) (LGC Biotecnologia), 100 g/mL streptomycin, and 100 units/mL penicillin at pH 7.2 and 37^{o}C under a 5% CO_2 atmosphere.

2.3.2 Isolation of PBMC from human blood

Peripheral blood was collected in EDTA tubes, diluted with an equal volume of Hank's balanced salt solution (HBSS) and mixed gently. All procedures were performed according to ethics considerations of the Declaration of Helsinki and were approved by the ethics committee of the Universidade Federal de Viçosa. Afterwards, samples were layered onto a cushion of Histopaque 1077 (Sigma) and centrifuged at room temperature for 30 min at 400 x*g*. Mononuclear cells were collected from the interface, washed twice in HBSS, and centrifuged at room temperature for 8 min 240 x*g*. These cells were resuspended in complete RPMI 1640 medium supplemented with 10% fetal bovine serum and 1% (v/v) phytohemagglutinin (Gibco) and counted using a Neubauer chamber for the following experiments.

2.3.3 SRPK inhibitor synthesis

Compound *N*-(2-(piperidin-1-yl)-5-(trifluoromethyl)phenyl)isonicotinamide (SRPIN340) was synthesized as published previously (Fukuhara et al., 2006).

2.3.4 MTT cell viability assay

Leukemic cells ($5x10^4$ cells/well) and isolated PBMCs ($8x10^4$ cells/well) were seeded in 96-well plates. Each well contained 100 µL of complete RPMI medium and 100 µL of SRPIN340 solution at different concentrations. The compound was diluted in RPMI medium with 10% fetal bovine serum and 0.4% DMSO (v/v). After 48 h of culture, MTT (5 mg/mL, Sigma) was added to the wells (3 h, 37^{o}C). The plates were centrifuged at room temperature for 30 min 500 x*g*, followed by the removal of the MTT solution and the addition of 100 µL/well of DMSO (Sigma) to solubilize the formazan. Absorbance was measured at 540 nm in a microplate reader (Sinergy HT, Biotek). Each experimental procedure was performed in triplicate.

2.3.5 Flow cytometry assays

Cultured cells were seeded on a 96-well plate at a density of 10^5 cells/well. After treatments, cells were labeled using an FITC Annexin V apoptosis detection kit I (BD Biosciences) according to the manufacturer's protocol. Subsequently, cell samples were submitted to analysis by flow cytometry (FACS Verse, BD Bioscience). Results were analyzed by FlowJo software.

2.3.6 RT-PCR and RT-qPCR Analysis

mRNA was extracted from leukemic cells using Tri Reagent (Sigma) according to the manufacturer's protocol. Samples were quantified by spectrophotometry (NanoDrop, Thermo

Scientific) and analyzed for integrity in 1% agarose gel. Afterwards, the RNA was used for first-strand cDNA synthesis using the Super Script First-Strand kit (Invitrogen) according to the manufacturer's protocol. Then, the cDNA was used to amplify each fragment of interest by PCR using the GoTaq Green Master Mix (Promega) kit, and the products were separated in 1% or 2% agarose gels. Quantitative gene expression analyses (RT-qPCR) were performed in an ABI Prism 7500 Sequence Detector system (Applied Biosystems) using SYBR Green I dye (SYBR Green PCR Master Mix, Applied Biosystems). cDNAs, obtained as described above, were used as the template for amplifications following the manufacturer's protocols. All primers used in the RT-PCR and RT-qPCR assays are listed in Supplementary Table 1.

2.6.7 Western Blot Analysis

Cells were counted using a Neubauer chamber and washed once in phosphate buffered saline (PBS). Cells were lysed in PBS containing 1% (v/v) NP40, 1 mM EDTA, 150 mM NaCl, protease and phosphatase inhibitors (Sigma), and 10 mM Tris (pH 7.4) at a concentration of $2x10^7$ cells/mL in lysis buffer. Samples were incubated on ice for 10 minutes, lysed by pipetting, and centrifuged for 10 minutes at 15000 x*g* to remove insoluble cellular debris. An equal volume of 2X sample buffer containing 4% (w/v) SDS, 0.2% (w/v) bromophenol blue, 20% (v/v) glycerol, and 100 mM Tris (pH 6.8) was added to the supernatant. Then, the samples were heated to 70^{o}C for 10 min. Approximately $1.5x10^5$ cell equivalents were loaded per well of 10% Bis-Tris SDS – polyacrylamide gel electrophoresis. Afterwards, proteins were transferred to a polyvinylidene difluoride (PVDF) membrane (GE Healthcare), blocked overnight in PBS containing 5% (w/v) skim milk powder, and then incubated for 2 h with primary antibody solutions. Specific kinases were detected using 1:4000 dilutions of anti-SRPK1 and anti-SRPK2 (BD Biosciences). Phosphorylated SR proteins were detected using a 1:1000 dilution of mAb1H4 (Invitrogen) specific for a phospho-epitope common to multiple SR proteins. Each blot was re-probed with a 1:1000 dilution of anti-actin (Sigma), used as an endogenous control in all experiments. Blots were washed in PBS-Tween (PBS-T) and incubated for 2 h in a 1:5000 dilution of a peroxidase-conjugated secondary antibody. Then, proteins were visualized using a Super Signal West Pico Chemiluminescent Substrate Kit (Thermo Scientific).

2.3.8 Cloning, expression and purification procedures

The clone pCMV-SPORT6-SRPK2 was purchased from the Mammalian Gene Collection (Invitrogen). This clone allowed amplification of full-length SRPK2 cDNA by PCR and subcloning into the pET28a-HIS-TEV vector (Carneiro et al., 2006), a modified version of the bacterial expression vector pET28a (Novagen). The following primers were used: forward primer 5'-

GAGCTCATGTCAGTTAACTCTGAGAAGTCG-3' and reverse primer 5'-GTCGACCTAAGAATTCAACCAAGGATGCC-3'. Expression of SRPK2 N-terminally fused to 6xHistidine (6xHis) was induced in *Escherichia coli* (BL21) by 0.25 mM isopropyl thio-β-D-galactoside (IPTG) for 2 h at 30°C. After harvesting, the pellets were resuspended in 20 mM phosphate, 500 mM NaCl, and 20 mM imidazole at pH 7.4. Lysis was performed by adding 5 U of DNAse (Fermentas) and 30 µg/mL of lysozyme (Sigma) followed by 30 min of incubation on ice and disruption by 10 cycles of sonication. Supernatants were obtained after centrifugation at 24586 x*g* for 15 min at 4^{o}C. The obtained supernatants were loaded onto a HiTrap Chelating HP column (GE Healthcare) coupled to an AKTA FPLC (GE Healthcare) equilibrated with lysis buffer. The 6xHis-SRPK2 was eluted by a gradient of 0 – 500 mM. The obtained Ni^{2+} affinity-purified fractions were dialyzed against a buffer containing 10 mM phosphate at pH 7.5. After a 2-fold dilution, samples were then loaded onto a CHT Ceramic Hidroxy Hepatite type II (Biorad) resin ion-exchange column. Proteins were eluted by a gradient of 0 - 500 mM phosphate. The efficiency of each purification step was verified by 10% SDS-PAGE. The following dialyses were performed against the sample buffer: 25 mM Tris-HCl, 100 mM NaCl, 1 mM β-mercaptoethanol, and 2 mM EDTA at pH 7.5.

2.3.9 Fluorescence Spectroscopy

Intrinsic tryptophan fluorescence emission was measured using a fluorescence spectrophotometer F-4500 (Hitachi). SRPK2 emission spectra were acquired at 20°C using 1 µM of protein dissolved in 25 mM Tris-HCl (pH 7.5) buffer, 100 mM NaCl, 1 mM EDTA and 1 mM β-mercaptoethanol in a 1.0 x 0.2 cm quartz cuvette. Tryptophan residues were excited at 295 nm, and the fluorescence emission was collected from 300 nm to 420 nm. SRPK2 spectra were analyzed by means of the maximum fluorescence wavelength (λ_{max}) and the spectral center of mass ($<\lambda>$) following the equation $<\lambda>=(\Sigma\lambda_i F_i)/(\Sigma F_i)$, where λ_i is the fluorescence wavelength and F_i is the fluorescence intensity at a given wavelength.

SRPK2 at 1 µM was titrated with SRPIN340 or the ATP analog adenosine 5'-(beta, gamma-imino)triphosphate (AMPPNP). All spectra were corrected by inner filter effects due to ligand absorption, and the dissociation constant (K_D) for the SRPK2-SRPIN340 interaction was calculated as described previously (Silva et al., 2013).

2.3.10 Computational Analyses

Atomic charges and optimal geometry of the tridimensional structure of SRPIN340 were calculated by DFT quantum calculations at the B3LYP/6-31G* level using the CHELPG method (Breneman and Wiberg, 1990). All calculations were carried out in GAMESS software (Schmidt

et al., 1993). Then, quantum charges were implemented to the topology generated by the PRODRG server (Schüttelkopf and Van Aalten, 2004). All SRPK2 structures found in the Protein Data Bank (PDB; www.pdb.org) repository are truncated forms lacking the spacer insert domain (SID), amino acids A236-R507. Structure PDB ID 2X7G was solved based on a SRPK2 recombinant version presenting the segments A236-P256 and A508-D510, generating a SID-like loop. Because this 2X7G crystal structure lacks some coordinates of SID-like loop atoms, they were modeled using the Swiss Model server. The obtained model SRPK2-SID-like loop comprising the amino acids A236-P256 and A508-D510 was then used as a target for SRPIN340 docking. For simplification, "SRPK2-SID-like loop structure" is herein named "SRPK2 structure". Docking assays were carried out inside of the SRPK2 ATP binding pocket, as previously identified for SRPK1 (Ngo et al., 2008). Fifty poses of SRPIN340 bound to SRPK2 were generated using the software Auto Dock 4.2.5.1, exploring the conformational space of the ligand through a genetic algorithm while the target protein was considered a rigid body (Morris et al., 2009). Poses were ranked according to the lowest energy and best interaction network using the Auto Dock 4 scoring function (Huey et al., 2007).

Molecular dynamics simulations were carried out on the SRPIN340/SRPK2 complexes using the GROMACS 4.5.5 software package (Pronk et al., 2013). First, SRPK2 topology was built using the Gromos53a6 force field (Oostenbrink et al., 2004). A single point charge extended (SPC/E) water model was used to fill up a cubic water box built around previously generated SRPIN340/SPRK2 complexes. Moreover, amounts of Na^+ and Cl^- corresponding to a concentration of 0.15 M were added to the system to neutralize protein net charges and mimic the cellular environment. After a careful minimization protocol, equilibration protocols were applied to ensure a proper thermodynamic description of the system. The system was equilibrated for 4 ns using *NVT assemble* (constant number of moles, volume and temperature) and *NPT assemble* (constant number of moles, pressure and temperature), consecutively. Additionally, restraint forces (Fc = 1000 kcal/mol.nm²) were used for all non-hydrogen atoms to reach a temperature stabilization of 298 K and pressure stabilization of 1 bar. Afterwards, a non-restrained production phase of molecular dynamics was performed using an integration step of 2 fs by the leap-frog algorithm for a trajectory of 400 ns. A cut-off of 10 Å was adopted to calculate long-range interactions. Simulations were performed in a cluster *Silicon Graphics International* (SGI Inc.).

2.3.11 Statistical analysis

All numeric data were derived from at least three independent experiments and are shown as means ± standard deviation. Analyses were performed using Microsoft Excel

(Microsoft Office Software), GraphPad Prism (GraphPad Software Inc.) and ImageJ. Statistical analyses were done by paired Student's T tests. *P <0.05 or **P <0.01 was considered significant.

2.4 Results

2.4.1 Expression of SRPK1 and SRPK2 in leukemia cells

To expand previous findings (Jang et al., 2008) and gain further information about the relative proportion between SRPK1 and SRPK2 expression among the leukemia cells used in this work, we evaluated the expression of SRPK1 and SRPK2 in a panel of leukemia cell lineages from different origins and genetic backgrounds.

Whereas no large differences in SRPK1 protein expression among the lineages were observed, at the protein level (**Figure 9A**), SRPK2 presented a distinct elevated expression in lineages of lymphoid origin, such as Molt4, TALL, Jurkat (ALL-T) and RS4 (ALL-B). Additionally, Molt4, TALL, Jurkat and RS4 cells presented a higher SRPK2 protein expression compared to SRPK1. Further RT-qPCR experiments revealed that among the nine lineages studied, only Molt4 and Jurkat presented correlations between mRNA and protein levels, indicating that additional layers of complexity involving the gene expression control of these kinases might exist in these cells, which deserves additional investigation in future studies (**Figure 9B**). We also used human PBMC as a control for non-transformed cells in Western blotting and RT-qPCR experiments. However, SRPK1 and SRPK2 were barely expressed (Supplementary Figure 1) or were even undetected in these assays (**Figure 9A**).

Taken together, these results demonstrate that the expression of SRPK1 and SRPK2 are proportionally distinct among the leukemia cells analyzed. Moreover, a clear correlation between mRNA and protein levels could not be found, reflecting the genetic diversity of these cells and possibly their outcomes during drug treatments.

2.4.2 Effect of SRPK pharmacological inhibition on leukemia cell viability and death

The emerging relevance of SRPKs as targets for pharmacological intervention has motivated the identification of the inhibitor SRPIN340 (SR Protein Inhibitor 340) and, more recently, its derivative SPHINX (SR Protein Inhibitor X). These compounds seem to possess equivalent biological properties in terms of potency, inhibition of SR protein phosphorylation, reduction in the expression of pro-angiogenic VEGF, and suppression of choroidal neovascularization (Gammons et al., 2013). Because SRPIN340 activity has been extensively characterized and used in different studies to date, it was chosen as a prototype for pharmacological intervention in leukemia cells here.

The cytotoxic potential of SRPIN340 was evaluated against CML, AML, ALL-B and ALL-T cell lineages. All evaluated cell lines were sensitive to the treatments, indicating that SRPK inhibition indeed yields an overall antileukemia effect *in vitro* (**Figure 10A**). Half-maximal inhibitory concentration values (IC_{50}) (**Table 1**) were determined and revealed that, in general, myeloid leukemias were more sensitive than lymphoid ones. In this case, the AML HL60 was the most sensitive (IC_{50} of 44.7 µM) compared with ALL-T Molt4 and Jurkat (IC_{50} values of 92.2 µM and 82.3 µM, respectively). Moreover, although an accurate IC_{50} value could not be determined at higher compound concentrations, PBMC seemed to be less sensitive to SRPIN340 than the leukemia lineages evaluated. This suggests that SRPK pharmacological inhibition can selectively affect tumor cell survival.

Furthermore, Annexin V/PI staining assays were performed to evaluate whether the effect of SRPIN340 treatment impacts Jurkat apoptosis. After 6 h of drug exposure, the cell population in the initial events of apoptosis (Annexin V positive) was approximately twice as high as the control group treated with DMSO for 12 h (values ranged from 1.6 to 4.5%) (**Figure 10B**). Increasing exposure time to the compound resulted in raising the PI/Annexin V positive cells, indicating the occurrence of later events of apoptosis (**Figure 10B**). Therefore, SRPIN340 can trigger early and later events of apoptosis in leukemia cells.

2.4.3 Impact on SRPK cellular activity

In the following experiments, we attempted to confirm whether SRPIN340 treatment affects cellular pathways targeted by SRPKs. As was previously reported, the expression or splicing pattern of transcripts encoding for MAP2K1, MAP2K2, VEGF and FAS are influenced by SR proteins or SRPK activity (Amin et al., 2011; Clery et al., 2013; Hayes et al., 2007). We observed that both MAP2K transcripts had their expression impaired during SRPIN340 treatment (**Figure 11**). These effects were more pronounced for MAP2K1, which had its expression reduced mainly at a prolonged incubation time. Additionally, we observed a reduction in the pro-angiogenic $VEGF_{165}$ isoform and an increase in the pro-apoptotic FAS isoform expression during the treatments. Although we could not detect clear changes in splicing in leukemias, SRPIN340 changed the splicing of MAP2K1 in HeLa cells (Supplementary Figure 2), suggesting that different cancer lineages may respond differently to SRPK inhibition.

The SR protein phosphorylation status was also investigated using a monoclonal antibody able to detect different phospho-SR protein epitopes (Kim et al., 2014; Zahler et al., 1992). As expected, the SR protein phospho-epitope signal decreased during treatments of both the HL60 and Jurkat lineages (**Figure 12**).

Overall, these results confirm that the observed decrease in leukemia cell viability upon SRPIN340 treatment is related to an effect on pathways targeted by SRPK activity.

2.4.4 Insights on SRPIN340-SRPK complexes

Once we observed the pharmacological effect of SRPIN340 in leukemia cells, we sought to investigate possible molecular interactions underlying its binding to SRPKs. While high-resolution crystallographic structures of the complex SRPIN340/SRPKs have not been solved to date, computational approaches were used to infer possible binding sites into SRPK structures currently available in PDB. A comparison of amino acid sequences revealed that both kinases are highly similar in their kinase domains (Wang et al., 1998) (Supplementary Figure 3), explaining why SRPIN340 can inhibit both SRPK1 and SRPK2 (Fukuhara et al., 2006). Considering this structural similarity, the position of the ATP analog, previously co-crystallized with SRPK1 (Ngo et al., 2008), allowed the prediction of its binding site into SRPK2 (**Figure 13A**), the paralog chosen to be studied herein, because its mechanisms in leukemia tumorigenesis have been previously well determined (Jang et al., 2008).

Because SRPIN340 behaves as an ATP competitive inhibitor (Fukuhara et al., 2006), docking assays were carried out inside the ATP binding pocket. To take into account protein flexibility and eventual induced fit effects, SRPIN340/SRPK2 complexes corresponding to the best two poses obtained by docking procedures, namely "pose A" and "pose B", were selected and used as inputs for molecular dynamics simulations. RMSD calculations demonstrated that both systems reached stability after 200 ns of simulation (data not shown). In both complexes, the SRPIN340 molecules displayed stable conformations inside the SRPK2 catalytic pocket after 200 ns, maintaining the same network interactions throughout the additional 200 ns. The space occupied by SRPIN340 on pose A and B throughout simulation is shown as a blue and green area, respectively (**Figure 13A**).

Interestingly, the ATP analog docked into ATP binding site (orange sticks) clearly shows higher superposition to the blue region occupied by SRPIN340 during the molecular dynamics of "pose A", which then seems to better explain the mechanism of competitive inhibition. In this sense, SRPIN340 at "pose A" is additionally stabilized by T-shaped and sandwich pi-stacking interactions with W89 during the last 200 ns (**Figure 13B**). The simulations also show residues L87, W89, V95, A108, F166, L169, Y228, A529 and P247 acting together to form a network of hydrophobic interactions with SRPIN340. These contacts on the SRPK2/SRPIN340 complex were measured throughout the trajectory in the last 200 ns (**Table 2**). The most prominent biding groups, with low distance standard deviations, were a benzene ring, CF_3 and a pyridine ring, either in pose A or B.

Furthermore, a solvent accessible surface area (SASA) analysis revealed more exposure to polar solvents of tryptophan amino acid residues in structures of "pose A" by approximately 100 $Å^2$ (**Figure 13C**). This finding might have interesting implications if considered together with the following intrinsic tryptophan fluorescence analysis confirmation (see below).

Together, these data can yield important information for the rational design of novel derivatives with increased potency and pharmacological potential.

2.4.5 Intrinsic tryptophan fluorescence studies

To further understand the structural aspects of SRPK inhibition by SRPIN340, fluorescence spectroscopy experiments using tryptophan residues as probes were carried out. The SRPK2 fluorescence spectrum at a λ_{max} of 340 ± 1 nm and a <λ> of 347.1 ± 0.6 nm, indicates that, on average, the SRPK2 W residues are partially exposed to the polar solvent (**Figure 14A**). For a control, the effect of DMSO (vehicle) on the tertiary structure was also evaluated. Concentrations up to 5% of DMSO did not affect the overall SRPK2 W emission spectrum, assuring that all observed effects are due to the presence of SRPIN340 in solution (**Figure 14A**).

The titration of SRPK2 with SRPIN340 resulted in a clear intrinsic fluorescence suppression (**Figure 14B**), as well as in a slight redshift in the λ_{max} and <λ> equal to 342 ± 1.0 nm and 351 ± 0.6 nm, respectively, at 15 µM SRPIN340 (**Figure 14B**). These results indicate an increase in W residues exposed to the solvent, suggesting that SRPK2 undergoes conformational changes in the presence of SRPIN340 (see also **Figure 13C**). The titration data additionally allowed the calculation of the dissociation constant (K_D) for the SRPK2/SRPIN340 interaction equal to 1.6 ± 0.3 µM (**Figure 14C**). Furthermore, tryptophan fluorescence analysis upon ATP analogue addition revealed no significant effects on the SRPK2 structure, even at higher ligand concentrations (**Figure 14D**). These data suggest that, compared to ATP, SRPIN340 may undergo different binding modes or access a different interaction network at the SRPK ATP binding pocket, but still act as its inhibitor, which agrees with the computational analyses performed (**Figure 13**).

2.5 Discussion

Dysregulation of SR protein phosphorylation by SRPKs has been shown to play a key role in cancer (Zhou and Fu, 2013). In leukemia cells, SRPK2 overexpression leads to hyperphosphorylation of the splicing factor acinus, which in turn is responsible for increasing the transcription level of cyclin A1 and affecting cell proliferation (Jang et al., 2008). SRPK1 and SRPK2 have also been observed to be overexpressed in various other human cancers, including pancreatic, breast, colon, lung and ovarian (Gout et al., 2012; Hayes et al., 2007, 2006; Odunsi

et al., 2012). SRPK-altered expression impacts the overall pre-mRNA normal splicing and gene expression program, allowing cancer cells to increase their proliferation, invasiveness, angiogenic potential and apoptosis escape (Jang et al., 2008; Naro and Sette, 2013). Moreover, high SRPK levels have also been co-related to tumor grade and resistance to chemotherapy (Hayes et al., 2007, 2006; Odunsi et al., 2012). Thus, much accumulated data points to the fact that SRPKs are functionally relevant for tumor cells, revealing that they can serve as a target for pharmacological intervention.

In previous immunoblotting analyses, high levels of SRPK2 have been found in leukemic bone marrows samples (n = 5), but SRPK2 is undetectable in normal bone marrow counterparts (Jang et al., 2008). To find additional information on SRPK expression in leukemia, we analyzed the protein and mRNA levels of SRPK1 and SRPK2 in different leukemia cell lineages herein (**Figure 9**). Both kinases were found with elevated expression in all cell lines evaluated, but none of them could be detected at significant levels in the PBMCs by Western blotting or RT-qPCR (**Figure 9** and Supplementary Figure 1). These data are in agreement with previous studies reporting that SRPK1 and SRPK2 are overexpressed in primary bone marrow leukemia samples in comparison with healthy ones (Hishizawa et al., 2005; Jang et al., 2008; Salesse et al., 2004).

Additionally, considering protein levels, the proportions of SRPK1 and SRPK2 were different among the lineages studied, reflecting the existence of different regulatory mechanisms operating in these cells to yield altered SRPK1 and SRPK2 expression. It is important to notice that the SRPK2 protein expression was higher than that of SRPK1 in the lineages ALL-T (Molt4, TALL and Jurkat) and ALL-B (RS4) (**Figure 9A**). This difference is intriguing and certainly would impact therapies based on compounds presenting specificity for SRPK1 or SRPK2. Therefore, these gene expression data, along with others previously reported (Hishizawa et al., 2005; Jang et al., 2008; Salesse et al., 2004), reinforce the fact that the therapeutic potential of SRPK inhibition should be considered against hematological malignances.

Based on these accumulated SRPK1 and SRPK2 gene expression data, we aimed to investigate the cytotoxic effect of the SRPK inhibitor SRPIN340 on leukemia cells (Fukuhara et al., 2006). This substance has been previously shown to be selective for SRPK1 and SRPK2 because no relevant inhibitory activity was observed against a panel of more than 140 kinases, including Cdc-like kinase family members (Clks) that are also involved in SR protein phosphorylation and regulation (Fukuhara et al., 2006). Although SRPIN340 was first described as an antiviral agent (Anwar et al., 2011; Fukuhara et al., 2006; Karakama et al., 2010), its pharmacological activity has also been evaluated in other studies. For instance, it was able to prevent neovascularization in a rodent model of choroidal retinopathy of prematurity (Oltean et al., 2012). In addition, this compound exhibits antiangiogenic and anti-melanoma effects both

in vitro and *in vivo* (Gammons et al., 2014). In the present investigation, SRPIN340 was shown to reduce cell viability of myeloid and lymphoid leukemias *in vitro* (**Figure 10** and **Table 1**). This effect seemed to be selective, as lower cytotoxicity was observed in PBMC treatments. This finding is in agreement with the low apparent toxic effect observed when SRPIN340 was evaluated in *in vivo* studies (Fukuhara et al., 2006).

Furthermore, Annexin V staining cell death assays showed that SRPIN340 cytotoxicity involves the triggering of early and late apoptosis, corroborating previous studies that have shown increased tumor cell sensitivity to cisplatin and gemcitabine during SRPK knockdown experiments (Hayes et al., 2007, 2006). Interestingly, the Jurkat and Molt4 lineages seemed more resistant to SRPIN340 treatment (**Table 1**). This finding might be due to the comparatively higher SRPK2 protein expression in these cells (**Figure 9A**). It is well known that SRPIN340 has a higher inhibitory activity over SRPK1 compared to SRPK2 (Fukuhara et al., 2006), implying that this compound would be less effective against tumor cells with higher SRPK2 expression.

Because the SR protein phosphorylation status was reduced during treatments, the SRPIN340 effect on leukemia cells seemed to be associated with SRPK inhibition (**Figure 12**). It is also interesting to notice that the effect on SR protein phosphorylation in HL60 seemed to be more effective than in Jurkat, which might be again explained by the differences in the proportion of SRPK1/SRPK2 in these cells.

Additionally, we observed in RT-PCR assays that SRPIN340 treatment impaired the expression of MAP2K1 and MAP2K2, both responsible for activating the MAPK3 and MAPK1 pathways (Hayes et al., 2007). The treatments led to a reduced expression principally of MAP2K1, in which decreased levels were also accompanied by a decreased expression of possible smaller variants (**Figure 11**). In contrast, when we treated HeLa cells with SRPIN340, a smaller splicing variant of MAP2K1 was expressed, indicating that the compound can favor spliced isoforms with less tumorigenic potential (Supplementary Figure 2). However, the same effect on splicing could not be observed for MAP2K2, VEGF or FAS in leukemia or HeLa cells, suggesting that different tumor lineages may respond differently to SRPK inhibition. When similar analyses were performed with breast, colonic, and pancreatic carcinoma lineages, the SRPK1 knockdown impacted the expression of MAP2K2 instead of MAP2K1 (Hayes et al., 2007), providing additional evidence for this different response according to each cell line. Regardless, the impaired gene expression observed in our assays indicates that cell survival pathways involving MAPK3, MAPK1 and Akt are affected by SRPIN340 treatment.

SRPIN340 reduced the expression of pro-angiogenic isoform $VEGF_{165}$ in all leukemia cell lines evaluated, mainly after 18 h of treatment. At the same time, pro-apoptotic FAS expression was induced (**Figure 11**). These data give more support, as previously described, that SRPK

inhibition may be related to triggering apoptosis (Hayes et al., 2007; Hong et al., 2011). Additionally, recent studies have shown that SRPK1 targeting is a reasonable strategy for cancer treatment due to the inhibition of angiogenesis (Amin et al., 2011; Gammons et al., 2014). Thus, the key role played by SRPKs in regulating cellular death or proliferation offers novel opportunities to develop antileukemia therapies.

The *in vivo* anti-melanoma effect of SRPIN340 has been recently demonstrated (Gammons et al., 2014). This effect was shown to be mediated by antiangiogenic activity and required dairy SRPIN340 administrations to the tumor locally due to the low pharmacological capacity of SRPIN340. This finding indicates that novel compounds with increased drug-like properties should be searched for in future studies. In recent years, a number of anticancer agents that reached clinical use were developed through 'target-based' approaches, mostly involving the knowledge of structural aspects of ligand-target interactions (Knight et al., 2010). Following this rationale, the possible interaction contacts between SRPIN340 and SRPK2 evaluated herein create a path to develop novel inhibitors with higher affinities and increased drug-like characteristics (Gammons et al., 2014).

Molecular dynamics simulation analyses revealed a high stability of the SRPK2/SRPIN340 complex, reinforcing the robustness of the docking assays that were performed (**Figure 13**). W exposure to the polar solvent across the trajectories analyzed was readily detected and indicates that the ligand binding induced conformational changes in the kinase structure. According to this finding, further intrinsic W fluorescence assays revealed that SRPIN340 caused a slight redshift and induced W fluorescence suppression in the SRPK2 spectrum (**Figure 14**). These observations may be explained by the exposure of W residues to the polar solvent or even by the formation of pi-stacking interactions observed between SRPIN340 and W89 in the molecular dynamics simulation of pose A, confirming that overall conformational changes occur upon SRPIN340 binding (**Figure 13B** and **C**).

SRPIN340 titration in the fluorescence assays also allowed estimation of the K_D value for the SRPK2/SRPIN340 complex at 1.6 ± 0.3 µM. Previous studies with the yeast SRPK homologue Sky1p revealed K_D values for the ATP analogue and ATP equal to 650 µM and 2000 µM, respectively (Aubol et al., 2003). Considering these values, SRPIN340 binding seems to occur with higher affinity than would be expected for adenine nucleotides. Although comparisons between these data should be made carefully, the huge differences in these values might indicate that the ATP-competitive SRPIN340 indeed accesses different interacting groups at the ATP binding pocket because they were obtained using different experimental methodologies.

The possible binding modes analyzed here presented different interactions made by SRPIN340. They were classified by their distances' standard deviations (**Table 2**) as good (SD <

0.5 Å), medium (0.5 Å < SD < 1.0 Å) and long (SD > 1 Å). For pose A, contacts on the benzenic ring (A108), CF_3 (P247) and the pyridine ring (W89) groups were more stable, corroborating the hypothesis of hydrophobic forces playing a critical role in SRPIN340 binding. In addition, interactions A108 and F166 with the piperidine ring and interactions L87 and V95 with the benzenic ring created a suitable environment for SRPIN340 accommodation. Together, these interactions led to a binding mode of a type I kinase inhibitor. However, these contacts can be further improved, along with the ones with higher deviations, to design more suitable SRPK inhibitors. Although all structural analyses were performed considering SRPK2, interpretations may also be applied to SRPK1, considering the high similarity in their kinase domains (Giannakouros et al., 2011; Wang et al., 1998) (Supplementary Figure 3). Additionally, SPHINX appears to be equivalent to SRPIN340 in terms of chemical properties and *in vitro* and *in vivo* activities (Gammons et al., 2013; Mavrou et al., 2015), and the structural information obtained here may therefore complement the biological and biochemical data already available in the literature for both compounds. Considered together, all of this information will certainly sustain efforts to pursue next-generation SRPK inhibitors.

In conclusion, SRPKs were found overexpressed in myeloid and lymphoid leukemia. The SRPK inhibitor SRPIN340 presented a selective cytotoxic effect against leukemia cell lines. This effect was accompanied by the triggering of apoptosis, and it was due to intracellular SRPK activity impairment. Finally, the structural insights obtained should favor the design of SRPK inhibitors with increased potency and drug-like properties.

Conflict of interest

The authors declare that it does not exist any conflict of interest.

Acknowledgments

The authors thank the Núcleo de Microscopia e Microanálise and Divisão de Suporte ao Desenvolvimento Científico e Tecnológico, Universidade Federal de Viçosa-UFV, for the available facilities and technical assistance with flow cytometry and computational cluster access, respectively. This work was supported by the Conselho Nacional de Desenvolvimento Científico e Tecnológico (CNPq; grant 485011/2012-3), Fundação de Amparo à Pesquisa do Estado de Minas Gerais (FAPEMIG; grant CBB-APQ-01637-13), Coordenação de Aperfeiçoamento de Pessoal de Nível Superior (CAPES; grant CAPES/CNPq 552459/2011-9), and Fundação Arthur Bernardes (FUNARBE/FUNARPEX). The funders had no involvement in the study design, in the collection, analysis or interpretation of data, in the writing of the report, or in the decision to

submit the article for publication. The authors also thank CNPq, FAPEMIG, CAPES and FUNARBE for the fellowships to students and researchers involved in this work.

2.6 Figures

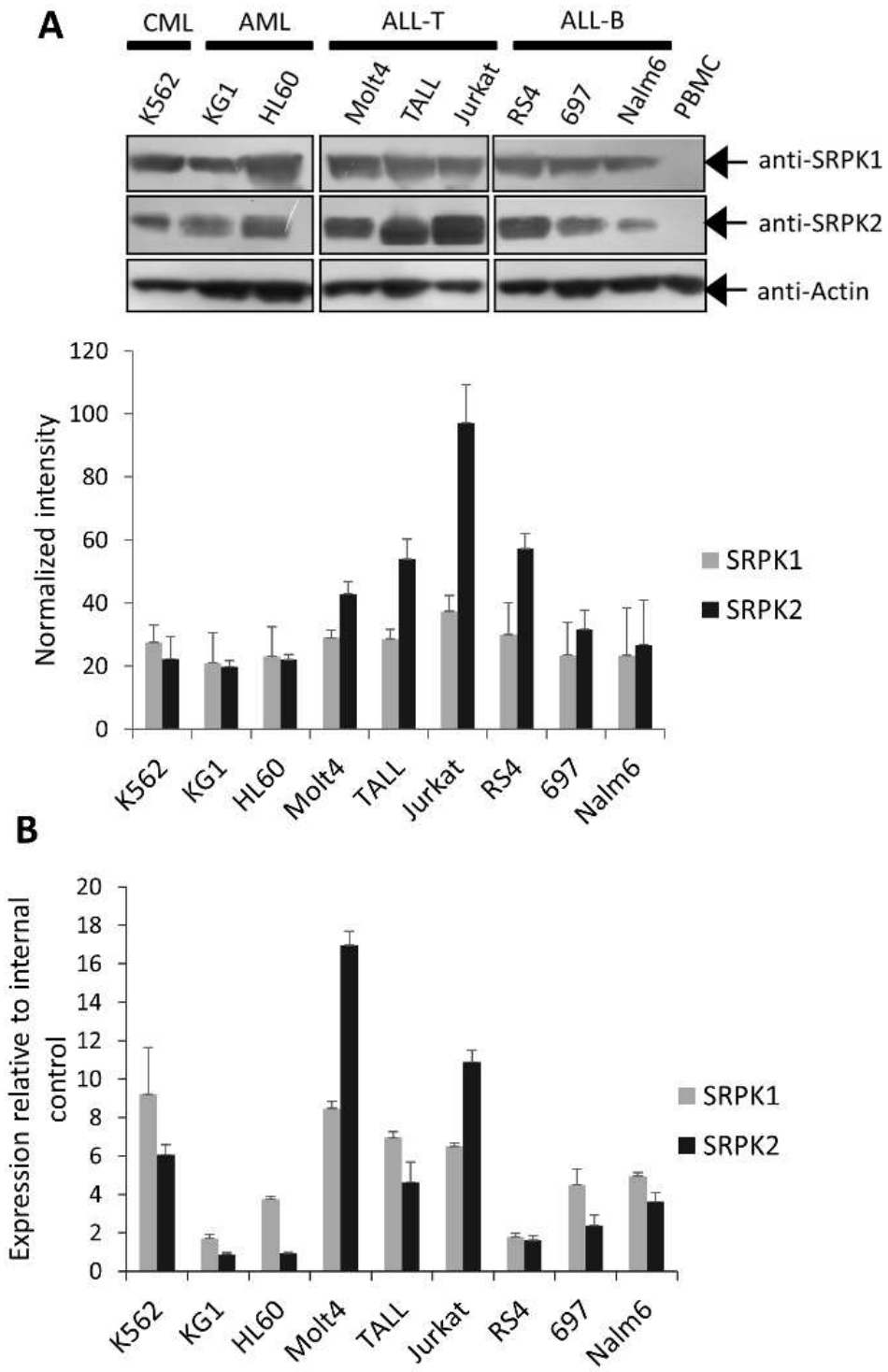

Figure 9: Analysis of SRPK1 and SRPK2 expression in leukemia cell lines. The expression of SRPK1 and SRPK2 were analyzed by (A) Western blotting and (B) RT-qPCR assays in different leukemia cell lines derived from chronic myelogenous leukemia (CML), acute myelogenous leukemia (AML), T-cell acute lymphoblastic leukemia (ALL-T), and B-cell acute lymphoblastic leukemia (ALL-B). (A) The histogram (below) represents the ratio of the band intensities of SRPK1

and SRPK2 normalized to the actin signal for each lineage. Densitometry analysis of the band intensity was performed using ImageJ software. Error bars represent means ± standard deviation from triplicate experiments. Because SRPK1 or SRPK2 signals in the PBMC samples could not be detected during the WB assays, even when higher amounts of material were used (data not shown), they were not considered for the densitometry analysis. Although we found that actin expression varied between leukemia cells and our PBMC samples (Supplementary Figure 1), actin was detected here to qualitatively control the presence of protein material. (B) Expression of SRPK1 and SRPK2 transcripts by relative quantification. Amplification of beta-2-microglobulin mRNA (B2M) was used as an endogenous control. B2M was equally expressed among all of the leukemia lineages evaluated (Supplementary Figure 1 and data not shown). SRPK1 and SRPK2 mRNA quantification in PBMC are discussed in Supplementary Figure 1. All primers used are detailed in Supplementary Table 1. The RT-PCR experiments were performed by Germanna Lima Riguetto.

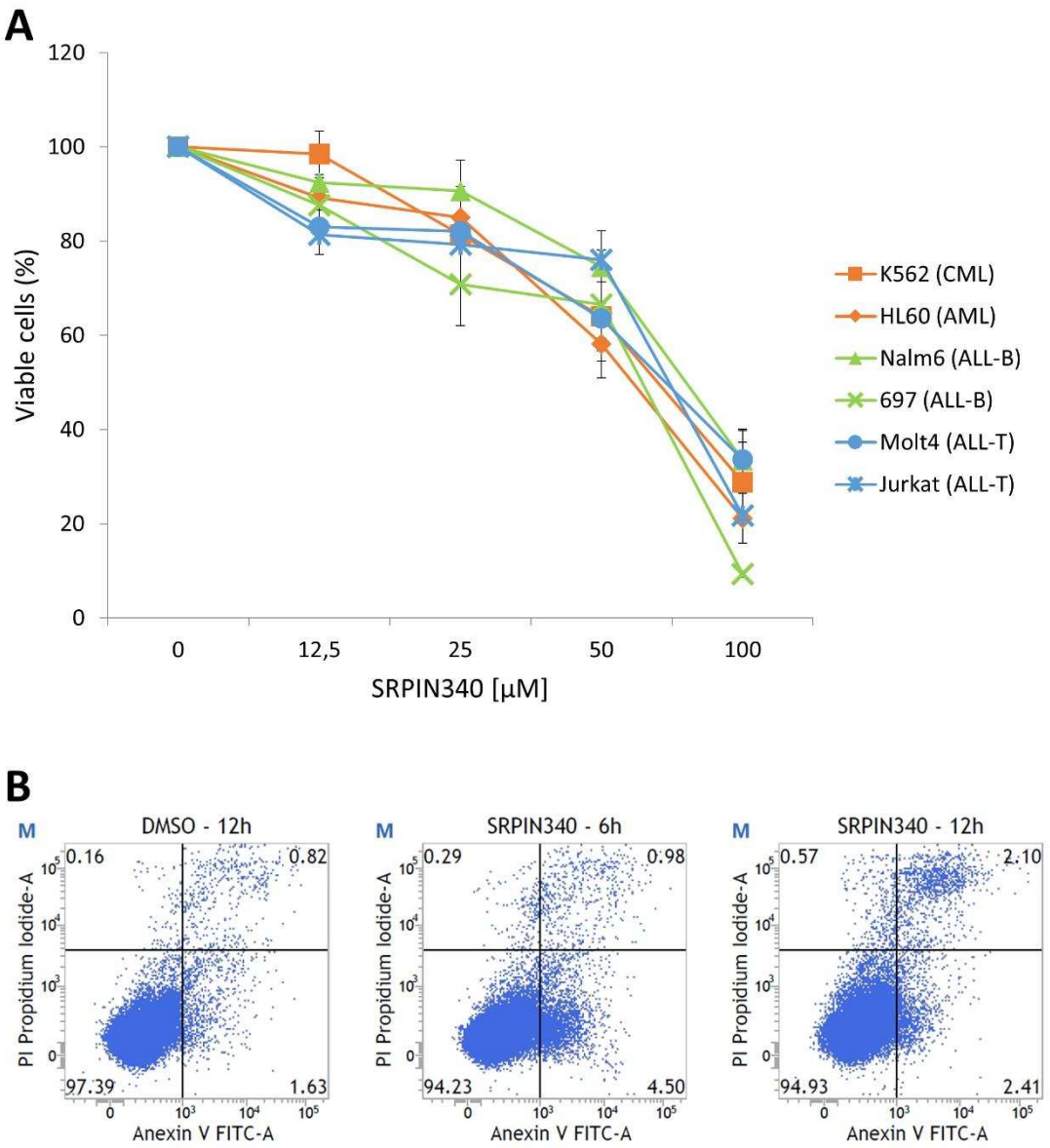

Figure 10: The effect of SRPIN340 treatment on leukemia cell viability and death. Different leukemia cell lines (A) were treated with increasing concentrations (0 – 100 µM) of SRPIN340 for 48 h. Cell viability was determined using the MTT assay. We considered the viability of 100% of the cells in the control treatment (vehicle). The percentage of inhibition was calculated relative to cells treated with the vehicle. The values are expressed as the means ± standard deviation of three independent experiments. To assess cell death (B), Jurkat cells were treated with 25 µM of SRPIN340 for 6 or 12 h. Cells treated with the vehicle were used as controls. Subsequently, the cell death was evaluated using annexin V-FITC (V) and PI (P) labels. One representative experiment of three is shown.

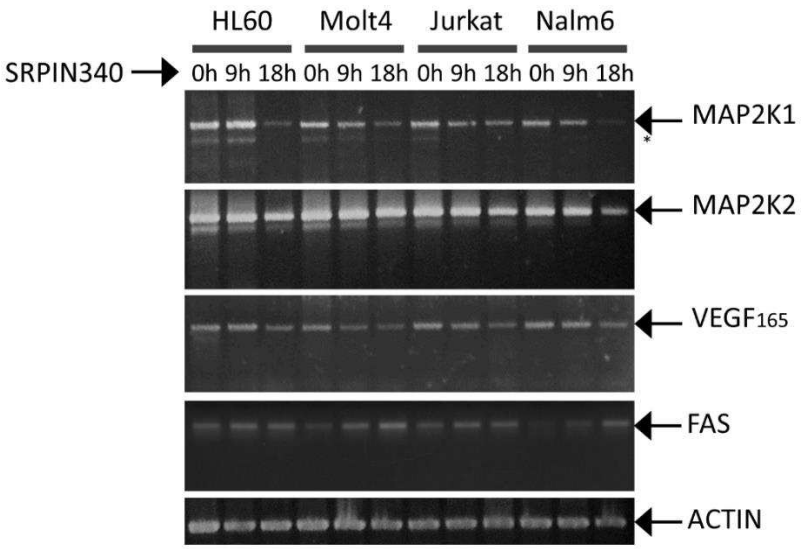

Figure 11: Effect of SRPIN340 treatment on MAP2K1, MAP2K2, VEGF and FAS expression in leukemia cells. cDNAs were derived from HL60, Jurkat, Molt4 and Nalm6 cells treated with SRPIN340 (100 µM) for different amounts of time (0, 9 and 18 h). One representative experiment of three is shown. (*) represent possible isoforms as previously described (Hayes et al., 2007).

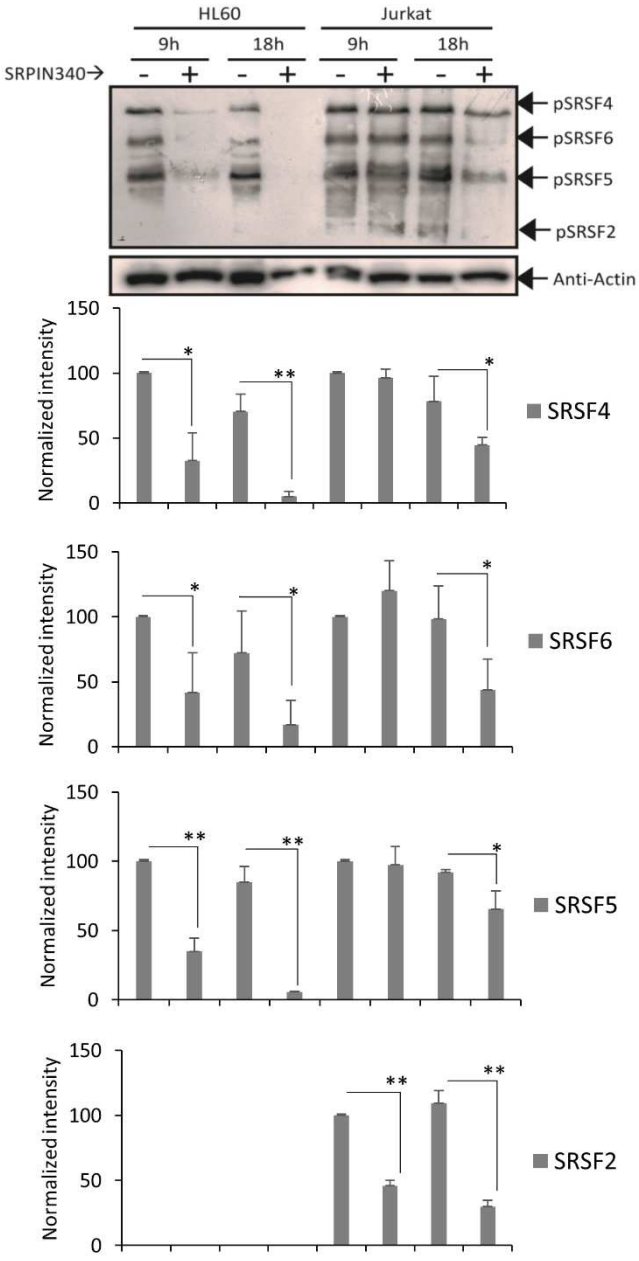

Figure 12: Effect of SRPIN340 treatment on SR protein phosphorylation. Western blotting analysis after treatment with SRPIN340 (100 µM) or negative control (vehicle) for 9 or 18 h. SR protein phosphorylation was detected using mAb1H4, which recognizes phosphorylated serine-arginine epitopes common to multiple SR factors. The blot was re-probed with actin and used as an endogenous control. Graphics (below) represent the percentage of the SR proteins' band intensity normalized to the actin signal for each HL60 and Jurkat negative control. Densitometry analysis was performed using ImageJ software. Error bars represent the means ± standard deviation from triplicate experiments. T tests, *P < 0.05, **P < 0.01.

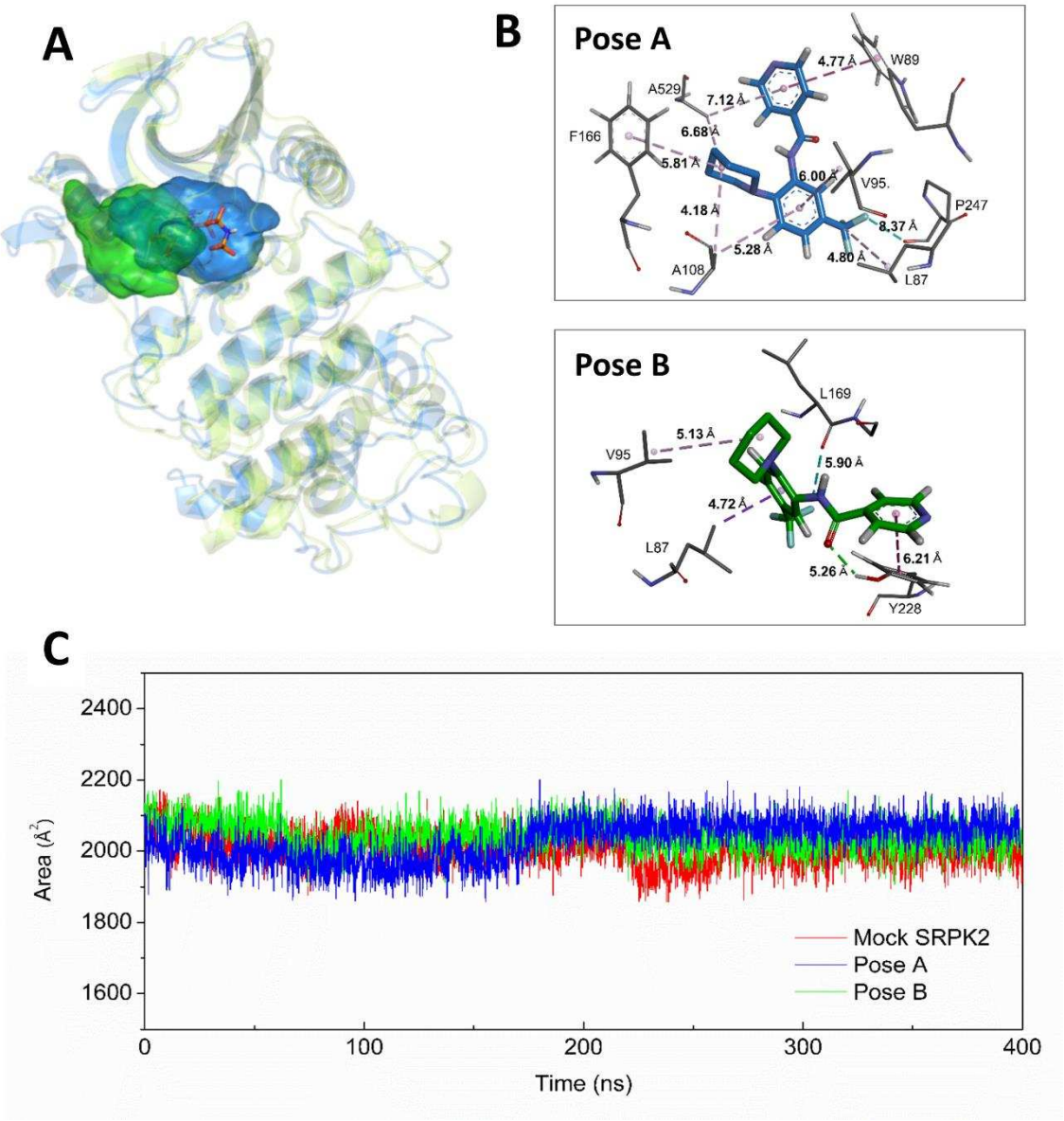

Figure 13: Molecular Dynamic Analysis. (A) Occupied space of SRPIN340 during simulations from poses A (blue) and B (green). Average protein structures are shown superposed in light blue for simulation A and in light green for simulation B. The ATP analogue ANP (shown in orange sticks) occupies the same region as SRPIN340 during both simulations. (B) Snapshot from pose A (upper) and pose B (bottom) simulations highlighting the possible SRPIN340 (orange sticks) interaction network. (C) Solvent accessible surface area (SASA) for tryptophan residues in the presence of the ligand, blue and green for poses A and B, respectively. The pose A simulation shows a signal increase at 175 ns, indicating a major exposure of residues to the polar solvent from this point of simulation. This is in agreement with the fluorescence spectroscopy analysis shown in **Figure 14**. The molecular dynamic and docking analysis were performed by Marcelo Depólo Polêto.

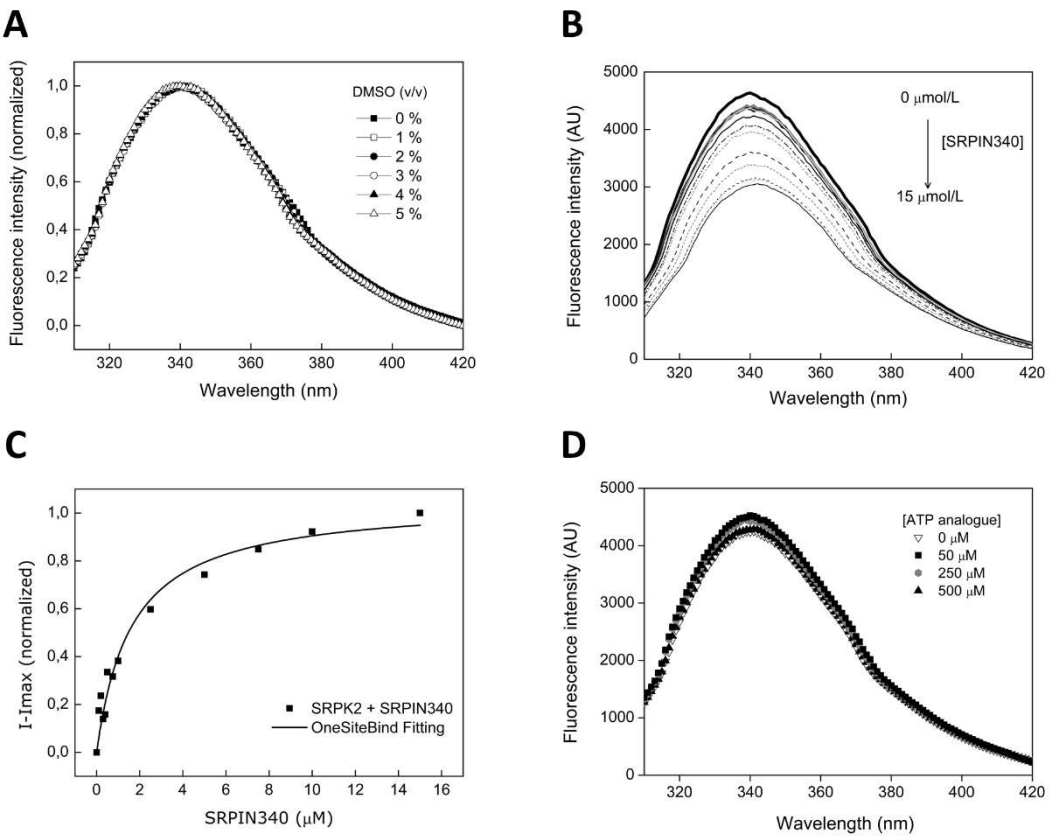

Figure 14: SRPK2/SRPIN340 interaction studied by fluorescence spectroscopy. (A) DMSO titration (0 – 5% v/v) of SRPK2 spectra showing no significant changes in the local tertiary structure of the W residues. (B) Fluorescence spectra of the SRPK2 titration with increasing concentrations (0 – 15 µM) of SRPIN340. (C) Data analysis of the spectra shown in (B) and SPRK2/SRPIN340 dissociation constant (K_D) determination. The K_D found for this interaction was 1.6 ± 0.3 µM. (D) SRPK2 (1 µM) fluorescence spectra upon addition of several concentrations of ATP analogue. The fluorescence spectroscopy analysis were performed by Éverton de Almeida Alves Barbosa.

2.7 Tables

Table 1: Half-maximal inhibitory concentration (IC_{50}) values for SRPIN340 treatments. Different leukemia cell lines and peripheral blood mononuclear cells (PBMC) were treated with increasing concentrations (0 – 200 µM) of SRPIN340 for 48 h. Cell viability was determined using the MTT assay. The values are expressed as the means ± standard deviation of three independent experiments.

Cell line	**SRPIN340 IC_{50} [µM]**
K562 (CML)	52.0 ± 0.6
HL60 (AML)	44.7 ± 2.4
Nalm6 (ALL-B)	66.6 ± 2.7
697 (ALL-B)	59.2 ± 0.6
Molt4 (ALL-T)	92.2 ± 15.2
Jurkat (ALL-T)	82.3 ± 1.2
PBMC	>100*

***** The precise IC_{50} value could not be determined due to the low solubility of SRPIN340 at higher concentrations.

Table 2: Average distances of SRPIN340 groups and SRPK2 binding site amino acid side-chains. Distances from the SRPIN340 groups and the amino acid side-chains' centers of mass were measured throughout both simulations. Standard deviation values were considered good for SD < 0.5 Å, medium for 0.5 Å < SD < 1.0 Å and long for SD > 1.0 Å.

Pose A		
	Distance Average (Å)	**Standard Deviation (Å)**
A108: Benzenic ring	5.28	0.39
L87: CF_3	4.80	0.45
W89: Pyridine ring	4.78	0.48
A108: Piperidine ring	4.18	0.53
F166: Piperidine ring	5.81	0.80
L87: Benzenic ring	5.66	0.57
V95: Benzenic ring	6.00	0.62
A529: Piperidine ring	6.68	1.28
A529: Pyridine ring	7.12	1.54
P247: CF_3	8.38	3.93
Pose B		
	Distance Average (Å)	**Standard Deviation (Å)**
L87: Benzenic ring	4.72	0.45
V95: Piperidine ring	5.13	0.38
Y228: N-cyclohexane	6.21	0.69
L169: CF_3	5.90	1.63
Y228: O-amide	5.26	1.77

Chapter 3: Research Article II

3. Research Article II

Trifluoromethyl Arylamides with Antileukemia Effect and Intracellular Inhibitory Activity Over Serine/arginine-rich Protein Kinases (SRPKs)

Raoni Pais Siqueira[1], Marcus Vinícius de Andrade Barros[2], Éverton de Almeida Alves Barbosa[1], Thiago Souza Onofre[1], Victor Hugo Sousa Gonçalves[1], Higor Sette Pereira[1], Abelardo Silva júnior[3], Leandro Licursi de Oliveira[4], Márcia Rogéria Almeida[1], Juliana Lopes Rangel Fietto[1], Robson Ricardo Teixeira[2] and Gustavo Costa Bressan[1]

[1]Departamento de Bioquímica e Biologia Molecular, Universidade Federal de Viçosa, Viçosa, Minas Gerais, Brasil.
[2]Departamento de Química, Universidade Federal de Viçosa, Viçosa, Minas Gerais, Brasil.
[3]Departamento de Veterinária, Universidade Federal de Viçosa, Viçosa, Minas Gerais, Brasil.
[4]Departamento de Biologia Geral, Universidade Federal de Viçosa, Viçosa, Minas Gerais, Brasil.

European Journal of Medicinal Chemistry, v. 134, p. 97 - 109, 2017

3.1 Abstract

The serine/arginine-rich protein kinases (SRPKs) have frequently been found with altered activity in a number of cancers, suggesting they could serve as potential therapeutic targets in oncology. Here we describe the synthesis of a series of twenty-two trifluoromethyl arylamides based on the known SRPKs inhibitor *N*-(2-(piperidin-1-yl)-5-(trifluoromethyl)phenyl) isonicotinamide (SRPIN340) and the evaluation of their antileukemia effects. Some derivatives presented superior cytotoxic effects against myeloid and lymphoid leukemia cell lines compared to SRPIN340. In particular, compounds **24**, **30**, and **36** presented IC_{50} values ranging between 6.0 – 35.7 μM. In addition, these three compounds were able to trigger apoptosis and autophagy, and to exhibit synergistic effects with the chemotherapeutic agent vincristine. Furthermore, compound **30** was more efficient than SRPIN340 in impairing the intracellular phosphorylation status of SR proteins as well as the expression of MAP2K1, MAP2K2, VEGF, and RON oncogenic isoforms. Therefore, novel compounds with increased intracellular effects against SRPK activity were obtained, contributing to medicinal chemistry efforts towards the development of new anticancer agents.

Keywords

Trifluoromethyl arylamides, SRPK, SRPIN340, serine/arginine-rich protein kinase, leukemia, pre-mRNA splicing.

3.2 Introduction

Serine/arginine-rich protein kinases (SRPKs) are serine-threonine kinases related to the phospho-regulation of serine-arginine proteins (SR proteins), a protein family involved in pre-mRNA splicing control (Giannakouros et al., 2011; Zhou and Fu, 2013). Overexpression of the SRPK1 and SRPK2 family members has been related to tumorigenesis and to poor patient prognosis of many human cancers including leukemia (Jang et al., 2008; Siqueira et al., 2015), colon (Hayes et al., 2007; Wang et al., 2016), pancreatic (Hayes et al., 2007, 2006), melanoma (Gammons et al., 2014), breast (Hayes et al., 2007; Van Roosmalen et al., 2015), prostate (Mavrou et al., 2015), and glioma (Wu et al., 2014). In the intracellular context of cancerous cells, dysregulated SRPKs activity promotes cell proliferation and apoptosis escape (Jang et al., 2008; Lin et al., 2014), suggesting that they are potential targets for the development of new anticancer agents (Da Silva et al., 2015; Lee and Abdel-Wahab, 2016).

SRPKs have also been associated with the infection mechanisms of multiple viruses, including HIV, hepatitis, dengue, and Epstein-Barr virus (Duarte et al., 2013; Fukuhara et al., 2006; Kim and Wu, 2014). Screening for SRPKs inhibitors with antiviral activity, Hagiwara and colleagues identified the isonicotinamide compound *N*-(2-(piperidin-1-yl)-5-(trifluoromethyl)phenyl) isonicotinamide (also called SRPIN340) (**Figure 8**), which is able to selectively inhibit SRPK1 and SRPK2 (Fukuhara et al., 2006).

Since the identification of SRPIN340, different studies have been conducted to evaluate its pharmacological potential in different *in vitro* and *in vivo* disease models, including viral infection (Anwar et al., 2011; Fukuhara et al., 2006; Karakama et al., 2010), angiogenesis (Amin et al., 2011; Oltean et al., 2012), and cancer (Gammons et al., 2014). Within this context, in our previous studies we evaluated the cytotoxic potential of SRPIN340 in a panel of leukemia cells with high expression levels of SRPK1 and SRPK2. This compound was able to reduce cell viability, decrease hyperphosphorylation of SR family members (SRSF2, SRSF4, SRSF5 and SRSF6), and to regulate the expression of genes involved in cell proliferation and survival (MAP2K1, MAP2K2, VEGF and FAS) (Siqueira et al., 2015). Recently, other SRPK inhibitors have also been described. Similar to SRPIN340, they displayed important biological effects (**Figure 8**) (Gammons et al., 2013; Morooka et al., 2015).

Even though these reports have indicated promising results for SRPK pharmacological inhibition in pre-clinical *in vitro* and *in vivo* assays, the search for novel compounds with increased biological efficiency is of potential interest (Gammons et al., 2014). Here we describe the design and synthesis of a series of twenty-two trifluoromethyl arylamides and the assessment of their potential antileukemia effects.

3.3 Results and discussion

3.3.1 Synthesis

Trifluoromethyl arylamide SRPIN340, as well as, compounds **15**-**36** were prepared in three steps. First, commercially available 1-fluoro-2-nitro-4-(trifluoromethyl)benzene (**1**) was treated with amines to obtain derivatives **2**-**7** with yields ranging 81% – 98% (**Scheme 1**).

After that, compounds **2** - **7** were submitted to reduction reactions with $SnCl_2$/HCl producing derivatives **8** - **13** (**Scheme 2**).

Finally, nucleophilic acyl substitution reactions (**Scheme 3, Table 3**), involving amines **8** - **13** and aromatic acyl chlorides, produced SRPIN340 (75% yield) and twenty-two other trifluoromethyl arylamides, compounds named **15 – 36** (30% – 91% yield). All synthesized compounds were fully characterized by infrared (IR) and nuclear magnetic resonance (NMR, ^{1}H and ^{13}C) spectroscopy techniques, as well as, by high resolution mass spectrometry (*vide infra*).

The synthesis of the compounds **15 - 36** was planned so that the influence on the biological activity of different groups attached to position **1** (see **Scheme 3** and **Table 3** for numbering) could be assessed. Thus, amines containing alicyclic, aliphatic and aromatic portions were chosen for the preparation of the compounds. In addition, we also decided to vary the type of aromatic group attached to the carbonyl functionality so that the impact of these modifications on biological activity could also be evaluated. Accordingly, four types of aromatic acyl chlorides were used in the preparation of the compounds **15 - 36**. In order to compare the biological effects of each derivative with SRPIN340, a well known SRPK inhibitor, the latter was also synthesized.

3.3.2 Effect of compounds on cell viability

The cytotoxic activity of the synthesized trifluoromethyl arylamides **15 - 36** and SRPIN340 was evaluated at different concentrations (0 – 200 μM) over HL60, Jurkat, and Nalm6 human leukemic cell lines and the half-maximal inhibitory concentration (IC_{50}) for each compound was determined. As shown in **Table 3**, among the twenty-two trifluoromethyl arylamides synthesized, ten of them were active against at least one of the leukemia cell lines (IC_{50} < 100 μM). The compounds **24**, **30**, and **36** were the most active ones (IC_{50} 14.2 – 35.7 μM, 8.5 – 17.8 μM, and 6.0 – 33.8 μM, respectively) and presented superior cytotoxicity in comparison to the SRPK inhibitor SRPIN340 (IC_{50} 38.3 - 75.4 μM). Although further structure-activity relationship studies should be performed, initial observations suggest that the presence of the aryl bromide group in novel compounds may be associated with their superior activity. These aryl halide groups (including groups with bromide or iodide) have been frequently found in the structures of kinase inhibitors, including the anticancer agents trametinib and vandetanib (Wu et al., 2016).

In order to evaluate if the most active compounds affect non-tumor cells, primary peripheral blood mononuclear cells (PBMC) were obtained and used in cytotoxic assays. As shown in **Figure 15**, PBMC cells were less sensitive to the treatments than the evaluated leukemia lineages (**Table 1**). Although compound **24** slightly reduced the lymphocytes viability at the dosage investigated, overall these compounds seem to be selective to leukemic cells.

3.3.3 Combinatorial effect with Vincristine

We further investigated potential interactions of compounds **24**, **30**, and **36** with vincristine, a component of many multi-drug pediatric and adult cancer chemotherapy, including leukemia (Silverman et al., 2013). For this purpose, Nalm6 was incubated for 48 h with two different doses, in isolation or in combination of compound **24** (8.9 and 17.9 µM), compound **30** (4.3 and 8.5 µM), and compound **36** (1.5 and 3.0 µM) with vincristine (0.5 and 1.0 nM). These doses correspond to 25% and 50% of the IC_{50} value previously obtained for each compound (**Table 3**). After treatments, cell viability was measured and the combination index (CI) for each drug combination was calculated using the Chou-Talalay method (Chou, 2010). According to this method, CI values significantly lower than 1.0 (CI < 1.0) indicate synergistic effect whereas values close to 1.0 indicate additive effect. Synergistic effects were observed for combinations containing lower concentrations of the compounds **24**, **30**, and **36** (i.e., 25% of the IC_{50}) as the calculated CI values were 0.57, 0.45, and 0.56, respectively (**Figure 16**). Moreover, combinations performed in concentrations corresponding to 50% of the IC_{50} indicated synergism for compound **30** (CI = 0.78) but additive effect for compounds **24** and **36** (CI = 1.02 and CI = 1.05, respectively). Despite this apparent incongruence, this has been previously reported and seems to be related to the saturation of drug-target complexes at higher concentrations or due to some interactions between compounds (Yadav et al., 2016), which is still unknown for our system. In addition, it is noteworthy that vincristine acts on a nanomolar scale while compounds **24**, **30**, and **36** act on a micromolar scale, resulting in dose-response curves with different maximum effects. Then, this can change the synergy to additive effect when drug concentrations are increased (Bulusu et al., 2016). Nevertheless, the data obtained indicates that pharmaceutical formulations containing these compounds maybe approached to increase the potency of chemotherapeutic agents, mainly at lower dosages, which is the overall goal of such a strategy.

3.3.4 Effect of compounds on cell death and proliferation

Once compounds **24**, **30**, and **36** were selected as the most active derivatives, they were used in additional experiments in order to gain insights on how they might act in leukemic cells.

Annexin V/PI staining assays were performed to evaluate whether the treatments impact in Nalm6 apoptosis. After 12 or 24 h exposure, the three compounds significantly increased annexin-V positive cells in comparison to control (**Figure 17A**). After 24 h of incubation, the percentage of cells in early events of apoptosis (annexin-V^+/PI^-) reached 11.9%, 14.6%, 24.7% when treated with compounds **24**, **30**, and **36,** respectively. Considering the percentage of total apoptotic cells (annexin-V^+/PI^- and annexin-V^+/PI^+), it was increased practically three times by treatment with compound **36** (**Figure 17B**). Importantly, necrotic cells (annexin-V^-/PI^+), which is considered a toxic and degradative process of cell death (Elmore, 2007), were barely noticed in these assays.

The effect of compounds on leukemic cells autophagy was also assessed by fluorescence microscopy. As shown in **Figure 17C**, there was an increase in red fluorescence when Nalm6 cells were treated with 20 μM of the compounds during 24 h. These findings indicate the presence of autophagosomes and intracellular acidification in these cells, very similarly to the observed for cytarabine, a drug that acts on leukemic cells by triggering apoptosis and autophagy (Bosnjak et al., 2014), which has been considered a complex cellular process that in some cases may increase cell death (Bai et al., 2013).

Finally, proliferation assays revealed that these three substances significantly impaired proliferation of HL60 and Nalm6 in a time-dependent manner (**Figure 18**). After 96 h of incubation, compounds **24**, **30**, and **36** inhibited, respectively, 33%, 38%, and 48% of HL60 growth in comparison to control (**Figure 18A**). Considering Nalm6, they inhibited cell growth in 37%, 66%, and 72%, respectively (**Figure 18B**). Thus, these data suggest that pathways affecting cell proliferation are subjected to inhibition upon treatments. This should be the case of the SRPK2 related activity, as it has been described to promote leukemia cell proliferation in a previous study (Hong et al., 2011).

3.3.5 Effect on intracellular SRPKs activity

The effect of compounds in altering SRPKs intracellular activity was firstly evaluated by monitoring the expression pattern of transcripts already known to be modulated by SRPKs (Amin et al., 2011; Clery et al., 2013; Hayes et al., 2007). With this approach, compound **30** was the most effective in impairing the expression of MAP2K1 and MAP2K2 as well as VEGF (**Figure 19A**). Additionally, compounds **30** and **36** seemed to alter the splicing pattern of the apoptosis related gene RON. Interestingly, no clear changes in gene expression was observed in Nalm6 treated with SRPIN340, indicating the necessity of higher concentrations of this inhibitor at the experimental conditions used (Gammons et al., 2014; Siqueira et al., 2015). No effects were

observed in the expression pattern of the actin transcript, used here as endogenous loading control.

Intracellular activity of SRPKs was also monitored by checking the SR protein phosphorylation status through Western blotting assays. As shown in **Figure 19B**, compound **30** was efficient in decreasing phospho-SR epitopes signals in Nalm6 lysates. Again, in the experimental condition used (treatments with 20 μM for 24 h), compound **30** was more efficient then the reference SRPK inhibitor SRPIN340. As controls, the expression of SRPK1, SRPK2 or actin proteins were checked but no difference was found during the treatments. These data suggest that we were able to obtain at least one compound with increased intracellular effect over SRPK activity, which the exact mechanism on SRPK inhibition *in vitro*, overall selectivity, membrane cell penetration, or *in vivo* effect in disease animal models deserve to be better elucidated in further studies.

3.4 Conclusions

A series of twenty-two trifluoromethyl arylamides were synthesized. Three compounds presented superior cytotoxicity against myelogenous and lymphoid leukemia cell lines as compared to the reference SRPK inhibitor SRPIN340. These three compounds impaired cell proliferation, presented synergistic effect in combination with the chemotherapeutic agent vincristine and were able to trigger apoptotic and autophagic cell death processes. Moreover, intracellular activity of SRPKs were affected by treatments with these compounds, mainly by compound **30**, which altered MAP2K1, MAP2K2, VEGF, and RON gene expression as well as SR protein phosphorylation status. Therefore, these data collectively contribute to medicinal chemistry efforts towards the development of novel anticancer chemotherapeutic agents based on SRPK inhibition.

3.5 Experimental procedures

3.5.1 Synthetic procedures

The synthesis procedures were performed in partnership with Dr. Robson Ricardo Teixeira and Marcus Vinícius Andrade Barros.

3.5.1.1 Generalities

Analytical grade 1-fluoro-2-nitro-4-trifluoromethyl benzene, piperidine, morpholine, cyclohexylamine, diethylamine, 4-bromoaniline, pyrrolidine, isonicotinoyl chloride hydrochloride, nicotinoyl chloride hydrochloride, 2-chloropyridine-3-carboxylic acid and benzoyl chloride were purchased from Sigma Aldrich (St. Louis, MO, USA) and used without further

purification. Anhydrous tin(II) chloride and triethylamine were purchased from Vetec (Rio de Janeiro, Brazil) and used as received. ^{1}H- and ^{13}C-NMR spectra were recorded on a Varian Mercury 300 instrument at 300 MHz and 75 MHz, respectively, using $CDCl_3$ and CD_3OD as solvents. Infrared spectra were recorded on either a Varian 660-IR, equipped with GladiATR scanning from 4000 to 500 cm^{-1} or a Perkin Elmer Paragon 1000 FTIR spectrophotometer, using potassium bromide (1% v/v) disks, scanning from 600 to 4000 cm^{-1}. Melting points are uncorrected and were obtained with a MQAPF-301 melting point apparatus (Microquimica, Campinas, Brazil). Analytical thin layer chromatography was carried out on TLC plates covered with 60GF254 silica gel. Column chromatography was performed over silica gel (60–230 mesh). Solvents utilized as eluents were used without further purification.

3.5.1.2 Synthesis of compounds 2 - 7

*1-(2-nitro-4-(trifluoromethyl)phenyl)piperidine (**2**)*

A 100 mL round bottom flask initially placed in an ice bath was charged with 8.60 mL (88.2 mmol) of piperidine, 4.10 mL of dimethylformamide (DMF), and 4.20 mL (28.7 mmol) of 1-fluoro-2-nitro-4-trifluoromethyl benzene (**1**). The ice bath was removed and the resulting mixture was magnetically stirred at room temperature for 1.5 h. After this time, water was added and the resulting mixture was transferred to a separatory funnel. The aqueous phase was extracted with ethyl acetate (4 x 80 mL). The organic extracts were combined and the resulting organic layer was washed with brine, dried over sodium sulphate, filtered and concentrated under reduced pressure. The resulting solid was recrystallized with methanol. Compound **2** was obtained as an orange solid in 91% yield (7.15 g, 26.1 mmol).

TLC R_f = 0.40 (ethyl acetate - hexane 16:1 v/v). mp 50.1 - 50.7 ºC. IR (ATR, cm^{-1}) $\bar{\nu}_{max}$: 2938, 2867, 2827, 1621, 1560, 1528, 1493, 1449, 1386, 1323, 1297, 1260, 1233, 1211, 1149, 1115, 1080, 1064, 1021, 974, 929, 906, 882, 856, 832, 789, 760, 724, 678, 629, 528.^{1}H NMR (300 MHz, $CDCl_3$) δ: 1.61-1.75 (m, 6H), 3.12 (t, 4H, *J* = 5.3 Hz), 7.14 (d, 1H, *J* = 8.7 Hz), 7.60 (dd, 1H, *J* = 8.7 Hz and *J* = 2.3 Hz), 8.03 (d, 1H,*J* = 2.3 Hz). ^{13}C NMR (75 MHz, $CDCl_3$) δ: 24.0, 25.8, 52.3, 120.6, 120.9 (q, J_{C-F} = 34.1 Hz), 123.7 (q, J_{C-F} = 269.6 Hz), 124.6 (q, J_{C-F} = 4.0 Hz), 130.1 (q, J_{C-F} = 3.4 Hz), 139.8, 148.8. HRMS ($M+H^+$): Calculated for $C_{12}H_{14}F_3N_2O_2$, 275.1007; found: 275.0926.

Nitro compounds **3** - **7** (**Scheme 1**) were synthesized using a procedure similar to that described for the preparation of compound **2**. Description of experimental data that support the structures of compounds **3**-**7** is provided below.

N-cyclohexyl-2-nitro-4-(trifluoromethyl)aniline (**3**)

The compound was obtained as a yellow solid after recrystallization with methanol in 81% yield. TLC R_f = 0.10 (hexane). mp 79.3 - 80.2 ºC. IR (ATR, cm^{-1}) $\bar{\nu}_{max}$: 3365, 3114, 2931, 2861, 1634, 1572, 1529, 1436, 1411, 1324, 1260, 1244, 1227, 1187, 1152, 1112, 1063, 976, 912, 899, 831, 763, 694, 642 . ^{1}H NMR (300 MHz, $CDCl_3$) δ: 1.30-2.07 (m, 10H), 3.51-3.61 (m, 1H), 6.95 (d, 1H, *J* = 9.3 Hz), 7.56 (dd, 1H, *J* = 9.3 Hz and *J* = 2.1 Hz), 8.34 (d 1H, *J* = 6.3 Hz), 8.45 (d, 1H, *J* = 2.1 Hz).^{13}C NMR (75 MHz, $CDCl_3$) δ: 24.6, 25.6, 32.7, 51.5, 115.0, 117.0 (q, J_{C-F}= 34.1 Hz), 123.9 (q, J_{C-F}= 269.0 Hz), 125.4 (q, *J* = 4.2 Hz), 132.1 (q, *J* = 3.0 Hz), 130.7, 146.2. HRMS ($M+H^+$): Calculated for $C_{13}H_{15}F_3N_2O_2$, 289.1086; found: 289.0994.

1-(2-nitro-4-(trifluoromethyl)phenyl)pyrrolidine (**4**)

The compound was obtained as an orange solid in 97% after purification by silica gel column chromatography eluted with hexane-ethyl acetate (5:1 v/v). TLC R_f = 0.45 (hexane-ethyl acetate 5:1 v/v). mp 52.3 - 53.8 ºC. IR (ATR, cm^{-1}) $\bar{\nu}_{max}$: 2975, 2871, 1622, 1554, 1504, 1428, 1388, 1322, 1268, 1150, 1103, 1074, 884, 808, 781, 719, 688, 634. ^{1}H NMR (300 MHz, $CDCl_3$) δ: 1.98 - 2.03 (m, 4H), 3.23 - 3.27 (m, 4H), 6.95 (d, 1H, *J* = 9.0 Hz), 7.53 (dd, 1H, *J* = 9.0 Hz and *J* = 2.4 Hz), 7.99 (brs, 1H). ^{13}C NMR (75 MHz, $CDCl_3$) δ: 25.8, 50.8, 116.4, 117.1 (q, J_{C-F} = 34.2 Hz), 124.0 (q, J_{C-F} = 269.1 Hz), 124.7 (q, J_{C-F} = 4.0 Hz), 129.4 (q, J_{C-F} = 3.2 Hz), 135.8, 144.4. HRMS ($M+H^+$): Calculated for $C_{11}H_{12}F_3N_2O_2$, 261.0851; found: 261.0770.

N,N-diethyl-2-nitro-4-(trifluoromethyl)aniline (**5**)

The compound was obtained as an orange oil in 98% yield after purification by silica gel column chromatography eluted with hexane-ethyl acetate (8:1 v/v). TLC R_f = 0.55 (hexane - ethyl acetate 8:1 v/v). IR (ATR, cm^{-1}) $\bar{\nu}_{max}$: 2979, 2939, 2877, 1621, 1531, 1322, 1258, 1114, 1083, 903, 877, 816, 784, 717, 669, 601. ^{1}H NMR (300 MHz, $CDCl_3$) δ: 1.16 (t, 6H, *J* = 7.1 Hz), 3.26 (q, 4H, *J* = 7.1 Hz), 7.14 (d, 1H, *J* = 9.0 Hz), 7.58 (dd, 1H, *J* = 9.0 Hz and *J* = 2.3 Hz), 7.96 (brs, 1H). ^{13}C NMR (75 MHz, $CDCl_3$) δ: 12.6, 46.1, 119.9 (q, J_{C-F} = 34.0 Hz),120.6, 123.8 (q, J_{C-F} = 269.3 Hz), 124.5 (q, J_{C-F} = 4.0 Hz), 129.4 (q, J_{C-F} = 3.3 Hz), 139.8, 146.6. HRMS ($M+H^+$): Calculated for $C_{11}H_{14}F_3N_2O_2$, 263.1007; found: 263.0944.

4-(2-nitro-4-(trifluoromethyl)phenyl)morpholine (**6**)

The compound was obtained as an orange oil in 97% yield after purification by silica gel column chromatography eluted with hexane-ethyl acetate (3:1 v/v). TLC R_f = 0.27 (hexane-ethyl

acetate 3:1 v/v). IR (ATR, cm^{-1}) $\bar{\nu}_{max}$: 2967, 2858, 1713, 1622, 1532, 1322, 1275, 1252, 1235, 1168, 1110, 1083, 1044, 938, 884, 824, 789, 720, 678, 640, 526. ^{1}H NMR (300 MHz, $CDCl_3$) δ: 3.13 (t, 4H, *J* = 4.7 Hz), 3.84 (t, 4H, *J* = 4.7 Hz), 7.16 (d, 1H, *J* = 8.7 Hz), 7.68 (dd, 1H, *J* = 8.7 Hz and *J* = 2.3 Hz), 8.05 (brs, 1H). ^{13}C NMR (75 MHz, $CDCl_3$) δ: 51.4, 66.6, 120.6, 123.4 (q, J_{C-F} = 269.9 Hz), 122.9 (q, J_{C-F} = 34.1 Hz), 124.4 (q, J_{C-F} = 3.9 Hz), 130.5 (q, J_{C-F} = 3.3 Hz), 141.0, 148.1. HRMS ($M+H^+$): Calculated for $C_{11}H_{12}F_3N_2O_3$, 277.0800; found: 277.0727.

N-(4-bromophenyl)-2-nitro-4-(trifluoromethyl)aniline (**7**)

The compound was obtained as an orange solid in 93% yield after purification by silica gel column chromatography eluted with hexane - ethyl acetate (5:1 v/v). TLC R_f = 0.78 (hexane - ethylacetate 5:1 v/v). mp 89.5 - 89.9 ºC. IR (ATR, cm^{-1}) $\bar{\nu}_{max}$: 3347, 3102, 1636, 1571, 1528, 1486, 1430, 1319, 1250, 1147, 1070, 1011, 909, 841, 805, 693, 632. ^{1}H NMR (300 MHz, $CDCl_3$) δ: 7.15-7.26 (m, 3H), 7.54-7.60 (m, 3H), 8.50 (brs, 1H), 9,63 (brs,1H). ^{13}C NMR (75 MHz, $CDCl_3$) δ: 116.8, 120.1 (q, J_{C-F} = 34.1 Hz), 120.2, 123.5 (q, J_{C-F} = 269.5 Hz), 125.0 (q, J_{C-F} = 4.2 Hz), 126.8, 132.1 (q, J_{C-F} = 3.2 Hz), 132.4, 133.3, 136.8, 144.9. HRMS ($M+H^+$): Calculated for $C_{13}H_8BrF_3N_2O_2$, 359.9721; found: 359.9648.

3.5.1.3 *Synthesis of compounds 8 - 13*

2-(piperidin-1-yl)-5-(trifluoromethyl)aniline (**8**)

A 50 mL round bottom flask initially placed in an ice bath was charged with 10.8 mL (129.6 mmol) of concentrated hydrocloric acid, 6.71 g (35.4 mmol) of tin(II) chloride, 20.0 mL of methanol, and 1.50 g (5.47 mmol) of 1-(2-nitro-4-(trifluoromethyl)phenyl)piperidine (**2**). The ice bath was removed and the resulting mixture was continuously stirred at room temperature for 42 h. After this time, sodium hydroxide solution was added to the mixture until pH was approximately equal to 10. Then, the mixture was transferred to a separatory funnel and extracted with ethyl acetate (4 x 80.0 mL). The organic extracts were combined and the resulting mixture was washed with brine, dried under sodium sulphate, filtered and concentrated under reduced pressure. The residue was purified by silica gel column chromatography eluted with hexane-ethyl acetate (11:1 v/v). The compound **8** was obtained as a white solid in 78% yield (1.34 g, 5.49 mmol).

TLC R_f = 0.48 (hexane-ethyl acetate 11:1 v/v). mp 50.0 - 50.5 ºC. IR (ATR, cm^{-1}) $\bar{\nu}_{max}$: 3452, 3355, 2950, 2865, 2805, 1611, 1589, 1512, 1469, 1439, 1379, 1328, 1288, 1256, 1227, 1205, 1160, 1104, 1064, 936, 892, 860, 810, 745, 722, 663, 643. ^{1}H NMR (300 MHz, $CDCl_3$) δ: 1.60-1.75

(m, 6H), 2.88 (brs, 4H), 4.11 (brs, 2H, N$\underline{H}_2$), 6.93-7.03 (m, 3H). ^{13}C NMR (75 MHz, $CDCl_3$) δ: 24.4, 26.8, 52.4, 111.5 (q, J_{C-F} = 3.5 Hz), 115.5 (q, J_{C-F} = 4.1 Hz), 119.7, 124.7 (q, J_{C-F} = 270.0 Hz), 126.1 (q, J_{C-F} = 31.9 Hz), 141.7, 143.4. HRMS ($M+H^+$): Calculated for $C_{12}H_{16}F_3N_2$, 245.1266; found: 245.1182.

The anilines **9** - **13** (**Scheme 2**) were synthesized from compounds **3**-**7** using a similar procedure to that described for the preparation of **8**. Description of experimental data that support the structures of compounds **9** - **13** is provided below.

N-cyclohexyl-4-(trifluoromethyl)benzene-1,2-diamine (**9**)

The compound was obtained as a white solid in 56% yield after purification by silica gel column chromatography eluted with hexane - ethyl acetate (14:1 v/v). TLC R_f = 0.25 (hexane-ethyl acetate 14:1 v/v). mp 71.6 - 72.0 ºC. IR (ATR, cm^{-1}) $\bar{\nu}_{max}$: 3421, 3350, 2928, 2855, 1625, 1601, 1528, 1470, 1440, 1362, 1324, 1300, 1240, 1217, 1146, 1107, 1084, 1055, 913, 885, 863, 808, 737, 668, 635. ^{1}H NMR (300 MHz, $CDCl_3$) δ: 1.17 - 2.15 (m, 10H), 3.25 - 3.37 (m, 4H), 6.65 (d, 1H, J = 8.4 Hz), 6.93 (d, 1H, J = 1.8 Hz), 7.08 (dd, 1H, J = 8.4 Hz and J = 1.8 Hz). ^{13}C NMR (75 MHz, $CDCl_3$) δ: 25.1, 26.0, 33.4, 51.8, 110.9, 113.9 (q, J_{C-F}= 3.7 Hz), 118.6 (q, J_{C-F}= 4.1 Hz), 119.3 (q, J_{C-F}= 32.1), 125.2 (q, J_{C-F}= 268.8 Hz), 133.2, 139.9. HRMS ($M+H^+$): Calculated for $C_{13}H_{18}F_3N_2$, 259.1422; found: 259.1341.

2-(pyrrolidin-1-yl)-5-(trifluoromethyl)aniline (**10**)

The compound was obtained as a red oil in 77% yield after purification by column chromatography eluted with hexane - ethyl acetate (3:1 v/v). TLC R_f = 0.68 (hexane - ethyl acetate 3:1 v/v). IR (ATR, cm^{-1}) $\bar{\nu}_{max}$: 3440, 3355, 2969, 2877, 2823, 1711, 1618, 1516, 1439, 1328, 1244, 1148, 1105, 954, 903, 866, 808, 661. ^{1}H NMR (300 MHz, $CDCl_3$) δ: 1.91 - 1.97(m, 4H), 3.09-3.13 (m, 4H), 3.92 (brs, 2H), 6.92 - 6.98 (m, 3H).^{13}C NMR (75 MHz, $CDCl_3$) δ: 24.3, 50.6, 112.1 (q, J_{C-F} = 3.8 Hz), 115.8 (q, J_{C-F} = 4.1 Hz), 117,8, 124.8 (q, J_{C-F} = 269.6 Hz), 124.8 (q, J_{C-F} = 31.8 Hz, C-5), 140.8. HRMS ($M+H^+$): Calculated for $C_{11}H_{14}F_3N_2$, 231.1109; found: 231.1026.

N,N-diethyl-4-(trifluoromethyl)benzene-1,2-diamine (**11**)

The compound was obtained as a yellow oil in 67% yield after purification by column chromatography eluted with hexane - ethyl acetate (12:1 v/v). TLC R_f = 0.22 (hexane -ethyl acetate 30:1 v/v). IR (ATR, cm^{-1}) $\bar{\nu}_{max}$: 3469, 3362, 2973, 2933, 2870, 2826, 1615, 1593, 1514, 1441, 1384, 1335, 1294, 1260, 1232, 1163, 1120, 928, 867, 817, 745, 666. ^{1}H NMR (300 MHz,

$CDCl_3$) δ: 0.99 (t, 6H, *J* = 7.1 Hz), 2.99 (q, 4H, *J* = 7.1 Hz), 4.19 (brs, 2H), 6.94-6.97 (m, 2H), 7.05 (d, 1H, *J* = 8.7 Hz).^{13}C NMR (75 MHz, $CDCl_3$) δ: 12.3, 46.6, 111.3 (q, J_{C-F} = 3.7 Hz), 114.6 (q, J_{C-F} = 3.9 Hz), 122.5, 124.4 (q, J_{C-F} = 270.0 Hz), 126.3 (q, J_{C-F} = 31.8 Hz), 139.9, 143.7. HRMS ($M+H^+$): Calculated for: $C_{11}H_{16}F_3N_2$, 233.1266; found: 233.1211.

2-*morpholino-5-(trifluoromethyl)aniline* (**12**)

Compound was obtained as a white solid in 94% yield without any further purification. TLC R_f = 0.48 (hexane - ethylacetate 3:1 v/v). mp 130.6 - 131.1 ºC. IR (ATR, cm^{-1}) $\bar{\nu}_{max}$: 3430, 3338, 2827, 2823, 1620, 1515, 1448, 1331, 1256, 1217, 1153, 1099, 938, 897, 860, 818, 651. ^{1}H NMR (300 MHz, $CDCl_3$) δ: 2.95 (t, 4H, *J* = 4.7 Hz), 3.87 (t, 4H, *J* = 4.7 Hz), 6.96 (brs, 1H), 6.96-7.05 (m, 2H). ^{13}C NMR (75 MHz, $CDCl_3$) δ: 51.2, 67.6, 111.9 (q, J_{C-F} = 3.7 Hz), 115.7 (q, J_{C-F} = 4.0 Hz), 119.7, 124.6 (q, J_{C-F} = 270.0 Hz), 126.9 (q, J_{C-F} = 32.0 Hz), 141.7. HRMS ($M+H^+$): Calculated for $C_{11}H_{14}F_3N_2O$, 247.1058; found: 247.0956.

N-(4-bromophenyl)-4-(trifluoromethyl)benzene-1,2-diamine (**13**)

Compound was obtained as a white solid in 79% yield after purification by silica gel column chromatography eluted with hexane-ethyl acetate (5:1 v/v). TLC R_f = 0.25 (hexane-ethyl acetate 5:1 v/v). mp 123.5-123.8 ºC. IR (ATR, cm^{-1}) $\bar{\nu}_{max}$: 3469, 3384, 1591, 1518, 1485, 1436, 1385, 1334, 1249, 1154, 1106, 928, 868, 820. ^{1}H NMR (300 MHz, $CDCl_3$) δ: 3.73 (brs, 2H), 5.39 (brs, 1H), 6.72 (d, 2H, *J* = 9.0 Hz), 6.97-7.91 (m, 2H), 7.16 (d, 1H, *J* = 8.1 Hz), 7.34 (d, 2H, *J* = 9.0 Hz). ^{13}C NMR (75 MHz, $CDCl_3$) δ: 113.0, 113.6 (q, J_{C-F} = 3.7 Hz), 117.0 (q, J_{C-F} = 3.9 Hz), 118.6, 121.9 (C-6), 124.4 (q, J_{C-F} = 270.3 Hz), 126.7 (q, J_{C-F} = 32.3 Hz), 132.5, 132.6, 139.5, 142.7.HRMS ($M+H^+$): Calculated for $C_{13}H_{11}BrF_3N_2$, 331.0058; found: 330.9987.

3.5.1.4 Synthesis of SRPIN340 and compounds 15 - 36

N-(2-(piperidin-1-yl)-5-(trifluoromethyl)phenyl)isonicotinamide (*SRPIN340*)

A 25 mL round bottom flask initially placed in an ice bath was charged with 0.629 g (3.389 mmol) of isonicotinoyl chloride hydrochloride, 0.800 mL of triethylamine, 8.00 mL of dichoromethane and 0.400 (1.64 mmol) of 2-(piperidin-1-yl)-5-(trifluoromethyl) aniline (**8**). The ice-bath was removed and the mixture was magnetically stirred at room temperature for 3 h. Then, 10.0 mL of distilled water was added, and the mixture was transferred to a separatory funnel. The aqueous layer was extracted with ethyl acetate (4 x 30.0 mL). The organic extracts were combined and the resulting organic layer was washed with brine, dried over sodium

sulphate, filtered, and concentrated under reduced pressure. The residue was purified by silica gel column chromatography eluted with hexane-ethyl acetate (3:1 v/v). The solid was further recrystallized with acetone. The compound SRPIN340 was obtained as a white solid in 75% yield (430 mg, 1.23 mmol).

TLC R_f = 0.13 (hexane - ethyl acetate 3:1 v/v). mp 95.6 - 96.7 ºC. IR (ATR, cm^{-1}) $\bar{\nu}_{max}$: 3347, 2945, 2917, 2811, 1679, 1611, 1587, 1556, 1527, 1455, 1434, 1380, 1334, 1308, 1239, 1165, 1107, 1093, 1061, 1022, 915, 895, 878, 839, 826, 751, 728, 681, 662, 644. ^{1}H NMR (300 MHz, $CDCl_3$) δ: 1.65 - 1.81 (m, 6H), 2.86 (t, 4H, *J* = 5.1 Hz), 7.28 (d, 1H, *J* = 8.4 Hz), 7.37 (dd, 1H, *J* = 8.4 Hz and *J* = 1.8 Hz), 7.76 (dd, 2H, *J* = 4.5 Hz and *J* = 1.5 Hz), 8.83 - 8.85 (m, 3H), 9.55 (s, 1H, NH). ^{13}C NMR (75 MHz, $CDCl_3$) δ: 24.0, 27.1, 53.8, 116.6, 120.8, 121.1, 121.6 (q, J_{C-F} = 3.7 Hz), 124.2 (q, J_{C-F} = 270.5 Hz), 127.5 (q, J_{C-F} = 32.3 Hz), 133.4, 141.8, 145.9, 151.1, 163.0. HRMS ($M+H^+$): Calculated for $C_{18}H_{19}F_3N_3O$, 350.1480; found: 350.1420.

The trifluoromethyl amides **15** - **36** (**Scheme 3**) were prepared by using a similar methodology to that described for the synthesis of SRPIN340. Description of experimental data that support the structures of compounds **15 - 36** is provided below.

N-(2-(cyclohexylamino)-5-(trifluoromethyl)phenyl)isonicotinamide (**15**)

The compound was obtained as a white solid in 82% yield after recrystallization with ethyl acetate. TLC R_f = 0.33 (hexane - ethyl acetate 1:1 v/v). mp 159.9 -160.2 ºC. IR (ATR, cm^{-1}) $\bar{\nu}_{max}$: 3262, 2931, 2851, 1657, 1617, 1543, 1510, 1485, 1441, 1324, 1205, 1254, 1238, 1147, 1133, 1103, 1069, 998, 931, 880, 841, 806, 754, 709, 687, 637. ^{1}H NMR (300 MHz, CD_3OD) δ: 1.10 – 2.20 (m, 10H), 3.30 (quint, 1H, *J* = 1.8 Hz), 3.32 - 3.43 (m, 1H), 6.87 (d, 1H, *J* = 8.7 Hz), 7.40 (dd, 1H, *J* = 8.7 Hz and *J* = 1.7 Hz), 7.47-7.46 (m, 1H), 7.93 (dd, 2H, *J* = 4.7 Hz and *J* = 1.8 Hz), 8.73 (dd, 2H, *J* = 4.7 Hz and *J* = 1.8 Hz).^{13}C NMR (75 MHz, CD_3OD) δ: 24.9, 25.7, 32.6, 51.3, 111.2, 116.9 (q, J_{C-F}= 32.7 Hz), 121.6, 122.1, 124.6 (q, *J* = 3.8 Hz), 125.1 (q, J_{C-F} = 3.9 Hz), 125.1 (q, *J* = 267.7 Hz), 142.4, 145.8, 149.7, 165.9. HRMS ($M+H^+$): Calculated for $C_{19}H_{21}F_3N_3O$, 364.1637; found: 364.1556.

N-(2-(pyrrolidin-1-yl)-5-(trifluoromethyl)phenyl)isonicotinamide (**16**)

The compound was obtained as a white solid in 70% yield after recrystallization with acetone. TLC R_f = 0.24 (hexane - ethyl acetate 1:1 v/v). mp 110.0 - 110.6 ºC. IR (ATR, cm^{-1}) $\bar{\nu}_{max}$: 3242, 2976, 2872, 1654, 1613, 1538, 1512, 1489, 1436, 1409, 1370, 1327, 1291, 1152, 1093, 929, 901, 849, 816, 755, 656. ^{1}H NMR (300 MHz, $CDCl_3$) δ: 1.94 - 1.98 (m, 4H), 3.13 - 3.17 (m, 4H), 7.10 (d, 1H, *J* = 8.7 Hz), 7.35 (dd, 1H, *J* = 8.7 Hz and *J* = 1.8 Hz), 7.71 - 7.73 (m, 2H), 8.31 (brs,

1H), 8.77 (brs, 2H), 8.97 (brs, 1H).[13]C NMR (75 MHz,$CDCl_3$) δ: 25.0, 51.9, 118.4, 121.0, 121.1, 123.0 (q. J_{C-F} = 3.6 Hz), 124.4 (q, J_{C-F} = 269.9 Hz), 124.3 (q, J_{C-F} = 32.6 Hz), 129.3, 141.7, 145.1, 150.9, 163.5. HRMS ($M+H^+$): Calculated for $C_{17}H_{17}F_3N_3O$, 336.1324; found: 336.1282.

N-(2-(diethylamino)-5-(trifluoromethyl)phenyl)isonicotinamide (**17**)

The compound was obtained as a white solid in 85% yield after purification by silica gel column chromatography eluted with hexane-ethyl acetate (2:1 v/v). TLC R_f = 0.60 (hexane - ethyl acetate 1:1 v/v). mp 73.8 - 74.3 ºC. IR (ATR, cm^{-1}) $\bar{\nu}_{max}$: 3326, 2976, 2925, 2856, 1680, 1588, 1530, 1439, 1333, 1241, 1164, 1094, 1060, 922, 895, 826, 746, 676, 562. ^{1}H NMR (300 MHz, $CDCl_3$) δ: 0.98 (t, 6H, *J* = 7.2 Hz), 3.02 (q, 4H, *J* = 7.2 Hz), 7.31 - 7.40 (m, 2H), 7.72 (dd, 2H, *J* = 4.5 Hz and *J* = 1.5 Hz), 8.82 - 8.89 (m, 3H), 9.92 (brs, 1H). ^{13}C NMR (75 MHz, $CDCl_3$) δ: 13.0, 49.5, 116.3, 120.9, 121.7 (q, J_{C-F} = 3.7 Hz), 123.7, 124.1 (q, J_{C-F} = 270.7 Hz), 128.3 (q, J_{C-F} = 32.8 Hz), 136.2, 141.9, 142.7, 151.0, 163.0. HRMS ($M+H^+$): Calculated for $C_{17}H_{19}F_3N_3O$, 338.1480; found: 338.1453.

N-(2-morpholino-5-(trifluoromethyl)phenyl)isonicotinamide (**18**)

The compound was obtained as a white solid in 78% yield after purification by silica gel column chromatography eluted with hexane-ethyl acetate (2:1 v/v). TLC R_f = 0.18 (hexane - ethyl acetate 2:1 v/v). mp 166.5 - 168.4 ºC. IR (ATR, cm^{-1}) $\bar{\nu}_{max}$: 3351, 2969, 2921, 2858, 1676, 1590, 1531, 1439, 1333, 1242, 1155, 1108, 918, 823, 750, 656. ^{1}H NMR (300 MHz, $CDCl_3$) δ: 2.95 (t, 4H, *J* = 4.5 Hz), 3.91 (t, 4H, *J* = 4.5 Hz), 7.32 (d, 1H, *J* = 8.4 Hz), 7.41 (dd, 1H, *J* = 8.4 Hz and *J* = 2.1 Hz), 7.74 (dd, 2H, *J* = 4.5 Hz and *J* = 2.8 Hz), 8.85 - 8.86 (m, 3H), 9.48 (brs, 1H).[13]C NMR (75 MHz, $CDCl_3$) δ: 52.6, 67.7, 117.0 (q, J_{C-F} = 3.9 Hz), 120.8, 121.3, 121.9 (q, J_{C-F} = 3.8 Hz), 124.0 (q, J_{C-F} = 270.6 Hz), 128.3 (q, J_{C-F} = 32.6 Hz), 133.5, 141.8, 144.2, 151.0, 162.9. HRMS ($M+H^+$): Calculated for $C_{17}H_{17}F_3N_3O_2$, 351.1273; found: 352.1218.

N-(2-(4-bromophenylamino)-5-(trifluoromethyl)phenyl)isonicotinamide (**19**)

The compound was obtained as a yellow solid in 81% yield after purification by silica gel column chromatography eluted with hexane-ethyl acetate (1:1 v/v). TLC R_f = 0.22 (hexane-ethylacetate 2:1 v/v). mp 203.5 - 203.9 ºC. IR (ATR, cm^{-1}) $\bar{\nu}_{max}$: 3386, 3243, 3081, 1675, 1589, 1510, 1469, 1324, 1249, 1163, 1101, 923, 885, 821, 804, 749. ^{1}H NMR (300 MHz, CD_3OD) δ: 7.06 (d, 2H, *J* = 8,7 Hz), 7.36-7.49 (m, 4H), 7.77-7.85 (m, 3H). 8.16 (brs, 1H), 8.75-8.77 (m, 2H), 10.14 (brs, 1H). ^{13}C NMR (75 MHz, CD_3OD) δ: 113.4, 117.5, 120.6 (q, J_{C-F} = 32.2 Hz), 121.8, 122.5, 124.5

(q, J_{C-F} = 3.8 Hz), 125.1 (q, J_{C-F} = 269.2 Hz), 125.3 (q, J_{C-F} = 3.8 Hz), 127.0, 132.6, 142.0, 142.3, 150.8, 165.2. HRMS ($M+H^+$): Calculated for $C_{19}H_{14}BrF_3N_3O$, 436.0272; found: 436.0202.

2-chloro-N-(2-(piperidin-1-yl)-5-(trifluoromethyl)phenyl)nicotinamide (**20**)

The compound was obtained as a white solid in 78% yield after purification by column chromatography eluted with hexane-ethyl acetate (3:1 v/v). mp 120.3 - 121.2 ºC. IR (ATR, cm^{-1}) $\bar{\nu}_{max}$: 3322, 2919, 2827, 1678, 1655, 1613, 1578, 1526, 1474, 1433, 1400, 1333, 1263, 1214, 1100, 915, 893, 858, 824, 754, 662, 642, 601 . ^{1}H NMR (300 MHz, $CDCl_3$) δ: 1.58 - 1.73 (m, 6H), 2.85 (t, 4H, *J* = 5.0 Hz), 7.30 (d, 1H, *J* = 8.4 Hz), 7.36 - 7.46 (m, 2H), 8.23 (dd, 1H, *J* = 8.4 Hz and *J* = 1.8 Hz), 8.54 (dd, 1H, *J* = 4.5 Hz and *J* = 1.8 Hz), 8.87 (s, 1H), 9.73 (brs, 1H).^{13}C NMR (75 MHz, $CDCl_3$) δ: 23.9, 26.6, 54.1, 116.8 (q, J_{C-F} = 3.7 Hz), 121.4, 121.7, 121.7 (q, J_{C-F} = 3.9 Hz), 123.2, 124.2 (q, J_{C-F} = 270.4 Hz), 127.6 (q, J_{C-F} = 32.1 Hz), 131.6, 133.8, 140.4, 146.1, 146.9, 151.6, 162.7. HRMS ($M+H^+$): Calculated for $C_{18}H_{18}ClF_3N_3O$, 384.1090; found: 384.1043.

2-chloro-N-(2-(pyrrolidin-1-yl)-5-(trifluoromethyl)phenyl)nicotinamide (**21**)

The compound was obtained as a white solid in 79% yield after purification by silica gel column chromatography eluted with hexane-ethyl acetate (2:1 v/v). TLC R_f = 0.52 (hexane - ethyl acetate 2:1 v/v). mp 147.5 - 148.7 ºC. IR (ATR, cm^{-1}) $\bar{\nu}_{max}$: 3232, 2968, 2882, 2818, 1659, 1615, 1581, 1535, 1508, 1405, 1368, 1331, 1275, 1151, 1095, 818, 802, 768, 708, 540. ^{1}H NMR (300 MHz, $CDCl_3$) δ: 1.94 - 2.01 (m, 4H), 3.13 (t, 4H, *J* = 6.3 Hz), 7.20 (d, 1H, *J* = 8.7 Hz), 7.38 (dd, 1H, *J* = 8.7 Hz and *J* = 1.5 Hz), 7.44 (dd, 1H, *J* = 7.8 Hz and *J* = 4.7 Hz), 8.32 (dd, 1H, *J* = 7.8 Hz and *J* = 1.8 Hz), 8.79 (dd, 1H, *J* = 4.7 Hz and *J* = 1.8 Hz), 8.56 (d, *J* = 1.5 Hz, 1H), 9.32 (brs, 1H). ^{13}C NMR (75 MHz, $CDCl_3$) δ: 24.8, 52.5, 119.3 (q, J_{C-F} = 3.8 Hz), 119.5, 122.6 (q, J_{C-F} = 3.7 Hz), 123.4, 125.3 (q, J_{C-F} = 32.5 Hz), 131.1, 131.3, 140.9, 144.7, 147.0 , 151.7, 162.6. The signal of the carbon of the CF_3 group presented low intensity and it was not noticed in the spectrum. HRMS ($M+H^+$): Calculated for $C_{17}H_{16}ClF_3N_3O$, 370.0934; found: 370.0851.

2-chloro-N-(2-(diethylamino)-5-(trifluoromethyl)phenyl)nicotinamide (**22**)

The compound was obtained as a yellow solid in 59% yield after purification by silica gel column chromatography eluted with hexane - ethyl acetate (3:1 v/v). TLC R_f = 0.75 hexane - ethyl acetate (1:1 v/v). mp 74.3 - 75.4 ºC. IR (ATR, cm^{-1}) $\bar{\nu}_{max}$: 3291, 2976, 2934, 2848, 1666, 1612, 1578, 1531, 1395, 1334, 1258, 1167, 1116, 1065, 926, 899, 829, 760, 696. ^{1}H NMR (300 MHz, $CDCl_3$) δ: 0.96 (t, 6H, *J* = 7.1 Hz), 3.00 (q, 4H, *J* = 7.1 Hz), 7.31 (d, 1H, *J* = 8.4 Hz), 7.38 - 7.40 (m,

2H), 8.25 (dd, 1H, *J* = 7.7 Hz and *J* = 2.0 Hz), 8.53 (dd, 1H, *J* = 4.7 Hz and *J* = 2.0 Hz), 8.92 (brs, 1H), 10.02 (brs, 1H). ^{13}C NMR (75 MHz, $CDCl_3$) δ: 12.5, 49.1, 116.7 (brs), 121.3 (q, J_{C-F} = 3.8 Hz), 123.2, 123.9, 124.2 (q, J_{C-F} = 270.8 Hz), 131.5, 136.4, 140.5, 147.0, 151.6, 162.7. Signal for the carbon attached to CF_3 was of low intensity and it is not observed. The signal for the carbon attached to the chlorine as well as the signal for the aromatic carbon attached to the $-N(Et)_2$ presented the same chemical shift. HRMS ($M+H^+$): Calculated for $C_{17}H_{18}ClF_3N_3O$, 372.1090; found: 372.1016.

2-chloro-N-(2-morpholino-5-(trifluoromethyl)phenyl)nicotinamide (**23**)

The compound was obtained as a yellow solid in 91% yield after purification by column chromatography eluted with hexane-ethyl acetate (3:1 v/v). TLC R_f = 0.43 hexane - ethyl acetate (1:1 v/v). mp 131.2 - 133.2 ºC. IR (ATR, cm^{-1}) $\bar{\nu}_{max}$: 3258, 2924, 2890, 2844, 1665, 1616, 1581, 1539, 1489, 1440, 1400, 1329, 1268, 1108, 923, 895, 828, 807, 754, 648. ^{1}H NMR (300 MHz, $CDCl_3$) δ: 2.94 (t, 4H, *J* = 4.5 Hz), 3.87 (t, 4H, *J* = 4.5 Hz), 7.36 (d, 1H, *J* = 8.4 Hz), 7.42-7.48 (m, 2H), 8.28 (dd, 1H, *J* = 7.8 Hz and *J* = 1.8 Hz), 8.55 (dd, 1H, *J* = 4.8 Hz and *J* = 1.8 Hz), 8.92 (brs, 1H), 9,82 (brs, 1H). ^{13}C NMR (75 MHz, $CDCl_3$) δ: 52.9, 67.3, 117.3 (q, J_{C-F} = 3.8 Hz), 121.8, 123.4, 124.1 (q, J_{C-F} = 270.5 Hz), 128.5 (q, J_{C-F} = 32.6 Hz), 131.2, 134.1, 140.9, 144.3, 146.6, 151.8, 162.7. HRMS ($M+H^+$): Calculated for $C_{17}H_{16}ClF_3N_3O_2$, 386.0883; found: 386.0842.

N-(2-(4-bromophenylamino)-5-(trifluoromethyl)phenyl)-2-chloronicotinamide (**24**)

The compound was obtained as a yellow solid in 37% yield after recrystallization with acetone. TLC R_f = 0.58 (hexane - ethyl acetate 1:1 v/v). mp 175.0 - 176.0 ºC. IR (ATR, cm^{-1}) $\bar{\nu}_{max}$: 3404, 3217, 3048, 1644, 1592, 1529, 1489, 1401, 1334, 1098, 1073, 882, 808, 751. ^{1}H NMR (300 MHz, $CDCl_3$) δ: 6,10 (brs, 1H), 6.81 (d, 2H, *J* = 8.7 Hz), 7.34 - 7.45 (m, 5H), 8.11 (s, 1H), 8.16 (dd, 1H, *J* = 7.8 Hz and *J* = 1.8 Hz), 8.49 (dd, 1H, *J* = 4.7 Hz and *J* = 2.0 Hz), 8.66 (brs, 1H). ^{13}C NMR (75 MHz, $CDCl_3$) δ: 114.5, 120.0, 121.3, 121.7 (q, J_{C-F} = 3.8 Hz), 123.2, 124.2 (q, J_{C-F} = 3.8 Hz), 125.6 (q, J_{C-F} = 32.8 Hz), 129.0, 130.5, 132.7, 138.9, 140.4, 141.9, 147.1, 151.9, 163.6. HRMS ($M+H^+$): Calculated for $C_{19}H_{13}BrClF_3N_3O$, 469.9883; found: 469.9707.

N-(2-(piperidin-1-yl)-5-(trifluoromethyl)phenyl)nicotinamide (**25**)

The compound was obtained as a white solid in 65% yield after purification by silica gel column chromatography eluted with hexane-ethyl acetate (1:1 v/v). TLC R_f = 0.45 (hexane - ethyl acetate 1:1 v/v). mp 129.8 - 130.3 ºC. IR (ATR, cm^{-1}) $\bar{\nu}_{max}$: 3332, 2940, 2856, 2811, 1664, 1588,

1529, 1467, 1435, 1332, 1243, 1163, 1105, 1023, 893, 834, 729, 703, 645, 584. ^{1}H NMR (300 MHz, $CDCl_3$) δ: 1.64 - 1.65 (m, 2H), 1.75 - 1.82 (m, 4H), 2.88 (t, 4H, *J* = 4.8 Hz), 7.28 (d, 1H, *J* = 8.4 Hz), 7.37 (dd, 1H, *J* = 8.4 Hz and *J* = 1.8 Hz), 7.50 (ddd, 1H, *J* = 7.8 Hz, *J* = 4.8 Hz and *J* = 0.8 Hz), 8.30 (dt, 1H, *J* = 7.8 Hz and *J* = 1.8 Hz), 8.80 (dd, 1H, *J* = 4.8 Hz and *J* = 1.8 Hz), 8.84 (brs, 1H), 9.15 (d, 1H, *J* = 1.8 Hz), 9.55 (brs, 1H).^{13}C NMR (75 MHz, $CDCl_3$) δ: 23.9, 27.0, 53.9, 116.7 (brs), 121.0, 121.4 (q, J_{C-F} = 3.8 Hz), 124.1, 124.2 (q, J_{C-F} = 270.6 Hz), 127.6 (q, J_{C-F} = 33.4 Hz), 130.6, 133.6, 135.6, 145.8, 147.7, 152.8, 163.2. HRMS ($M+H^+$): Calculated for $C_{18}H_{19}F_3N_3O$, 350.1480; found: 350.1396.

N-(2-(cyclohexylamino)-5-(trifluoromethyl)phenyl)nicotinamide (**26**)

The compound was obtained as a white solid in 53% yield after purification by silica gel column chromatography eluted with hexane-ethyl acetate (1:1 v/v). TLC R_f = 0.38 (hexane - ethylacetate 1:1 v/v). mp 137.0 - 138.4 ºC. IR (ATR, cm^{-1}) $\bar{\nu}_{max}$: 3434, 3234, 3046, 2930, 2852, 1643, 1615, 1591, 1532, 1456, 1331, 1105, 883, 813, 712, 636. ^{1}H NMR (300 MHz, $CDCl_3$) δ: 1.12 - 2.03 (m, 10H), 3.28 - 3.29 (m, 1H), 4.19 (brs, 1H), 6.79 (d, 1H, *J* = 8.4 Hz), 7.36-7.46 (m, 2H), 7.52 (brs, 1H), 8.19 - 8.25 (m, 2H), 8.72 (d, 1H, *J* = 4.2 Hz), 9.08 (brs, 1H). ^{13}C NMR (75 MHz, $CDCl_3$) δ: 24.7, 25.6, 32.9, 51.6, 112.5, 118.5 (q, J_{C-F}= 32.6 Hz), 124.4 (q, *J* = 269.1 Hz), 122.0, 123.7, 125.1, 129.6, 135.7, 144.6, 147.9, 152.6, 164.5. HRMS ($M+H^+$): Calculated for $C_{19}H_{21}F_3N_3O$, 364.1638; found: 364.1549.

N-(2-(pyrrolidin-1-yl)-5-(trifluoromethyl)phenyl)nicotinamide (**27**)

The compound was obtained as a white solid in 73% yield after recrystallization with ethyl acetate. TLC R_f = 0.33 (hexane - ethyl acetate 1:2 v/v). mp 127.8 - 128.5 ºC. IR (ATR, cm^{-1}) $\bar{\nu}_{max}$: 3289, 3056, 2972, 2870, 2842, 1644, 1615, 1592, 1530, 1372, 1332, 1266, 1249, 1152, 1109, 1082, 1024, 932, 897, 875, 827, 707, 656. ^{1}H NMR (300 MHz, $CDCl_3$) δ: 1.96 - 2.01 (m, 4H), 3.20 (t, 4H, *J* = 6.2 Hz), 7.14 (d, 1H, *J* = 8.4 Hz), 7.35 - 7.38 (m, 1H), 7.48 (dd, 1H, *J* = 7.8 Hz and 4.8 Hz), 8.26 (dt,1H, *J* = 7.8 Hz and *J* = 1.8 Hz), 8.47 (brs, 1H), 8.79 (dd, 1H, *J* = 4.8 Hz and *J* = 1.8 Hz), 8.82 (brs, 1H), 9.10 (d,1H, *J* = 1.8 Hz). ^{13}C NMR (75 MHz, $CDCl_3$) δ: 24.9, 52.2, 118.8, 119.6 (brs), 122.5 (q, J_{C-F} = 3.6 Hz), 124.4 (q, J_{C-F} = 270.2 Hz), 124.9 (q, J_{C-F} = 32.6 Hz), 124.1, 130.5, 130.6, 135.6, 144.8, 147.8, 152.9, 163.6. HRMS ($M+H^+$): Calculated for $C_{17}H_{17}F_3N_3O$, 336.1324; found: 336.1201.

N-(2-(diethylamino)-5-(trifluoromethyl)phenyl)nicotinamide (**28**)

The compound was obtained as a white solid in 87% yield after purification by silica gel column chromatography eluted with hexane - ethyl acetate (1:1 v/v). TLC R_f = 0.50 (hexane - ethyl acetate 1:1 v/v). mp 64.8 - 66.8 ºC. IR (ATR, cm^{-1}) $\bar{\nu}_{max}$: 3334, 2975, 2932, 2854, 1678, 1614, 1586, 1534, 1483, 1440, 1336, 1247, 1167, 1150, 1114, 1062, 1021, 923, 898, 828, 716, 567. ^{1}H NMR (300 MHz, $CDCl_3$) δ: 0.99 (t, 6H, *J* = 7.2 Hz), 3.05 (q, 4H, *J* = 7.2 Hz), 7.32 (d, 1H, *J* = 8.1 Hz), 7.39 (dd, 1H, *J* = 8.1 Hz and *J* = 1.5 Hz), 7.49 (dd, 1H, *J* = 8.3 Hz and *J* = 4.7 Hz), 8.27 (dt, 1H, *J* = 8.3 Hz and *J* = 1.8 Hz), 8.80 (dd, 1H, *J* = 4.8 Hz and *J* = 1.8 Hz), 8.92 (d, 1H, *J* = 1.5 Hz), 9.12 (d, 1H, *J* = 1.8 Hz), 9.90 (brs, 1H). ^{13}C NMR (75 MHz, $CDCl_3$) δ: 13.0, 49.5, 116.3 (q, J_{C-F} = 3.9 Hz), 121.0 (q, J_{C-F} = 3.9 Hz), 123.6, 124.1, 124.2 (q, J_{C-F} = 270.5 Hz), 128.3 (q, J_{C-F} = 32.3 Hz), 130.6, 135.6, 136.5, 142.6, 147.8, 152.9, 163.2. HRMS ($M+H^+$): Calculated for $C_{17}H_{19}F_3N_3O$, 338.1480; found: 338.1399.

N-(2-morpholino-5-(trifluoromethyl)phenyl)nicotinamide (**29**)

The compound was obtained as a white solid in 74% yield after purification by silica gel column chromatography eluted with hexane - ethyl acetate (1:1 v/v). TLC R_f = 0.18 (hexane - ethyl acetate 1:1 v/v). 157.5 - 159.0 mp ºC. IR (ATR, cm^{-1}) $\bar{\nu}_{max}$: 3344, 2970, 2846, 1674, 1588, 1534, 1469, 1441, 1339, 1247, 1198, 1156, 1114, 1022, 936, 918, 897, 880, 833, 734, 707, 661. ^{1}H NMR (300 MHz, $CDCl_3$) δ: 2.95 (t, 4H, *J* = 4.5 Hz), 3.91 (t, 4H, *J* = 4.5 Hz), 7.33 (d, 1H, *J* = 8.1 Hz), 7.43 (dd, 1H, 8.4 Hz and *J* = 2.1 Hz), 7.51 (dd, 1H, *J* = 7.8 Hz and *J* = 4.8 Hz), 8.28 (td, 1H, *J* = 7.8 Hz and 1.8 Hz), 8.81 - 8.88 (m, 2H), 9,13 (brs, 1H), 9.45 (brs, 1H). ^{13}C NMR (75 MHz, $CDCl_3$) δ: 52.6, 67.7, 117.0 (q, J_{C-F} = 3.9 Hz), 121.3, 121.6 (q, J_{C-F} = 3.7 Hz), 124.1 (q, J_{C-F} = 270.3 Hz), 124.2, 128.4 (q, J_{C-F} = 32.5 Hz), 130.4, 133.7, 135.5, 144.1, 147.6, 153.1, 163,1. HRMS ($M+H^+$): Calculated for $C_{17}H_{17}F_3N_3O_2$ 352.1273; found: 352.1201.

N-(2-(4-bromophenylamino)-5-(trifluoromethyl)phenyl)nicotinamide (**30**)

The compound was obtained as a white solid in 30% yield after recrystallization with acetone. TLC R_f = 0.38 (hexane - ethyl acetate 1:1 v/v). mp 166.7 - 167.2 ºC. IR (ATR, cm^{-1}) $\bar{\nu}_{max}$: 3314, 3188, 3068, 1663, 1621, 1592, 1514, 1440, 1337, 1250, 1162, 1114, 1074, 1025, 1008, 887, 808, 709. ^{1}H NMR (300 MHz, $CDCl_3$) δ: 6.34 (brs, 1H), 6.82 (d, 2H, *J* = 8.7 Hz), 7.33 - 7.46 (m, 5H), 8.08 – 8.12 (m, 2H), 8.72 (dd, 1H, *J* = 4.8 Hz and *J* = 1.5 Hz), 8.96 (d, 1H, *J* = 1.5 Hz), 8.53 (brs, 1H). ^{13}C NMR (75 MHz, $CDCl_3$) δ: 114.4, 120.0, 121.3, 121.6 (q, J_{C-F} = 3.6 Hz), 123.9 (q, J_{C-F} = 3.7 Hz), 124.1, 124.1 (q, J_{C-F} = 270.0 Hz), 125.5 (q, J_{C-F} = 33.4 Hz), 129.2, 129.7, 132.7, 135.8, 138.9,

141.9, 148.0, 152.9, 164.5. HRMS (M+H$^+$): Calculated for $C_{19}H_{14}BrF_3N_3O$, 436.0272; found: 436.0200.

N-(2-(piperidin-1-yl)-5-(trifluoromethyl)phenyl)benzamide (**31**)

The compound was obtained as a white solid in 88% yield after purification by silica gel column chromatography eluted with hexane-ethyl acetate (5:1 v/v). TLC R_f = 0.55 (hexane - ethyl acetate 5:1 v/v). mp 116.0 - 117.0 ºC. IR (ATR, cm^{-1}) $\bar{\nu}_{max}$: 3338, 2932, 2846, 1675, 1588, 1530, 1472, 1439, 1378, 1337, 1272, 1240, 1162, 1116, 1026, 932, 913, 902, 877, 828, 796, 697, 648. ^{1}H NMR (300 MHz, $CDCl_3$) δ: 1.64 - 1.66 (m, 2H), 1.74 - 1.82 (m, 4H), 2.88 (t, 4H, *J* = 5.1 Hz), 7.26 (d, 1H, *J* = 8.1 Hz), 7.35 (d, 1H, *J* = 8.1 Hz), 7.51-7.62 (m, 3H), 7.94-7.96 (m, 2H), 8.91 (brs, 1H), 9.45 (brs, 1H).^{13}C NMR (75 MHz, $CDCl_3$) δ: 24.1, 27.1, 53.7, 116.5 (q, J_{C-F} = 3.8 Hz), 120.8, 124.4 (q, J_{C-F} = 269.9 Hz), 127.1, 129.2, 132.2, 134.0, 134.8, 145.8, 165.1. HRMS (M+H$^+$): Calculated for $C_{19}H_{20}F_3N_2O$, 349.1528; found: 349.1451.

N-(2-(cyclohexylamino)-5-(trifluoromethyl)phenyl)benzamide (**32**)

The compound was obtained as a white solid in 55% yield after purification by column chromatography eluted with hexane-ethyl acetate (5:1 v/v). TLC R_f = 0.43 (hexane-ethyl acetate 5:1 v/v). mp 157.5-158.8 ºC. IR (ATR, cm^{-1}) $\bar{\nu}_{max}$:3396, 3214, 3058, 2935, 2862, 1636, 1613, 1552, 1334, 1243, 1213, 1161, 1105, 1073, 880, 812, 707, 624. ^{1}H NMR (300 MHz, $CDCl_3$) δ: 1.13-2.04 (m, 10H), 3.27-3.33 (m, 1H), 4.10-4.22 (brs, 1H), 6.79 (d, 1H, *J* = 8.7 Hz), 7.38 (dd, 1H, *J* = 8.6 Hz and*J* = 1.4 Hz), 7.46-7.60 (m, 4H), 7.76 (brs, 1H), 7.89 (d, 2H, *J* = 7.5 Hz). ^{13}C NMR (75 MHz, $CDCl_3$) δ: 25.0, 25.9, 33.2, 51.8, 112.7, 118.3 (q, J_{C-F}= 32.7 Hz), 122.9, 125.1 (q, J_{C-F} = 3.6 Hz), 127.5, 129.0, 132.5, 133.9, 145.0, 166.5. The signal of the carbono of the CF_3 group was of low intensity and it was not noticed in the spectrum. HRMS (M+H$^+$): Calculated for $C_{20}H_{22}F_3N_2O$, 363.1684; found: 363.1613.

N-(2-(pyrrolidin-1-yl)-5-(trifluoromethyl)phenyl)benzamide (**33**)

The compound was obtained in 80% yield as a white solid after purification by silica gel column chromatography eluted with hexane - ethyl acetate (5:1 v/v). TLC R_f = 0.30 (hexane-ethyl acetate 5:1 v/v). mp 122.2 - 122.8 ^{o}C.IR (ATR, cm^{-1}) $\bar{\nu}_{max}$: 3242, 2986, 2948, 2870, 1637, 1616, 1578, 1519, 1488, 1366, 1331, 1266, 1149, 1098, 1082, 874, 799, 695, 656. ^{1}H NMR (300 MHz, $CDCl_3$) δ: 1.96 - 2.01 (m, 4H), 3.13 - 3.17 (t, 4H, *J* = 6.3 Hz), 7.15 (d, 1H, *J* = 8.4 Hz), 7.34 (dd, 1H, *J* = 8.4 Hz and *J* = 1.5 Hz), 7.49 - 7.61 (m, 3H), 7.89 - 7.91 (m, 2H), 8.51 (brs,1H), 8.70 (brs, 1H).

^{13}C NMR (75 MHz, $CDCl_3$) δ: 24.9, 52.0, 118.5, 119.6 (q, J_{C-F} = 3.8 Hz), 122.0 (q, J_{C-F} = 3.9 Hz), 124.5 (q, J_{C-F} = 269.9 Hz), 124.8 (q, J_{C-F} = 32.5 Hz), 127.2, 129.2, 131.1, 132.2, 134.7, 144.6, 165.3. HRMS ($M+H^+$): Calculated for $C_{18}H_{18}F_3N_2O$, 335.1371; found: 335.1277.

N-(2-(diethylamino)-5-(trifluoromethyl)phenyl)benzamide (**34**)

The compound was obtained in 84% yield as a white solid after purification by silica gel column chromatography eluted with hexane-ethyl acetate (5:1 v/v). TLC R_f = 0.65 (hexane - ethyl acetate 5:1 v/v). mp 65.1 - 66.0 ºC. IR (ATR, cm^{-1}) $\bar{\nu}_{max}$: 3334, 2975, 2932, 2858, 1678, 1586, 1534, 1483, 1440, 1336, 1247, 1167, 1150, 923, 828, 716. ^{1}H NMR (300 MHz, $CDCl_3$) δ: 1.00 (t, 6H, *J* = 7.2 Hz), 3.03 (q, 4H, *J* = 7.2 Hz), 7.30 (d, 1H, *J* = 8.4 Hz), 7,36 (dd, 1H, *J* = 8.4 Hz and *J* = 1.5 Hz), 7.50 - 7.61(m, 3H), 7.92 (dd, 2H, *J* = 8.1 Hz and *J* = 1.5 Hz), 8.97 (brs, 1H), 9.81 (brs, 1H). ^{13}C NMR (75 MHz, $CDCl_3$) δ: 13.0, 49.3, 116.2 (q, J_{C-F} = 3.9 Hz), 120.5 (q, J_{C-F} = 3.8 Hz), 123.4, 124.3 (q, J_{C-F} = 270.7 Hz), 128.1 (q, J_{C-F} = 32.3 Hz), 127.2, 129.1, 132.2, 134.9, 136.9, 142.5, 165.1. HRMS ($M+H^+$): Calculated for $C_{18}H_{20}F_3N_2O$, 337.1528; found: 337.1449.

N-(2-morpholino-5-(trifluoromethyl)phenyl)benzamide (**35**)

The compound was obtained as a white solid in 78% yield after recrystallization with acetone. TLC R_f = 0.18 (hexane-acetate 5:1 v/v). mp 137.3 - 138.5 ºC. IR (ATR, cm^{-1}) $\bar{\nu}_{max}$: 3369, 2967, 2896, 2851, 1668, 1589, 1534, 1465, 1438, 1335, 1238, 1157, 1112, 1075, 1025, 937, 917, 897, 877, 821, 801, 707, 659. ^{1}H NMR (300 MHz, $CDCl_3$) δ: 2.96 (t, 4H, *J* = 4.5 Hz), 3.92 (t, 4H, *J* = 4.5 Hz), 7.30 (d, 1H, *J* = 8.4 Hz), 7.38 (dd, 1H, *J* = 8.4 Hz and *J* = 1.5 Hz), 7.52 - 7.63 (m, 3H), 7.93 (dd, 2H, *J* = 8.1 Hz and *J* = 1.5 Hz), 8.91 (brs, 1H), 9.39 (brs, 1H). ^{13}C NMR (75 MHz, $CDCl_3$) δ: 52.5, 67.8, 116.9 (q, J_{C-F} = 3.8 Hz), 121.0, 121.1 (q, J_{C-F} = 3.9 Hz), 124.2 (q, J_{C-F} = 270.5 Hz), 127.0, 128,2 (q, J_{C-F} = 32.5 Hz), 129.2, 132.5, 134.1, 134.6, 144.0, 165.0. HRMS ($M+H^+$): Calculated for $C_{18}H_{18}F_3N_2O_2$, 351.1320; found: 351.1266.

N-(2-(4-bromophenylamino)-5-(trifluoromethyl)phenyl)benzamide (**36**)

The compound was obtained as a white solid in 58% yield. TLC R_f = 0.25 (hexane - ethyl acetate 5:1 v/v). mp 157.3 - 158.0 ºC. IR (ATR, cm^{-1}) $\bar{\nu}_{max}$: 3366, 2967, 2892, 2852, 1668, 1589, 1534, 1465, 1438, 1335, 1238, 1157, 1112, 937, 917, 897, 877, 821, 802, 707, 659. ^{1}H NMR (300 MHz, $CDCl_3$) δ: 6.30 (brs, 1H), 6.83 (d, 2H, *J* = 8.7 Hz), 7.31 - 7.47 (m, 6H), 7.55 (t, *J* = 7.4 Hz, 1H), 7.75 (d, 2H, *J* = 8.7 Hz), 8,05 (brs, 1H), 8.22 (brs, 1H). ^{13}C NMR (75 MHz, $CDCl_3$) δ: 113.9, 119.7, 120.9, 121.1 (q, J_{C-F} = 3.9 Hz), 123.3 (q, J_{C-F} = 3.7 Hz), 123.9 (q, J_{C-F} = 270.1 Hz), 125.1 (q, J_{C-F} = 33.0

Hz), 127.1, 128.9, 129.3, 132.4, 133.3, 138.6, 141.8, 166.3. HRMS ($M+H^+$): Calculated for $C_{20}H_{15}BrF_3N_2O$, 435.0320; found: 435.0300.

3.5.2 Biological assays

3.5.2.1 Cell culture

Human leukemia cell lines HL60 (acute myelogenous leukemia - AML), Nalm6 (B-cell acute lymphoblastic leukemia – ALL-B), and Jurkat (T-cell acute lymphoblastic leukemia - ALL-T) were kindly provided by Dr. Jose Andrés Yunes (Centro Infantil Boldrini, Campinas, São Paulo, Brazil). Cell lines were grown in RPMI-1640 medium (Sigma) supplemented with 10% (v/v) fetal bovine serum (FBS) (LGC Biotecnologia), 100 g/mL streptomycin, and 100 units/mL penicillin (Sigma) at pH 7.2 and 37 ºC under 5% CO_2 atmosphere. Peripheral blood mononuclear cells (PBMC) were isolated from human-heparinized blood using Histopaque-1077 (Sigma) according to the manufacturer's protocol. The isolated lymphocytes were resuspended in complete RPMI-1640 medium supplemented with 10% FBS and stimulated with 1% (v/v) phytohemagglutinin (Gibco). The cells were counted using a Neubauer chamber for the following experiments.

3.5.2.2 Cell viability assay

HL60, Nalm6, and Jurkat cells ($7x10^4$ cells/well) and PBMC ($1x10^5$ cells/well) were seeded in 96-well plates. Each well contained 100 µL of complete RPMI medium and 100 µL of each compound solution at different concentration. The compounds were diluted in RPMI medium with 10% FBS and 0.4% DMSO (v/v, Sigma). After 48 h of culture, MTT (5 mg/mL, Sigma) was added to the wells. After 3 h at 37 ºC, the MTT solution was removed and it was added 100 µL/well of DMSO to solubilize the formazan. Absorbance was measured at 540 nm in a microplate reader (SpectraMax M5, Molecular Devices).

3.5.2.3 Drug combination studies

Cell viability of leukemia cells treated with a combination of compounds **24**, **30**, or **36** with vincristine was assessed by seeding $7x10^4$ Nalm6 cells in each well of a 96-well plate. The cells were then incubated with each compound (at concentrations corresponding to 25 and 50% of the IC_{50}), vincristine (0.5 or 1.0 nM, Sigma) or a combination of each compound and vincristine for 48 h. The cell viability was determined by MTT assay and CompuSyn software was used to calculate the combination index (CI) as previously described (Chou, 2010).

3.5.2.4 Apoptosis assay by flow cytometry

Nalm6 cells were seeded on 96-well plate at density of $7x10^4$ cells per well and treated with compounds **24**, **30** and **36** [20 µM]. DMSO (0.4% v/v) was used as vehicle control. After treatments, cells were labeled by using Annexin V/FITC apoptosis detection kit I (BD Biosciences) according to manufacturer's protocol. Then the cell samples were analyzed by flow cytometry (FACS Verse, BD Bioscience).

3.5.2.5 Autophagy detection with acridine orange staining

Nalm6 cells were seeded on 96-well plate at density of $7x10^4$ cells per well and treated with compounds **24**, **30** and **36** [20 µM] or DMSO (0.4% v/v). After, cells were washed with phosphate-buffered saline (PBS), suspended in PBS and stained by acridine orange (1 µM, Sigma) at 37 ºC for 15 min; then the cells were washed with PBS and resuspended in 0.5 mL of PBS. For visual examination of autophagosomes, cells were analyzed under a fluorescence microscope Evos FL (Life technologies).

3.5.2.6 Cell proliferation assay

Proliferation assays were performed in 96-well plates containing $1x10^4$ Nalm6 cells per well or $1.5x10^4$ HL60 cells per well. The compounds **24**, **30**, and **36** were added at 20 µM and DMSO (0.4% v/v) were used as control. The effect of each treatments on cell growth were determined by trypan blue (Invitrogen) dye exclusion. After 24, 48, 72, and 96 h cells were loaded on a hemocytometer to obtain the viable cell count.

3.5.2.7 RT-PCR assay

Nalm6 cells were exposed to 20 µM of compounds **24**, **30**, and **36** or SRPIN340 for 24 h. Cells treated with DMSO (0.4% v/v) were used as control. After incubation, mRNA was extracted using Tri Reagent (Sigma) according to the manufacturer's protocol. Samples were quantified by spectrophotometry (NanoDrop, Thermo Scientific) and analyzed for integrity in 1% agarose gel. Afterwards, the RNA was used for first-strand cDNA synthesis using the Super Script First-Strand kit (Invitrogen) according to the manufacturer's protocol. Then, the cDNA was used to amplify each fragment of interest by PCR using the GoTaq Green Master Mix (Promega) kit, and the products were separated in 1% or 2% agarose gels. All primers used in these assays are listed in Supplementary Table 1.

3.5.2.8 Western blotting assay

Nalm6 cells were treated with 20 µM of compounds **24**, **30**, and **36** or SRPIN340 for 24 h. After, cells were lysed in PBS containing 1% (v/v) NP40, 1 mM EDTA, 150 mM NaCl, protease and phosphatase inhibitors (Sigma), and 10 mM Tris (pH 7.4) at a concentration of $2x10^7$cells/mL in lysis buffer. Samples were incubated on ice for 10 minutes, briefly sonicated, and centrifuged for 10 minutes at 15000 x*g* to remove insoluble cellular debris. Proteins were resolved by SDS polyacrylamide gel electrophoresis, transferred to a polyvinylidene difluoride (PVDF) membrane (GE Healthcare), blocked overnight in PBS containing 5% (w/v) skim milk powder, incubated for 2 h with primary antibody, and then incubated for 2 h with secondary antibody solutions. Primary antibodies used were mouse anti-SRPK1 (BD Biosciences), mouse anti-SRPK2 (BD Biosciences), rabbit anti-actin (Sigma) and mouse anti-phospho SR proteins mAb1H4 (Invitrogen). The last one is able to detect different phospho-SR proteins epitopes (Siqueira et al., 2015; Zahler et al., 1992). The secondary antibodies used were anti-mouse peroxidase-conjugated (Sigma) and anti-rabbit peroxidase-conjugated (Sigma). Then, proteins were visualized using 3,3'-Diaminobenzidine tetrahydrochloride (Sigma) according to the manufacturer's protocol.

3.5.2.9 Statistical analysis

All numeric data were obtained from three independent experiments and are shown as means ± standard deviation. Analyses were performed using Microsoft Excel (Microsoft Office Software) and GraphPad Prism (GraphPad Software Inc.). Statistical analyses were done by one-way ANOVA followed by Dunnett's test. $*P < 0.05$ was considered significant.

Acknowledgments

The authors thank the Núcleo de Microscopia e Microanálise for the available facilities and technical assistance with flow cytometry assays. This work was supported by the Conselho Nacional de Desenvolvimento Científico e Tecnológico (CNPq) (Grant 485011/2012-3 to GCB), Fundação de Amparo à Pesquisa do Estado de Minas Gerais (FAPEMIG) (Grant CBB-APQ-01637-13 and CBB-APQ-02556-15 to GCB and CBB-APQ-01287-14/PRONEM), Coordenação de Aperfeiçoamento de Pessoal de Nível Superior (CAPES), and Fundação Arthur Bernardes (FUNARBE/FUNARPEX fellowship program to GCB). The funders had no involvement in the study design, in the collection, analysis or interpretation of data, in the writing of the report, or in the decision to submit the article for publication. The authors also thank CNPq, FAPEMIG, CAPES and FUNARBE for the fellowships to students and researchers involved in this work.

3.6 Figures

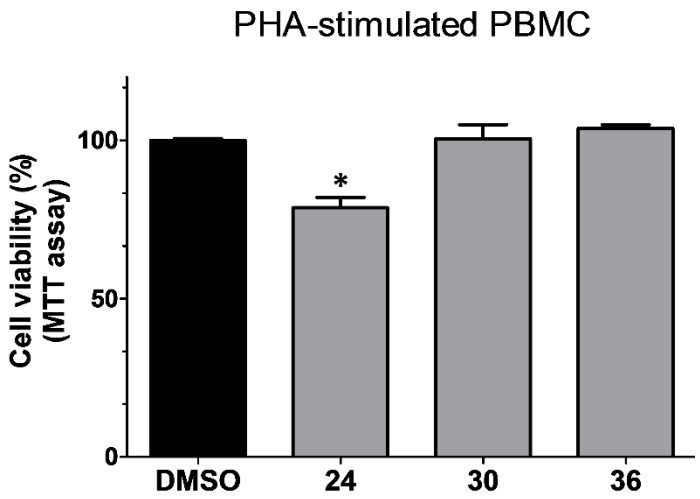

Figure 15: Effect of compounds 24, 30, and 36 over peripheral blood mononuclear cells (PBMC) stimulated with phytohemagglutinin (PHA). Cells were treated with 25 µM of each compound for 48 h. Cell viability was determined using MTT assay. Control treatment (vehicle) was considered 100% of viability. Data are shown as means ± standard deviation of triplicate experiments (*$P < 0.05$).

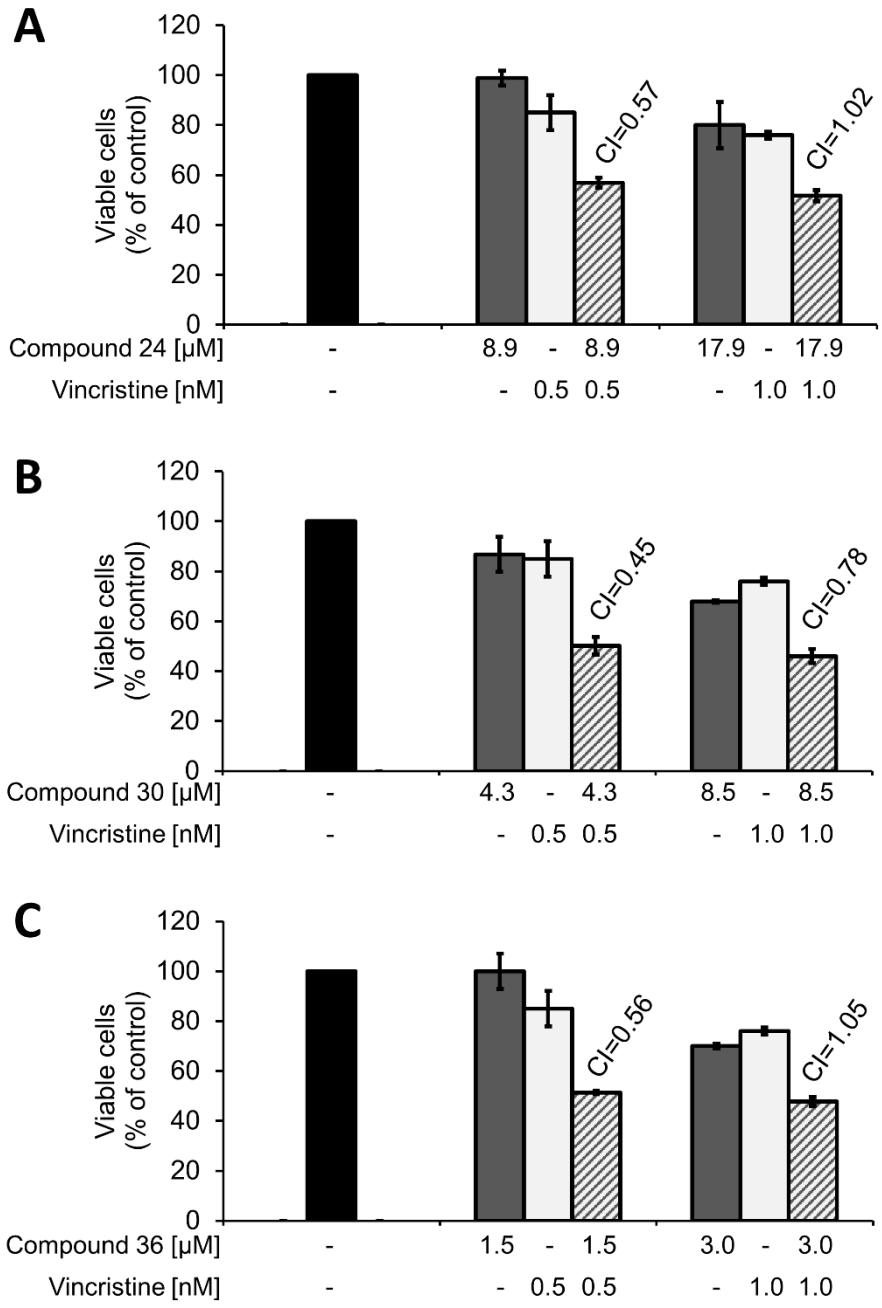

Figure 16: Effect of compounds 24, 30, and 36, in combination with vincristine, on the growth inhibition of Nalm6 cells. Cells were plated onto 96-well plates containing indicated concentrations of compound **24** (A), compound **30** (B), and compound **36** (C) or vincristine alone or in combinations with a fixed ratio for 48 h. The percentages of surviving cells as compared to controls, defined as 100% of viable cells, were determined by MTT assay. The combination index (CI) values were calculated using CompuSyn software according to the Chou–Talalay equation (Chou, 2010). Synergistic effect is characterized by CI < 1.0, additive effect by CI close to 1.0 and antagonistic effect by CI > 1.0. Data are shown as means ± standard deviation of triplicate experiments.

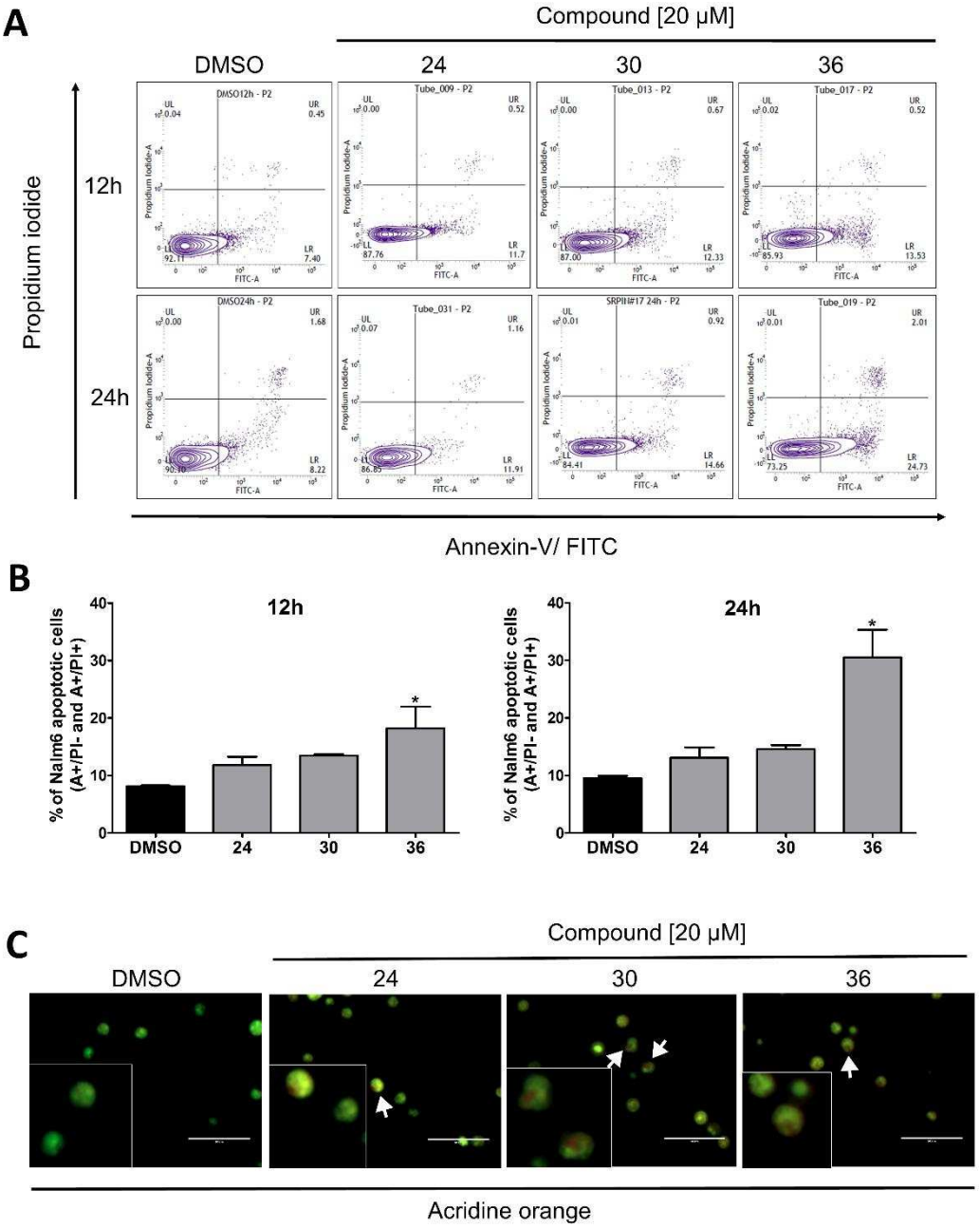

Figure 17: Effect of compounds 24, 30, and 36 on leukemia cell death. (A) Nalm6 cells were treated with 20 µM of each compound for 12 and 24 h. Cells treated with vehicle (DMSO) were used as control. Apoptosis/necrosis was evaluated using annexin-V/FITC and PI labels. One representative experiment is shown. (B) The graphs show averaged percentage of apoptotic cells (annexin-V positive cells) of triplicate experiments. **P* < 0.05. To assess the autophagossome induction (C), Nalm6 cells were treated with 20 µM of each compound or DMSO for 24 h. Subsequently, cells were stained with acridine orange and visualized under fluorescent microscopy. White arrows point to the autophagosomes. One representative experiment of three is shown.

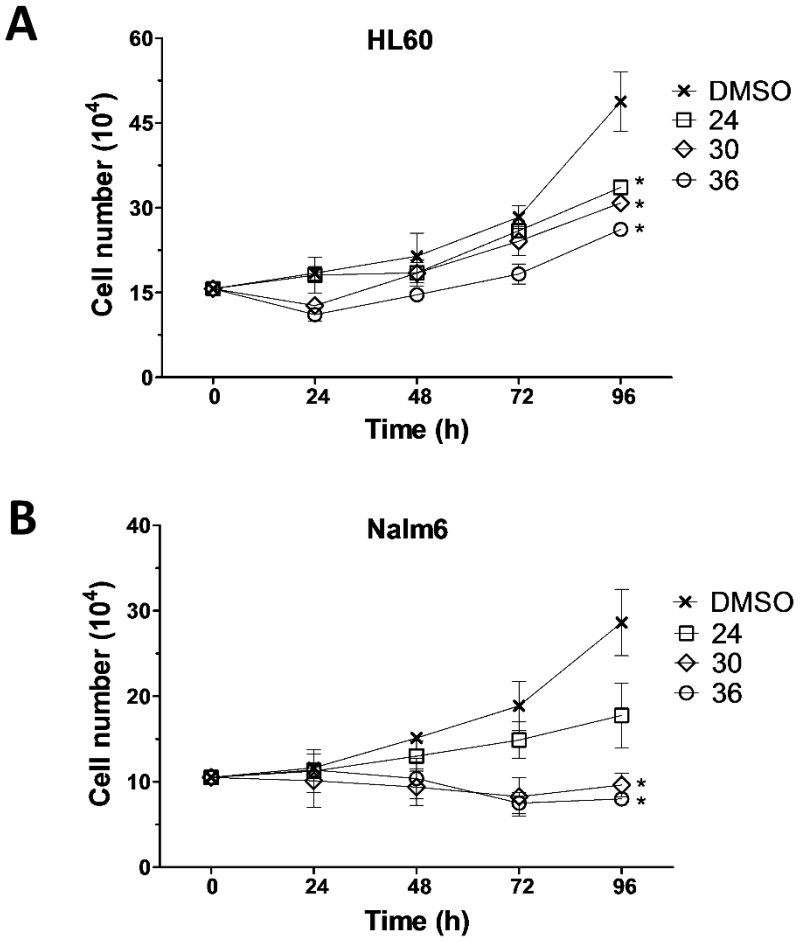

Figure 18: Effect of compounds 24, 30, and 36 on leukemia cell proliferation. (A) HL60 and (B) Nalm6 cells were treated with 20 µM of each compound. Cells treated with vehicle (DMSO) were used as control. Cell growth was determined with trypan blue exclusion at 0, 24, 48, 72, and 96 h after incubation (*$P < 0.05$).

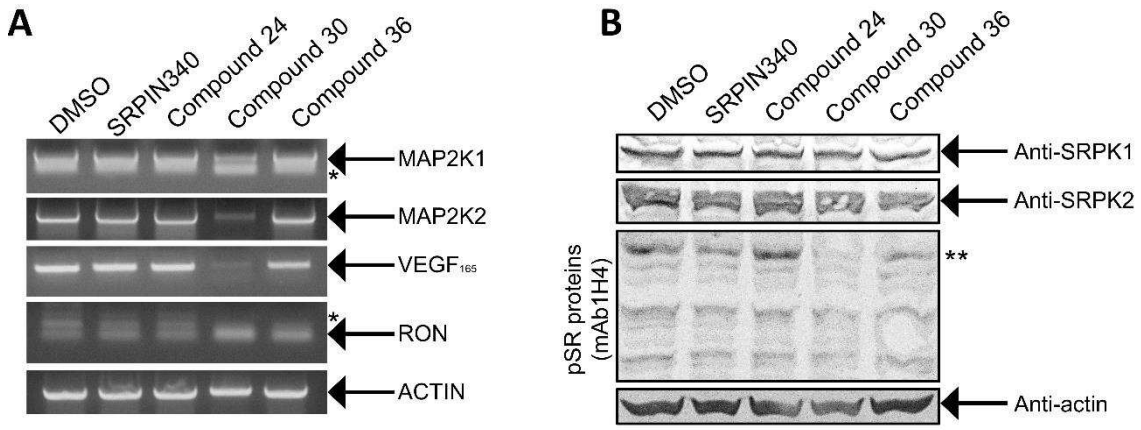

Figure 19: Effect of compounds 24, 30, and 36 in the intracellular activity of SRPKs. Nalm6 cells were treated with 20 µM of each compound for 24 h in order to investigate the effect on gene expression by RT-PCR assays (A) and SR protein phosphorylation pattern by Western blotting assays (B). Cells treated with vehicle (DMSO) or SRPIN340 [20 µM] were used as control. One representative experiment of three is shown for each analysis. (*) represent possible spliced isoforms and (**) represent the phosphorylated SRSF5 splicing factor.

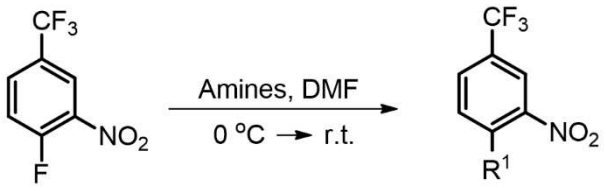

(**1**) (**2-7**)

Amines = piperidine, ciclohexylamine, pirrolidine, diethylamine, morpholine, 4-bromo aniline

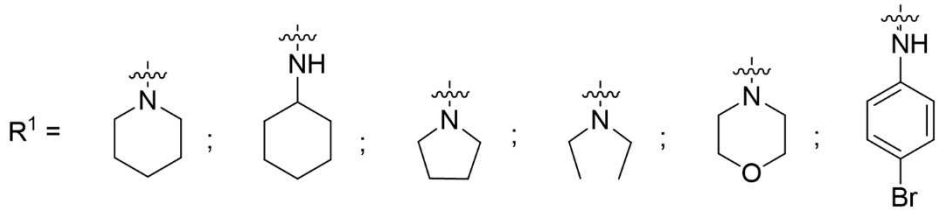

(**2**, 91%) (**3**, 81%) (**4**, 97%) (**5**, 98%) (**6**, 97%) (**7**, 93%)

Scheme 1: Nucleophilic aromatic substitution reactions between compound **1** and different amines involved in the preparation of compounds **2**-**7**.

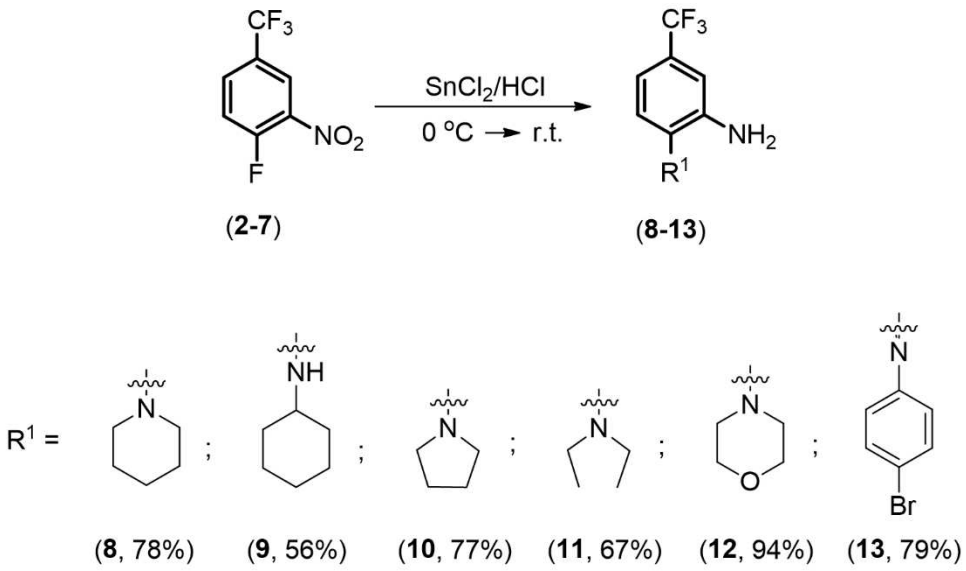

Scheme 2: Reduction of compounds **2**-**7** with $SnCl_2$/HCl.

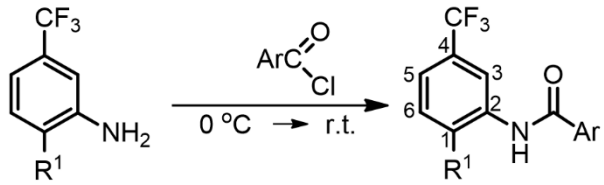

(**8-13**) **SRPIN340 and Compounds 15-36**

Scheme 3: Final step involved in the preparation of SRPIN340 and compounds **15**-**36**.

3.7 Table

Table 3: Synthesized compounds and half-maximal inhibitory concentration (IC_{50}) values over leukemic cell lines. HL60 (AML), Jurkat (LLA-T) and Nalm6 (LLA-B) cells were treated with increasing concentrations (0 – 200 µM) of each compound for 48 h. Cell viability was determined using the MTT assay. The IC_{50} values are expressed as the means ± standard deviation of three independent experiments.

Compound	R^1	Ar	Yield (%)	IC_{50}		
				HL60	Jurkat	Nalm6
SRPIN340		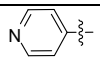	75	38.3±8.7	75.4±5.7	70.6±5.0
15	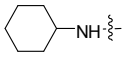		82	59.2±5.0	80.9±6.7	59.0±2.8
16			70	NA	NA	NA
17			85	89.7±12.8	NA	63.6±6.6
18			78	NA	NA	NA
19	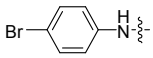		81	NA	NA	51.9±0.8
20			78	NA	NA	NA
21			79	NA	NA	NA
22			59	84.1±6.0	88.4±11.9	NA
23			91	NA	NA	NA
24	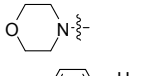		37	14.2±0.9	20.6±4.0	35.7±1.0
25			65	NA	NA	NA
26	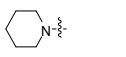		53	48.3±3.9	NA	52.3±3.7
27			73	NA	NA	NA
28			87	71.0±2.3	NA	63.2±2.0
29			74	NA	NA	NA
30	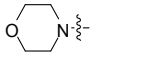		30	8.5±0.2	17.8±1.1	17.0±1.0
31			88	NA	NA	NA
32	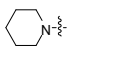		55	34.9±1.7	NA	NA
33			80	NA	NA	NA
34			84	NA	NA	NA
35			78	NA	NA	NA
36			58	11.8±0.4	33.8±1.8	6.0±2.4

NA: Not active within the concentration range evaluated (0-200 µM); IC_{50} values expressed in µM; AML: acute myelogenous leukemia; ALL-T: T-cell acute lymphoblastic leukemia; ALL-B: B-cell acute lymphoblastic leukemia.

Chapter 4: Concluding Remarks

4.1 Concluding Remarks

The abnormal activity of SRPKs has been demonstrated in different tumors and has been linked to an increased tumor cell proliferation and apoptosis evasion. Considering leukemias, the overexpression of both SRPK1 and SRPK2 in patient has been also previously reported (Hishizawa et al., 2005; Jang et al., 2008; Salesse et al., 2004). Mechanistically, the overexpression of SRPK2 in leukemia cells has been linked to cell proliferation due to the hiperphosphorylation of the SR protein acinus, which increases the expression levels of cyclin A1 (Jang et al., 2008). These findings suggest that strategies of SRPK inhibition would impact leukemia treatment regimes.

Within this context, the major aim of this work was to investigate the antileukemia potential of the pharmacological inhibition of SRPKs.

In a first study (Chapter 2), it was shown that SRPK1 and SRPK2 are overexpressed in a panel of myeloid and lymphoid leukemia cells but not in non transformed PBMCs. Along with a significant cytotoxic activity of a known SRPK pharmacological inhibitor (SRPIN340), its impact on SR proteins phosphorylation as well as in the expression of MAP2K1/2, FAS, and VEGF genes was observed. In addition, pharmacological treatments with this compound triggered early and late events of apoptosis. Furthermore, the *in vitro* structural data obtained with a recombinant SRPK2 form together with the analysis of docking and molecular dynamics provided possible mechanisms of SRPIN340 inhibitory activity. These findings were further corroborated and complemented by crystallographic studies on SRPK1/SRPIN340 complexes (Batson et al., 2017; Morooka et al., 2015).

Aiming to obtain novel SRPIN340 derivatives with increased pharmacological properties, in a second study (Chapter 3) a series of trifluoromethyl arylamides was obtained in collaboration with Dr. Robson Ricardo Teixeira from the Department of Chemistry of UFV. Three compounds was selected with increased cytotoxic activity - compounds **24**, **30**, and **36**. These compounds presented synergistic effect when combined with the chemotherapeutic agent vincristine, were able to induce apoptosis and autophagy in Nalm6 cells and displayed low toxicity against peripheral blood mononuclear cells (PBMCs). Remarkably, treatments of Nalm6 cells with these compounds changed the expression pattern of oncogenic isoforms of MAP2K1/2, VEGF, and RON genes as well as decreased the phospho-SR protein signal.

Taken together, these results suggest that SRPIN340 and its derivatives may be considered as valuable molecular probes to study the impact of splicing machinery in cancer cells as well as starting points for the development of a novel class of antitumor agents.

It is important to point out that the data presented here indicated the compound **30** was the most effective in reducing the phosphorylation status of SR protein in comparison to

SRPIN340. These *in vitro* data have been corroborated by additional *in vivo* studies carried out in parallel by our group in a murine model of metastatic melanoma (Moreira, 2016; Moreira et al., 2018; in preparation). This fact is particularly relevant in the context of previous studies that have shown SRPIN340 as a compound with low potency and poor pharmacokinetic (Gammons et al., 2014). In this context, it is important to mention that two new SRPK inhibitors, named SRPIN803 and SPHINX31, have been recently described (Batson et al., 2017; Morooka et al., 2015), and their likely antitumor activity remains to be demonstrated. In fact, it would be very interesting to considerer the *in vitro* and *in vivo* results obtained with these three substances in future medicinal chemistry efforts to obtain novel SRPKs inhibitors with relevant clinical potential.

In conclusion, we showed in this work that SRPIN340 and its derivatives obtained possess antileukemic potential, a finding that also contributes to the consolidation of SRPK as interesting therapeutic targets. Furthermore, the newly obtained substances here may serve as scaffolds for developing novel classes of anticancer agents. Future studies should investigate the mechanism of action of these compounds *in vitro* as well as their pharmacokinetic properties *in vivo*.

4.2 Acknowledgements

I would like to express my gratitude to all who has contributed throughout this time.

Thank to prof. Gustavo, for the guidance, confidence and support during the development of this study.

Thanks to professors and co-advisors Márcia, Juliana, and Abelardo, for the support in their labs.

Thanks to all of my colleagues, for the companionship, sharing knowledge and experience. In particular, I thank to Thiago Onofre, Éverton Barbosa, Marcelo Polêto, and Germanna Riguetto, for conducting the experiments in the published studies.

Thanks to Victor and Higor, not only by helping in the experiments, but also for the opportunity to share the acquired knowledge.

Thanks to the PhD colleagues in *Bioquímica Aplicada,* for the companionship.

Thanks to prof. Róbson and Marcus Vinícius, for their dedication to providing us with precious milligrams of SRPIN340 and its analogues and for the opportunity to collaborate in other studies.

Thanks to Universidade Federal de Viçosa and Departamento de Bioquímica e Biologia Molecular, for the institutional support through these ten years.

Thanks to CAPES, CNPq and FAPEMIG, for the granting of scholarships and financial

support to carry out ours projects.

Thanks to Dr. Patrick Eyers, Dr. Tiago Monteiro, and Dra. Luciana Maria, who promptly agreed to participate as members of the examining committee of this thesis.

Thanks to my friends, for share the fun times.

Thank to my sister Nathane, for her active support and constructive criticism.

Thanks to my parents, José Natalino and Maria Lúcia, for the word of authority, for teaching me to work, to be creative and to have expectations.

Thanks to God, I can do all things through him who strengthens me.

Thank you very much!

4.3 List of publications, co-authors and other relevant works

This thesis

Siqueira, R.P., Barros, M.V. de A., Barbosa, E.A.A., Onofre, T.S., Gonçalves, V.H.S., Pereira, H.S., Silva Júnior, A., de Oliveira, L.L., Almeida, M.R., Fietto, J.L.R., Teixeira, R.R., Bressan, G.C., 2017. Trifluoromethyl arylamides with antileukemia effect and intracellular inhibitory activity over serine/arginine-rich protein kinases (SRPKs). Eur. J. Med. Chem. 134, 97–109. doi:10.1016/j.ejmech.2017.03.078

Siqueira, R.P., Barbosa, E.A.A., Polêto, M.D., Righetto, G.L., Seraphim, T.V., Salgado, R.L., Ferreira, J.G., Barros, M.V.A., de Oliveira, L.L., Laranjeira, A.B.A., Almeida, M.R., Júnior, A.S., Fietto, J.L.R., Kobarg, J., de Oliveira, E.B., Teixeira, R.R., Borges, J.C., Yunes, J.A., Bressan, G.C., 2015. Potential antileukemia effect and structural analyses of SRPK inhibition by N-(2-(Piperidin-1-yl)-5-(Trifluoromethyl)Phenyl) isonicotinamide (SRPIN340). PLoS One 10. doi:10.1371/journal.pone.0134882

Other publications

Gazolla, P.A.R., Teixeira, R.R., da Silva, A.M., Vaz, B.G., Vasconcelos, G.A., Siqueira, R.P., Gonçalves, V.H.S., Pereira, H.S., Bressan, G.C., 2018. Synthesis and Cytotoxic Activity of 1,2,3-Triazole Derivatives of Eugenol. Química Nova. Accepted manuscript.

Teixeira, R.R., de Andrade Barros, M.V., Bressan, G.C., Siqueira, R.P., dos Santos, F.S., Bertazzini, M., Kiralj, R., Ferreira, M.M.C., Forlani, G., 2017. Synthesis, theoretical studies, and effect on the photosynthetic electron transport of trifluoromethyl arylamides. Pest Manag. Sci. 73, 2360–2371. doi:10.1002/ps.4623

Da Silva Maia, A.F., Siqueira, R.P., De Oliveira, F.M., Ferreira, J.G., Da Silva, S.F., Caiuby, C.A.D.,

De Oliveira, L.L., De Paula, S.O., Souza, R.A.C., Guilardi, S., Bressan, G.C., Teixeira, R.R., 2016. Synthesis, molecular properties prediction and cytotoxic screening of 3-(2-aryl-2-oxoethyl)isobenzofuran-1(3H)-ones. Bioorganic Med. Chem. Lett. 26, 2810–2816. doi:10.1016/j.bmcl.2016.04.065

Da Silva, M.R., Moreira, G.A., Silva, R.A.G., Barbosa, E.A.A., Siqueira, R.P., Teixeira, R.R., Almeida, M.R., Silva-Júnior, A., Fietto, J.L.R., Bressan, G.C., 2015. Splicing regulators and their roles in cancer biology and therapy. Biomed Res. Int. doi:10.1155/2015/150514

Inoue, F.A., Purgato, G.A., Maia, T. F., Siqueira, R.P., Lima, S., Diaz, G., Diaz, M.A.N., 2015. Chemical constituents and an alternative medicinal veterinary herbal soap made from Senna macranthera. Evidence-based Complement. Altern. Med. 2015. doi:10.1155/2015/217598

Patents

Bressan, G.C., Teixeira, R.R., Silva-Júnior, A., Fietto, J.L.R., Almeida, A.A., Neves, M.M., Siqueira, R.P., Moreira, G.A., Paiva, J.C., Lima, G.D.A., Barros, M.V.A., Viol, L.C.S., Carvalho, O.V., Santos, M.R., Assao, V.S., Gonçalves, V.H.S., Loterio, R.K., Barbosa, E.A.A., Pereira, H.S. Composto, Composições Farmacêuticas e Usos Desses. 2016, Brazil. Patent: Privilege of Innovation. Registration number: BR1020160293294, title: "Composto, Composições Farmacêuticas e Usos Desses", Registration institution: INPI - Instituto Nacional da Propriedade Industrial, Deposit date: 14/12/2016.

Bressan, G.C., Teixeira, R.R., Silva-Júnior, A., Fietto, J.L.R., Almeida, A.A., Neves, M.M., Siqueira, R.P., Moreira, G.A., Lima, G.D.A., Barros, M.V.A., Viol, L.C.S., Gonçalves, V.H.S., Loterio, R.K., Barbosa, E.A.A., Pereira, H.S. Compostos Sintéticos Antitumorais e Antimetastáticos, Composições Farmacêuticas e os Usos Desses. 2016, Brazil. Patent: Privilege of Innovation. Registration number: BR10201602934, title: "Compostos Sintéticos Antitumorais e Antimetastáticos, Composições Farmacêuticas e os Usos Desses", Registration institution: INPI - Instituto Nacional da Propriedade Industrial, Deposit date: 14/12/2016.

Award received

Siqueira, et al. 2016. SBBq Award, Brazilian Society of Biochemistry and Molecular Biology. Abstract Achievement Award. Title: Serine/ arginine-rich Protein Kinases (SRPKs) Inhibition as a Potential Targeted Therapeutic Strategy against Leukemia. In: 45ª Annual Meeting of the Brazilian Society of Biochemistry and Molecular Biology, Natal-RN. SBBq/2016.

4.4 References

Al Omair, S., 2015. Regulators of VEGF-a major isoforms in leukemia. Kent State Univ. 1–75.

Amin, E.M., Oltean, S., Hua, J., Gammons, M.V.R., Hamdollah-Zadeh, M., Welsh, G.I., Cheung, M.K., Ni, L., Kase, S., Rennel, E.S., Symonds, K.E., Nowak, D.G., Royer-Pokora, B., Saleem, M.A., Hagiwara, M., Schumacher, V.A., Harper, S.J., Hinton, D.R., Bates, D.O., Ladomery, M.R., 2011. WT1 Mutants Reveal SRPK1 to Be a Downstream Angiogenesis Target by Altering VEGF Splicing. Cancer Cell 20, 768–780. doi:10.1016/j.ccr.2011.10.016

Anczuków, O., Krainer, A.R., 2016. Splicing-factor alterations in cancers. RNA 22, 1285–301. doi:10.1261/rna.057919.116

Anwar, A., Hosoya, T., Leong, K.M., Onogi, H., Okuno, Y., Hiramatsu, T., Koyama, H., Suzuki, M., Hagiwara, M., Garcia-Blanco, M.A., 2011. The kinase inhibitor sfv785 dislocates dengue virus envelope protein from the replication complex and blocks virus assembly. PLoS One 6. doi:10.1371/journal.pone.0023246

Arber, D.A., Orazi, A., Hasserjian, R., Thiele, J., Borowitz, M.J., Le Beau, M.M., Bloomfield, C.D., Cazzola, M., Vardiman, J.W., 2016. The 2016 revision to the World Health Organization classification of myeloid neoplasms and acute leukemia. Blood. doi:10.1182/blood-2016-03-643544

Aubol, B.E., Adams, J.A., 2014. Recruiting a silent partner for activation of the protein kinase SRPK1. Biochemistry 53, 4625–4634. doi:10.1021/bi500483m

Aubol, B.E., Nolen, B., Shaffer, J., Ghosh, G., Adams, J.A., 2003. Novel Destabilization of Nucleotide Binding by the ?? Phosphate of ATP in the Yeast SR Protein Kinase Sky1p. Biochemistry 42, 12813–12820. doi:10.1021/bi035200c

Aubol, B.E., Plocinik, R.M., Hagopian, J.C., Ma, C.T., McGlone, M.L., Bandyopadhyay, R., Fu, X.D., Adams, J.A., 2013. Partitioning RS domain phosphorylation in an SR protein through the CLK and SRPK protein kinases. J. Mol. Biol. 425, 2894–2909. doi:10.1016/j.jmb.2013.05.013

Aubol, B.E., Wu, G., Keshwani, M.M., Movassat, M., Fattet, L., Hertel, K.J., Fu, X.D., Adams, J.A., 2016. Release of SR Proteins from CLK1 by SRPK1: A Symbiotic Kinase System for Phosphorylation Control of Pre-mRNA Splicing. Mol. Cell 63, 218–228. doi:10.1016/j.molcel.2016.05.034

Bai, L.Y., Weng, J.R., Chiu, C.F., Wu, C.Y., Yeh, S.P., Sargeant, A.M., Lin, P.H., Liao, Y.M., 2013. OSU-A9, an indole-3-carbinol derivative, induces cytotoxicity in acute myeloid leukemia through reactive oxygen species-mediated apoptosis. Biochem. Pharmacol. 86, 1430–1440. doi:10.1016/j.bcp.2013.09.002

Batson, J., Toop, H.D., Redondo, C., Babaei-Jadidi, R., Chaikuad, A., Wearmouth, S.F., Gibbons, B., Allen, C., Tallant, C., Zhang, J., Du, C., Hancox, J.C., Hawtrey, T., Da Rocha, J., Griffith, R.,

Knapp, S., Bates, D.O., Morris, J.C., 2017. Development of Potent, Selective SRPK1 Inhibitors as Potential Topical Therapeutics for Neovascular Eye Disease. ACS Chem. Biol. 12, 825–832. doi:10.1021/acschembio.6b01048

Bosnjak, M., Ristic, B., Arsikin, K., Mircic, A., Suzin-Zivkovic, V., Perovic, V., Bogdanovic, A., Paunovic, V., Markovic, I., Bumbasirevic, V., Trajkovic, V., Harhaji-Trajkovic, L., 2014. Inhibition of mTOR-dependent autophagy sensitizes leukemic cells to cytarabine-induced apoptotic death. PLoS One 9. doi:10.1371/journal.pone.0094374

Bourgeois, C.F., Lejeune, F., Stévenin, J., 2004. Broad specificity of SR (serine/arginine) proteins in the regulation of alternative splicing of pre-messenger RNA. Prog. Nucleic Acid Res. Mol. Biol. 78, 37–88. doi:10.1016/S0079-6603(04)78002-2

Breneman, C.M., Wiberg, K.B., 1990. Determining atom-centered monopoles from molecular electrostatic potentials. The need for high sampling density in formamide conformational analysis. J. Comput. Chem. 11, 361–373. doi:10.1002/jcc.540110311

Bullock, N., Potts, J., Simpkin, A.J., Koupparis, A., Harper, S.J., Oxley, J., Oltean, S., 2016. Serine-arginine protein kinase 1 (SRPK1), a determinant of angiogenesis, is upregulated in prostate cancer and correlates with disease stage and invasion. J. Clin. Pathol. 69, 171–175. doi:10.1136/jclinpath-2015-203125

Bulusu, K.C., Guha, R., Mason, D.J., Lewis, R.P.I., Muratov, E., Kalantar Motamedi, Y., Cokol, M., Bender, A., 2016. Modelling of compound combination effects and applications to efficacy and toxicity: State-of-the-art, challenges and perspectives. Drug Discov. Today. doi:10.1016/j.drudis.2015.09.003

Bustin, S.A., 2000. Absolute quantification of mrna using real-time reverse transcription polymerase chain reaction assays. J. Mol. Endocrinol. doi:JME00927 [pii]

Carneiro, F.R.G., Silva, T.C.L., Alves, A.C., Haline-Vaz, T., Gozzo, F.C., Zanchin, N.I.T., 2006. Spectroscopic characterization of the tumor antigen NY-REN-21 and identification of heterodimer formation with SCAND1. Biochem. Biophys. Res. Commun. 343, 260–268. doi:10.1016/j.bbrc.2006.02.140

Chan, C.B., Ye, K., 2013. Serine-arginine protein kinases: New players in neurodegenerative diseases? Rev. Neurosci. 24, 401–413. doi:10.1515/revneuro-2013-0014

Cho, S., Hoang, A., Chakrabarti, S., Huynh, N., Huang, D. Bin, Ghosh, G., 2011. The SRSF1 linker induces semi-conservative ESE binding by cooperating with the RRMs. Nucleic Acids Res. 39, 9413–9421. doi:10.1093/nar/gkr663

Chou, T.C., 2010. Drug combination studies and their synergy quantification using the chou-talalay method. Cancer Res. doi:10.1158/0008-5472.CAN-09-1947

Clery, A., Sinha, R., Anczukow, O., Corrionero, A., Moursy, A., Daubner, G.M., Valcarcel, J.,

Krainer, A.R., Allain, F.H.-T., 2013. Isolated pseudo-RNA-recognition motifs of SR proteins can regulate splicing using a noncanonical mode of RNA recognition. Proc. Natl. Acad. Sci. 110, E2802–E2811. doi:10.1073/pnas.1303445110

Courtney, K.D., Corcoran, R.B., Engelman, J.A., 2010. The PI3K pathway as drug target in human cancer. J. Clin. Oncol. 28, 1075–83. doi:10.1200/JCO.2009.25.3641

Cunningham, T.J., Palumbo, I., Grosso, M., Slater, N., Miles, C.G., 2013. WT1 regulates murine hematopoiesis via maintenance of VEGF isoform ratio. Blood 122, 188–192. doi:10.1182/blood-2012-11-466086

Da Silva, M.R., Moreira, G.A., Gonçalves Da Silva, R.A., De Almeida Alves Barbosa, É., Pais Siqueira, R., Teixera, R.R., Almeida, M.R., Silva Júnior, A., Fietto, J.L.R., Bressan, G.C., 2015. Splicing regulators and their roles in cancer biology and therapy. Biomed Res. Int. doi:10.1155/2015/150514

Dong, Z.Y., Noda, K., Kanda, a, Fukuhara, J., Ando, R., Murata, M., Saito, W., Hagiwara, M., Ishida, S., 2013. Specific inhibition of serine/arginine-rich protein kinase attenuates choroidal neovascularization. Mol. Vis. 19, 536–543.

Duarte, M., Wang, L., Calderwood, M.A., Adelmant, G., Ohashi, M., Roecklein-Canfield, J., Marto, J.A., Hill, D.E., Deng, H., Johannsen, E., 2013. An RS Motif within the Epstein-Barr Virus BLRF2 Tegument Protein Is Phosphorylated by SRPK2 and Is Important for Viral Replication. PLoS One 8. doi:10.1371/journal.pone.0053512

Elmore, S., 2007. Apoptosis: A Review of Programmed Cell Death. Toxicol. Pathol. doi:10.1080/01926230701320337

Fedorov, O., Huber, K., Eisenreich, A., Filippakopoulos, P., King, O., Bullock, A.N., Szklarczyk, D., Jensen, L.J., Fabbro, D., Trappe, J., Rauch, U., Bracher, F., Knapp, S., 2011. Specific CLK inhibitors from a novel chemotype for regulation of alternative splicing. Chem. Biol. 18, 67–76. doi:10.1016/j.chembiol.2010.11.009

Fukuhara, T., Hosoya, T., Shimizu, S., Sumi, K., Oshiro, T., Yoshinaka, Y., Suzuki, M., Yamamoto, N., Herzenberg, L.A., Herzenberg, L.A., Hagiwara, M., 2006. Utilization of host SR protein kinases and RNA-splicing machinery during viral replication. Proc. Natl. Acad. Sci. U. S. A. 103, 11329–11333. doi:10.1073/pnas.0604616103

Gammons, M.V.R., Dick, A.D., Harper, S.J., Bates, D.O., 2013. SRPK1 inhibition modulates VEGF splicing to reduce pathological neovascularization in a rat model of retinopathy of prematurity. Investig. Ophthalmol. Vis. Sci. 54, 5797–5806. doi:10.1167/iovs.13-11634

Gammons, M. V., Fedorov, O., Ivison, D., Du, C., Clark, T., Hopkins, C., Hagiwara, M., Dick, A.D., Cox, R., Harper, S.J., Hancox, J.C., Knapp, S., Bates, D.O., 2013. Topical antiangiogenic SRPK1 inhibitors reduce choroidal neovascularization in rodent models of exudative AMD.

Investig. Ophthalmol. Vis. Sci. 54, 6052–6062. doi:10.1167/iovs.13-12422

Gammons, M. V., Lucas, R., Dean, R., Coupland, S.E., Oltean, S., Bates, D.O., 2014. Targeting SRPK1 to control VEGF-mediated tumour angiogenesis in metastatic melanoma. Br. J. Cancer 111, 477–485. doi:10.1038/bjc.2014.342

Gammons, M. V, Lucas, R., Dean, R., Coupland, S.E., Oltean, S., Bates, D.O., 2014. Targeting SRPK1 to control VEGF-mediated tumour angiogenesis in metastatic melanoma. Br. J. Cancer 111, 477–485. doi:10.1038/bjc.2014.342

Giannakouros, T., Nikolakaki, E., Mylonis, I., Georgatsou, E., 2011. Serine-arginine protein kinases: A small protein kinase family with a large cellular presence. FEBS J. 278, 570–586. doi:10.1111/j.1742-4658.2010.07987.x

Goncalves, V., Henriques, A., Pereira, J., Neves Costa, A., Moyer, M.P., Moita, L.F., Gama-Carvalho, M., Matos, P., Jordan, P., 2014. Phosphorylation of SRSF1 by SRPK1 regulates alternative splicing of tumor-related Rac1b in colorectal cells. RNA 20, 474–482. doi:10.1261/rna.041376.113

Gout, S., Brambilla, E., Boudria, A., Drissi, R., Lantuejoul, S., Gazzeri, S., Eymin, B., 2012. Abnormal Expression of the Pre-mRNA Splicing Regulators SRSF1, SRSF2, SRPK1 and SRPK2 in Non Small Cell Lung Carcinoma. PLoS One 7. doi:10.1371/journal.pone.0046539

Gui, J.-F., Lane, W.S., Fu, X.-D., 1994. A serine kinase regulates intracellular localization of splicing factors in the cell cycle. Nature 369, 678–682. doi:10.1038/369678a0

Harper, S.J., Bates, D.O., 2008. VEGF-A splicing: The key to anti-angiogenic therapeutics? Nat. Rev. Cancer. doi:10.1038/nrc2505

Hayes, G.M., Carrigan, P.E., Beck, A.M., Miller, L.J., 2006. Targeting the RNA splicing machinery as a novel treatment strategy for pancreatic carcinoma. Cancer Res. 66, 3819–3827. doi:10.1158/0008-5472.CAN-05-4065

Hayes, G.M., Carrigan, P.E., Miller, L.J., 2007. Serine-arginine protein kinase 1 overexpression is associated with tumorigenic imbalance in mitogen-activated protein kinase pathways in breast, colonic, and pancreatic carcinomas. Cancer Res. 67, 2072–2080. doi:10.1158/0008-5472.CAN-06-2969

Hishizawa, M., Imada, K., Sakai, T., Ueda, M., Hori, T., Uchiyama, T., 2005. Serological identification of adult T-cell leukaemia-associated antigens. Br. J. Haematol. 130, 382–390. doi:10.1111/j.1365-2141.2005.05619.x

Hong, Y., Jang, S.W., Ye, K., 2011. The N-terminal fragment from caspase-cleaved serine/arginine protein-specific kinase2 (SRPK2) translocates into the nucleus and promotes apoptosis. J. Biol. Chem. 286, 777–786. doi:10.1074/jbc.M110.193441

House, A.E., Lynch, K.W., 2008. Regulation of alternative splicing: More than just the ABCs. J.

Biol. Chem. doi:10.1074/jbc.R700031200

Huey, R., Morris, G.M., Olson, A.J., Goodsell, D.S., 2007. Software news and update a semiempirical free energy force field with charge-based desolvation. J. Comput. Chem. 28, 1145–1152. doi:10.1002/jcc.20634

Jang, S.W., Yang, S.J., Ehlén, Å., Dong, S., Khoury, H., Chen, J., Persson, J.L., Ye, K., 2008. Serine/arginine protein-specific kinase 2 promotes leukemia cell proliferation by phosphorylating acinus and regulating cyclin A1. Cancer Res. 68, 4559–4570. doi:10.1158/0008-5472.CAN-08-0021

Karakama, Y., Sakamoto, N., Itsui, Y., Nakagawa, M., Tasaka-Fujita, M., Nishimura-Sakurai, Y., Kakinuma, S., Oooka, M., Azuma, S., Tsuchiya, K., Onogi, H., Hagiwara, M., Watanabe, M., 2010. Inhibition of hepatitis C virus replication by a specific inhibitor of serine-arginine-rich protein kinase. Antimicrob. Agents Chemother. 54, 3179–3186. doi:10.1128/AAC.00113-10

Kim, H., Choi, K., Kang, H., Lee, S.Y., Chi, S.W., Lee, M.S., Song, J., Im, D., Choi, Y., Cho, S., 2014. Identification of a novel function of CX-4945 as a splicing regulator. PLoS One 9. doi:10.1371/journal.pone.0094978

Kim, J., Wu, J., 2014. A theoretical study of SRPK interaction with the flexible domains of hepatitis B capsids. Biophys. J. 107, 1453–1461. doi:10.1016/j.bpj.2014.07.032

King, K.Y., Goodell, M.A., 2011. Direct conversion of skin cells into blood: Alchemy or science? Mol. Ther. doi:10.1038/mt.2010.291

Klaeger, S., Heinzlmeir, S., Wilhelm, M., Polzer, H., Vick, B., Koenig, P., Reinecke, M., Ruprecht, B., Petzoldt, S., Meng, C., Zecha, J., Reiter, K., Qiao, H., Helm, D., Koch, H., Schoof, M., Canevari, G., Casale, E., Depaolini, S., Feuchtinger, A., Wu, Z., Schmidt, T., Rueckert, L., Becker, W., Huenges, J., Garz, A., Gohlke, B., Zolg, D., Kayser, G., Vooder, T., Preissner, R., Hahne, H., Tõnisson, N., Kramer, K., Götze, K., Bassermann, F., Schlegl, J., Ehrlich, H., Aiche, S., Walch, A., Greif, P., Schneider, S., Felder, E., Ruland, J., Médard, G., Jeremias, I., Spiekermann, K., Kuster, B., 2017. The target landscape of clinical kinase drugs. Science (80-.). 358, pii: eaan4368.

Knight, Z.A., Lin, H., Shokat, K.M., 2010. Targeting the cancer kinome through polypharmacology. Nat. Rev. Cancer. doi:10.1038/nrc2787

Kornblihtt, A.R., Schor, I.E., Alló, M., Dujardin, G., Petrillo, E., Muñoz, M.J., 2013. Alternative splicing: A pivotal step between eukaryotic transcription and translation. Nat. Rev. Mol. Cell Biol. doi:10.1038/nrm3525

Koutroumani, M., Papadopoulos, G.E., Vlassi, M., Nikolakaki, E., Giannakouros, T., 2017. Evidence for disulfide bonds in SR Protein Kinase 1 (SRPK1) that are required for activity

and nuclear localization. PLoS One 12. doi:10.1371/journal.pone.0171328

Kozlovski, I., Siegfried, Z., Amar-Schwartz, A., Karni, R., 2017. The role of RNA alternative splicing in regulating cancer metabolism. Hum. Genet. doi:10.1007/s00439-017-1803-x

Kuroyanagi, N., Onogi, H., Wakabayashi, T., Hagiwara, M., 1998. Novel SR-protein-specific kinase, SRPK2, disassembles nuclear speckles. Biochem. Biophys. Res. Commun. 242, 357–64. doi:10.1006/bbrc.1997.7913

La Cognata, V., Iemmolo, R., D'Agata, V., Scuderi, S., Drago, F., Zappia, M., Cavallaro, S., 2014. Increasing the Coding Potential of Genomes Through Alternative Splicing: The Case of PARK2 Gene. Curr. Genomics 15, 203–216. doi:10.2174/1389202915666140426003342

Lee, G., Zheng, Y., Cho, S., Jang, C., England, C., Dempsey, J., Yu, Y., Liu, X., He, L., Cavaliere, P., Chavez, A., Zhang, E., Isik, M., Couvillon, A., Dephoure, N., Blackwell, T., Yu, J., Rabinowitz, J., Cantley, L., Blenis, J., 2017. Post-transcriptional Regulation of De Novo Lipogenesis by mTORC1-S6K1-SRPK2 Signaling. Cell In press.

Lee, S.C.W., Abdel-Wahab, O., 2016. Therapeutic targeting of splicing in cancer. Nat. Med. doi:10.1038/nm.4165

Lee, Y., Rio, D.C., 2015. Mechanisms and Regulation of Alternative Pre-mRNA Splicing. Annu. Rev. Biochem. 84, 291–323. doi:10.1146/annurev-biochem-060614-034316

Lin, J.-C., Lin, C.-Y., Tarn, W.-Y., Li, F.-Y., 2014. Elevated SRPK1 lessens apoptosis in breast cancer cells through RBM4-regulated splicing events. RNA 20, 1621–1631. doi:10.1261/rna.045583.114

Long, J.C., Caceres, J.F., 2009. The SR protein family of splicing factors: master regulators of gene expression. Biochem. J. 417, 15–27. doi:10.1042/BJ20081501

Mahiet, C., Swanson, C.M., 2016. Control of HIV-1 gene expression by SR proteins. Biochem. Soc. Trans. 44, 1417 LP-1425. doi:10.1042/BST20160113

Matera, A.G., Wang, Z., 2014. A day in the life of the spliceosome. Nat. Rev. Mol. Cell Biol. doi:10.1038/nrm3742

Mavrou, A., Brakspear, K., Hamdollah-Zadeh, M., Damodaran, G., Babaei-Jadidi, R., Oxley, J., Gillatt, D.A., Ladomery, M.R., Harper, S.J., Bates, D.O., Oltean, S., 2015. Serine–arginine protein kinase 1 (SRPK1) inhibition as a potential novel targeted therapeutic strategy in prostate cancer. Oncogene 34, 4311–4319. doi:10.1038/onc.2014.360

Moreira, G.A., 2016. Efeito Citotóxico e Antimetastático da Inibição das Cinases SRPKs em Células de Melanoma Cutâneo. Unniversidade Fed. Viçosa 1–76.

Moreira, G.A., Lima, G., Siqueira, R.P., Adjanohoun, A.L.M., Santos, V.C., Barros, M.V. de A., Barbosa, É. de A.A., Loterio, R., Paiva, J., Gonçalves, V.H.S., Viol, L., Silva, E., Silva Júnior, A., Almeida, M.R., Fietto, J.L.R., Neves, M., Ferreira, R., Teixera, R.R., Bressan, G.C., 2018.

Antimetastatic Effect of the Pharmacological Inhibition of Serine/Arginine-rich Protein Kinases (SRPK) in Murine Melanoma. Prep. 1–34.

Morlando, M., Ballarino, M., Fatica, A., 2015. Long Non-Coding RNAs: New Players in Hematopoiesis and Leukemia. Front. Med. 2. doi:10.3389/fmed.2015.00023

Morooka, S., Hoshina, M., Kii, I., Okabe, T., Kojima, H., Inoue, N., Okuno, Y., Denawa, M., Yoshida, S., Fukuhara, J., Ninomiya, K., Ikura, T., Furuya, T., Nagano, T., Noda, K., Ishida, S., Hosoya, T., Ito, N., Yoshimura, N., Hagiwara, M., 2015. Identification of a Dual Inhibitor of SRPK1 and CK2 That Attenuates Pathological Angiogenesis of Macular Degeneration in Mice. Mol. Pharmacol. 88, 316–325. doi:10.1124/mol.114.097345

Morris, G.M., Ruth, H., Lindstrom, W., Sanner, M.F., Belew, R.K., Goodsell, D.S., Olson, A.J., 2009. Software news and updates AutoDock4 and AutoDockTools4: Automated docking with selective receptor flexibility. J. Comput. Chem. 30, 2785–2791. doi:10.1002/jcc.21256

Nakagawa, O., Arnold, M., Nakagawa, M., Hamada, H., Shelton, J.M., Kusano, H., Harris, T.M., Childs, G., Campbell, K.P., Richardson, J.A., Nishino, I., Olson, E.N., 2005. Centronuclear myopathy in mice lacking a novel muscle-specific protein kinase transcriptionally regulated by MEF2. Genes Dev. 19, 2066–2077. doi:10.1101/gad.1338705

Naro, C., Sette, C., 2013. Phosphorylation-mediated regulation of alternative splicing in cancer. Int. J. Cell Biol. doi:10.1155/2013/151839

Ngo, J.C.K., Giang, K., Chakrabarti, S., Ma, C.T., Huynh, N., Hagopian, J.C., Dorrestein, P.C., Fu, X.D., Adams, J.A., Ghosh, G., 2008. A Sliding Docking Interaction Is Essential for Sequential and Processive Phosphorylation of an SR Protein by SRPK1. Mol. Cell 29, 563–576. doi:10.1016/j.molcel.2007.12.017

Nowak, D.G., Amin, E.M., Rennel, E.S., Hoareau-Aveilla, C., Gammons, M., Damodoran, G., Hagiwara, M., Harper, S.J., Woolard, J., Ladomery, M.R., Bates, D.O., 2010. Regulation of Vascular Endothelial Growth Factor (VEGF) splicing from pro-angiogenic to anti-angiogenic isoforms: A novel therapeutic strategy for angiogenesis. J. Biol. Chem. 285, 5532–5540. doi:10.1074/jbc.M109.074930

Odunsi, K., Mhawech-Fauceglia, P., Andrews, C., Beck, A., Amuwo, O., Lele, S., Black, J.D., Huang, R.Y., 2012. Elevated expression of the serine-arginine protein kinase 1 gene in ovarian cancer and its role in Cisplatin cytotoxicity in vitro. PLoS One 7, e51030. doi:10.1371/journal.pone.0051030\rPONE-D-12-26848 [pii]

Oltean, S., Gammons, M., Hulse, R., Hamdollah-Zadeh, M., Mavrou, A., Donaldson, L., Salmon, A.H., Harper, S.J., Ladomery, M.R., Bates, D.O., 2012. SRPK1 inhibition in vivo: modulation of VEGF splicing and potential treatment for multiple diseases. Biochem. Soc. Trans. 40, 831–835. doi:10.1042/BST20120051

Oostenbrink, C., Villa, A., Mark, A.E., Van Gunsteren, W.F., 2004. A biomolecular force field based on the free enthalpy of hydration and solvation: The GROMOS force-field parameter sets 53A5 and 53A6. J. Comput. Chem. 25, 1656–1676. doi:10.1002/jcc.20090

Pronk, S., P??ll, S., Schulz, R., Larsson, P., Bjelkmar, P., Apostolov, R., Shirts, M.R., Smith, J.C., Kasson, P.M., Van Der Spoel, D., Hess, B., Lindahl, E., 2013. GROMACS 4.5: A high-throughput and highly parallel open source molecular simulation toolkit. Bioinformatics 29, 845–854. doi:10.1093/bioinformatics/btt055

Salesse, S., Dylla, S.J., Verfaillie, C.M., 2004. p210BCR/ABL-induced alteration of pre-mRNA splicing in primary human CD34+ hematopoietic progenitor cells. Leuk. Off. J. Leuk. Soc. Am. Leuk. Res. Fund, U.K 18, 727–33. doi:10.1038/sj.leu.2403310

Salton, M., Misteli, T., 2016. Small Molecule Modulators of Pre-mRNA Splicing in Cancer Therapy. Trends Mol. Med. doi:10.1016/j.molmed.2015.11.005

Sanidas, I., Kotoula, V., Ritou, E., Daans, J., Lenz, C., Mairhofer, M., Daniilidou, M., Kolbus, A., Kruft, V., Ponsaerts, P., Nikolakaki, E., 2010. The ratio of SRPK1/SRPK1a regulates erythroid differentiation in K562 leukaemic cells. Biochim. Biophys. Acta - Mol. Cell Res. 1803, 1319–1331. doi:10.1016/j.bbamcr.2010.07.008

Schmidt, M.W., Baldridge, K.K., Boatz, J.A., Elbert, S.T., Gordon, M.S., Jensen, J.H., Koseki, S., Matsunaga, N., Nguyen, K.A., Su, S., Windus, T.L., Dupuis, M., Montgomery, J.A., 1993. General atomic and molecular electronic structure system. J. Comput. Chem. 14, 1347–1363. doi:10.1002/jcc.540141112

Schüttelkopf, A.W., Van Aalten, D.M.F., 2004. PRODRG: A tool for high-throughput crystallography of protein-ligand complexes. Acta Crystallogr. Sect. D Biol. Crystallogr. 60, 1355–1363. doi:10.1107/S0907444904011679

Silva, K.P., Seraphim, T. V, Borges, J.C., 2013. Structural and functional studies of Leishmania braziliensis Hsp90. Biochim. Biophys. Acta 1834, 351–61. doi:10.1016/j.bbapap.2012.08.004

Silverman, J.A., Reynolds, L., Deitcher, S.R., 2013. Pharmacokinetics and Pharmacodynamics of Vincristine Sulfate Liposome Injection (VSLI) in adults with acute lymphoblastic leukemia. J. Clin. Pharmacol. 53, 1139–1145. doi:10.1002/jcph.155

Singh, B., Eyras, E., 2017. The role of alternative splicing in cancer. Transcription 8, 91–98.

Siqueira, R.P., Barbosa, É.D.A.A., Polêto, M.D., Righetto, G.L., Seraphim, T.V., Salgado, R.L., Ferreira, J.G., De Andrade Barros, M.V., De Oliveira, L.L., Laranjeira, A.B.A., Almeida, M.R., Júnior, A.S., Fietto, J.L.R., Kobarg, J., De Oliveira, E.B., Teixeira, R.R., Borges, J.C., Yunes, J.A., Bressan, G.C., 2015. Potential antileukemia effect and structural analyses of SRPK inhibition by N-(2-(Piperidin-1-yl)-5-(Trifluoromethyl)Phenyl) isonicotinamide (SRPIN340).

PLoS One 10. doi:10.1371/journal.pone.0134882

Syed, N.H., Kalyna, M., Marquez, Y., Barta, A., Brown, J.W.S., 2012. Alternative splicing in plants - coming of age. Trends Plant Sci. doi:10.1016/j.tplants.2012.06.001

Tzelepis, K., Koike-Yusa, H., De Braekeleer, E., Li, Y., Metzakopian, E., Dovey, O.M., Mupo, A., Grinkevich, V., Li, M., Mazan, M., Gozdecka, M., Ohnishi, S., Cooper, J., Patel, M., McKerrell, T., Chen, B., Domingues, A.F., Gallipoli, P., Teichmann, S., Ponstingl, H., McDermott, U., Saez-Rodriguez, J., Huntly, B.J.P., Iorio, F., Pina, C., Vassiliou, G.S., Yusa, K., 2016. A CRISPR Dropout Screen Identifies Genetic Vulnerabilities and Therapeutic Targets in Acute Myeloid Leukemia. Cell Rep. 17, 1193–1205. doi:10.1016/j.celrep.2016.09.079

Van Roosmalen, W., Le Dévédec, S.E., Golani, O., Smid, M., Pulyakhina, I., Timmermans, A.M., Look, M.P., Zi, D., Pont, C., De Graauw, M., Naffar-Abu-Amara, S., Kirsanova, C., Rustici, G., 'T Hoen, P.A.C., Martens, J.W.M., Foekens, J.A., Geiger, B., Van De Water, B., 2015. Tumor cell migration screen identifies SRPK1 as breast cancer metastasis determinant. J. Clin. Invest. 125, 1648–1664. doi:10.1172/JCI74440

Wahl, M.C., Will, C.L., Lührmann, R., 2009. The Spliceosome: Design Principles of a Dynamic RNP Machine. Cell. doi:10.1016/j.cell.2009.02.009

Wang, E.T., Sandberg, R., Luo, S., Khrebtukova, I., Zhang, L., Mayr, C., Kingsmore, S.F., Schroth, G.P., Burge, C.B., 2008. Alternative isoform regulation in human tissue transcriptomes. Nature 456, 470–476. doi:10.1038/nature07509

Wang, H.Y., Lin, W., Dyck, J.A., Yeakley, J.M., Songyang, Z., Cantley, L.C., Fu, X.D., 1998. SRPK2: A differentially expressed SR protein-specific kinase involved in mediating the interaction and localization of pre-mRNA splicing factors in mammalian cells. J. Cell Biol. 140, 737–750. doi:10.1083/jcb.140.4.737

Wang, J., Wu, H.-F., Shen, W., Xu, D.-Y., Ruan, T.-Y., Tao, G.-Q., Lu, P., 2016. SRPK2 promotes the growth and migration of the colon cancer cells. Gene 586, 41–47. doi:10.1016/j.gene.2016.03.051

Wang, P., Zhou, Z., Hu, A., Pontede Albuquerque, C., Zhou, Y., Hong, L., Sierecki, E., Ajiro, M., Kruhlak, M., Harris, C., Guan, K.L., Zheng, Z.M., Newton, A.C., Sun, P., Zhou, H., Fu, X.D., 2014. Both decreased and increased SRPK1 levels promote cancer by interfering with PHLPP-mediated dephosphorylation of Akt. Mol. Cell 54, 378–391. doi:10.1016/j.molcel.2014.03.007

Wang, Y., Liu, J., Huang, B.O., Xu, Y.-M., Li, J., Huang, L.-F., Lin, J., Zhang, J., Min, Q.-H., Yang, W.-M., Wang, X.-Z., 2015. Mechanism of alternative splicing and its regulation. Biomed. reports 3, 152–158. doi:10.3892/br.2014.407

Wang, Y., Xiao, X., Zhang, J., Choudhury, R., Robertson, A., Li, K., Ma, M., Burge, C.B., Wang, Z.,

2013. A complex network of factors with overlapping affinities represses splicing through intronic elements. Nat. Struct. Mol. Biol. 20, 36–45. doi:10.1038/nsmb.2459

Ward, A.J., Cooper, T.A., 2010. The pathobiology of splicing. J. Pathol. doi:10.1002/path.2649

Wong, K.-K., Engelman, J.A., Cantley, L.C., 2010. Targeting the PI3K signaling pathway in cancer. Curr. Opin. Genet. Dev. 20, 87–90. doi:10.1016/j.gde.2009.11.002

Wong, M.L., Medrano, J.F., 2005. Real-time PCR for mRNA quantitation. Biotechniques. doi:10.2144/05391RV01

Wu, P., Nielsen, T.E., Clausen, M.H., 2016. Small-molecule kinase inhibitors: An analysis of FDA-approved drugs. Drug Discov. Today. doi:10.1016/j.drudis.2015.07.008

Wu, Q., Chang, Y., Zhang, L., Zhang, Y., Tian, T., Feng, G., Zhou, S., Zheng, Q., Han, F., Huang, F., 2014. SRPK1 dissimilarly impacts on the growth, metastasis, chemosensitivity and angiogenesis of glioma in normoxic and hypoxic conditions. J. Cancer 4, 727–735. doi:10.7150/jca.7576

Xu, X., Wei, Y., Wang, S., Luo, M., Zeng, H., 2017. Serine-arginine protein kinase 1 (SRPK1) is elevated in gastric cancer and plays oncogenic functions. Oncotarget 8, 61944–61957. doi:10.18632/oncotarget.18734

Yadav, S.S., Li, J., Stockert, J.A., O'Connor, J., Herzog, B., Elaiho, C., Galsky, M.D., Tewari, A.K., Yadav, K.K., 2016. Combination effect of therapies targeting the PI3K- and AR-signaling pathways in prostate cancer. Oncotarget 7, 76181–76196. doi:10.18632/oncotarget.12771

Zahler, A.M., Lane, W.S., Stolk, J.A., Roth, M.B., 1992. SR proteins: A conserved family of pre-mRNA splicing factors. Genes Dev. 6, 837–847. doi:10.1101/gad.6.5.837

Zhong, X.Y., Ding, J.H., Adams, J.A., Ghosh, G., Fu, X.D., 2009. Regulation of SR protein phosphorylation and alternative splicing by modulating kinetic interactions of SRPK1 with molecular chaperones. Genes Dev. 23, 482–495. doi:10.1101/gad.1752109

Zhou, Z., Fu, X.D., 2013. Regulation of splicing by SR proteins and SR protein-specific kinases. Chromosoma. doi:10.1007/s00412-013-0407-z

Zhou, Z., Qiu, J., Liu, W., Zhou, Y., Plocinik, R.M., Li, H., Hu, Q., Ghosh, G., Adams, J.A., Rosenfeld, M.G., Fu, X.D., 2012. The Akt-SRPK-SR Axis Constitutes a Major Pathway in Transducing EGF Signaling to Regulate Alternative Splicing in the Nucleus. Mol. Cell 47, 422–433. doi:10.1016/j.molcel.2012.05.014

4.5 Supporting Information

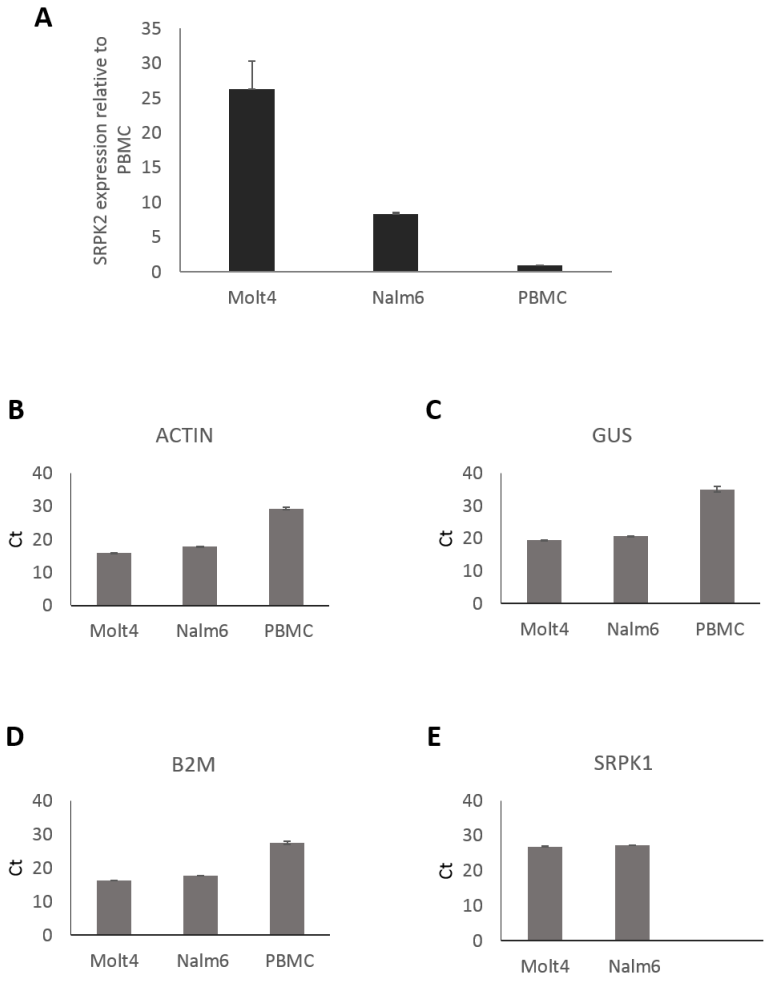

Supplementary Figure 1. RT-qPCR analysis comparing SRPK2 mRNA expression in Molt4 and Nalm6 leukemia cells in relation to PBMC. mRNA expression analysis (A) shows that SRPK2 has higher expression in Molt4 and Nalm6 compared with non-transformed PBMC. Because all genes amplified to be used as endogenous controls strongly varied between the PBMC and leukemia cells (see graphs B-D), the data were normalized using the unit of mass of the starting material (Bustin, 2000; Wong and Medrano, 2005). For this analysis, equal amounts of total RNA and cDNAs were carefully determined spectrophotometrically, allowing us to plot the relative expression values as $2^{\Delta Ct}$, where PBMC was used as a calibrator ($\Delta Ct = Ct_{(PBMC)} — Ct_{(SRPK)}$). The same approach was attempted with SRPK1, but its expression could not be precisely compared with the leukemia cells (see graph E) because it was barely detected in the PBMC samples. Nevertheless, this indicates that SRPK1 has very low expression in PBMC, which is in good agreement with our WB assays (**Figure 9A**) and with previous RT-qPCR reports (Hishizawa et al., 2005; Salesse et al., 2004). The primers used in these experiments are detailed in Supplementary Table 1.

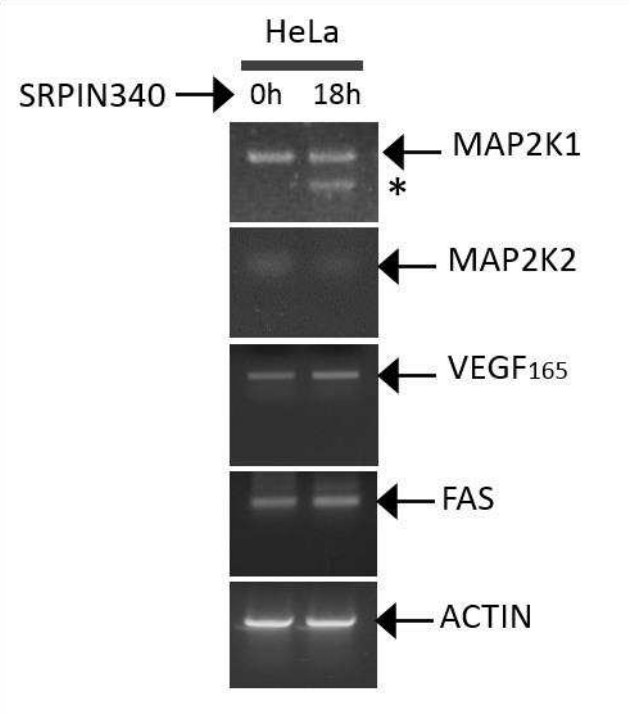

Supplementary Figure 2. Effect of SRPIN340 treatment on MAP2K1, MAP2K2, VEGF and FAS expression in HeLa cells. RT-PCR was performed using primers specific for MAP2K1, MAP2K2, VEGF, and FAS genes, and cDNA were derived from HeLa cells after 18 h of treatment with SRPIN340 (100 µM). Cells treated with the vehicle DMSO were used as a control. One representative experiment of three is shown. (*) MAP2K1 splicing variant as previously described (Hayes et al., 2007).

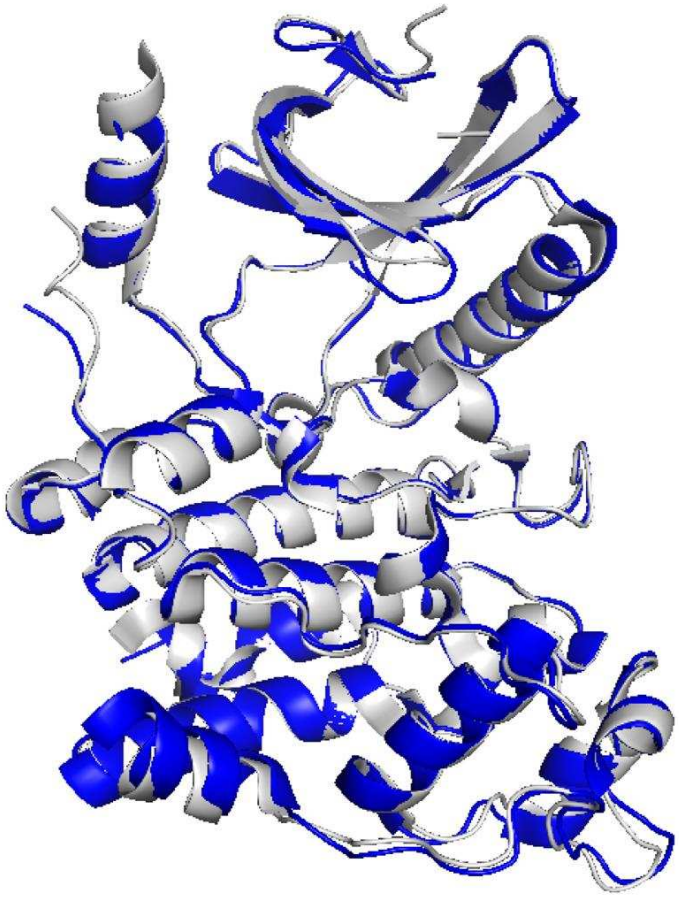

Supplementary Figure 3. Superposition of SRPK1 and SRPK2 crystallographic structures. SRPK1 (PDB ID 1WAK, grey) and SRPK2 (PDB ID 2X7G, blue) structures were aligned attesting their high similarity.

Supplementary Table 1: List of primers. List of primers used for RT-PCR and quantitative RT-PCR assays.

RT-PCR primers:		
Primer Name	Primer sequence 5'→3'	Reference
ACTIN_F	CCAGCTCACCATGGATGATGATATCG	Hayes et al., 2007
ACTIN_R	GGAGTTGAAGGTAGTTTCGTGGATGC	
FAS_F	TCAAGGAATGCACACTCACC	Clery et al., 2013
FAS_R	TCCTTTCTGTGCTTTCTGCAT	
MAP2K1_F	CCAAAATGCCCAAGAAGAAGCCG	Hayes et al., 2007
MAP2K1_R	CCAAACACTTAGACGCCAGCAGC	
MAP2K2_F	CACCATCAACCCTACCATCGCC	Hayes et al., 2007
MAP2K2_R	CCACTTCTTCCACCTCGGACC	
VEGF_F	GTAAGCTTGTACAAGATCCGCAGACG	Amin et al., 2011
VEGF_R	ATGGATCCGTATCAGTCTTTCCTGG	
RON_F	CTGAATATGTGGTCCGAGACC	Clery et al., 2013
RON_R	TAGCTGCTTCCTCCGCCACC	
Quantitative RT-PCR primers:		
Primer Name	Primer sequence 5'→3'	Reference
ACTIN_F	TGGATCAGCAAGCAGGAGTATG	_
ACTIN_R	GCATTTGCGGTGGACGAT	
GUS_F	GAAAATATGTGGTTGGAGAGCTCATT	_
GUS_R	CAGCACTCTCGTCGGTGACTGTTCA	
B2M_F	GAGTATGCCTGCCGTGTG	_
B2M_R	CCTCCATGATGCTGCTTACATGTCTC	
SRPK1_F	TGCTTGTTGGGTGCACAAA	_
SRPK1_R	CGATTAGAACTTCCAAGGAACGA	
SRPK2_F	GCAAAGGACAATGGTGAAGCTGAGG	_
SRPK2_R	CATCATCATCTTCATCGTCCAGTTGC	

F: Forward primer; R: Reverse primer.